INDUCTION OF IMMUNOGENIC CELL DEATH VIA NANOPARTICLE-MEDIATED DUAL CHEMOTHERAPY AND PHOTOTHERMAL THERAPY

by

Niloofar Heshmati Aghda, B.S., M.S.

A dissertation submitted to the Graduate Council of
Texas State University in partial fulfillment
of the requirements for the degree of
Doctor of Philosophy
with a Major in Materials Science, Engineering, and Commercialization
May 2020

Committee Members:

Tania Betancourt, Chair

Jennifer Irvin

Kevin Lewis

James Tunnell

Shannon Weigum

FAIR USE AND AUTHOR'S PERMISSION STATEMENT

Fair Use

Duplication Permission

DEDICATION

To

Mohammad Hossein Heshmati and Afsar (Zohre) Afkhami

ACKNOWLEDGEMENTS

I would like to thank the people without whom I would not have been able made it through this project.

First, I would like to express my sincere gratitude and appreciation for my amazing advisor, Dr. Tania Betancourt. She was smart, knowledgeable, supportive, extremely kind and attentive. She consistently provided guidance and support to push the project forward. She was a great mentor whom I was fortunate enough to meet and work with in the past three years. Not only she generously shared her knowledge, but also, she patiently taught me the skills that I would never have learned anywhere else. She always encouraged me, trusted on me, supported and guided me to accomplish my goals. I am truly grateful for this opportunity and thank her for all of these.

I would like to thank Dr. Jennifer Irvin, Dr. Kevin Lewis, Dr. James Tunnel, and Dr. Shannon Weigum for taking the time to be on my advisory committee and giving valuable feedback on my project.

I would like to thank Dr. Irvin, as the director of MSEC program, for her constant support and help. I will never forget that how difficult it was for me to get here and it would not have been possible without her help. I would also thank her and Dr. Tunnell for letting me use his laboratory facilities whenever I needed.

I would like to thank my undergraduate collaborators who were great teammates and awesome friends, Juan Castillo, Carli Severson, Emilio Lara, Shahad Abdulsahib and Grayson Ard. I also thank Dr. Susana Torres for her collaboration.

I also want to thank Dr. Jonathan Tyner, Ms. Karla Pizana and Ms. Kelsie Crumpton for always being patient, supportive and for their consistent help.

I also thank all members of Dr. Betancourt's research laboratory, my wonderful friends and finally my lovely family from whom I always received encouragement, motivation and sympathy.

TABLE OF CONTENTS

Page

LIST OF TABLES

Table **Page**

LIST OF FIGURES

Figure **Page**

LIST OF ABBREVIATIONS

Abbreviation	Description
APC	Antigen Presenting Cells
ATCC	American Type Culture Collection
ATP	Adenosine Triphosphate
BODIPY	Boron-Dipyrromethane
BSA	Bovine Serum Albumin
CD	Carbon Dot
CNH	Carbon Nanohorn
CNT	Carbon Nanotube
DAMP	Damage-Associated Molecular Pattern
DAPI	4′,6-Diamidine-2′-Phenylindole
DC	Dendritic Cell
DL	Drug Loading
DLS	Dynamic Light Scattering
DMEM	Dulbecco's Modified Eagle's Medium
Dox	Doxorubicin
EDC	1-Ethyl-3-(3-Dimethylaminopropyl) carbodiimide
EPR	Enhanced Permeability and Retention
ER	Endoplasmic Reticulum
ER	Estrogen Receptor
FDA	Food and Drug Administration

GD	Graphene Dot
GMP	Good Manufacturing Practice
GO	Graphene Oxide
GPC	Gel Permeation Chromatography
HSA	Human Serum Albumin
HEPES	4-(2-hydroxyethyl)-1-piperazineethanesulfonic acid
HMGB1	High Mobility Group Box 1
HSP	heat shock proteins
ICD	Immunogenic cell death
ICG	Indocyanine Green
ICP	Immune Checkpoint Therapy
IL	Interleukin
INF	Interferon
IR	Infrared
LALS	Left-Angel Light Scattering
MBL	Mannose-Binding Lectin
MHC	Major Histocompatibility Complex
MTT	Thiazolyl Blue Tetrazolium Bromide
NIR	Near Infrared
NK	Natural Killer
NP	Nanoparticle

NT	No Treatment
PBS	Phosphate Buffer Saline
PDI	Polydispersity Index
PEDOT	poly(ethylene dioxythiophene)
PEDOT:PSS	Poly(3,4-ethylene dioxythiophene)-poly(styrene sulfonate)
PEO	Poly(ethylene oxide)
PLA-PEG	Poly(lactic acid)-b-poly(ethylene glycol)
PLGA	Poly(lactic-co-glycolic acid))
PMPC	Poly(2-methacryloyloxyethyl phosphorylcholine)
PNIPAAm	Poly(N-isopropyl acrylamide)
PR	Progesterone Receptor
PS	Polystyrene
PTT	Photothermal Therapy
PVA	Polyvinyl Alcohol
RALS	Right-Angel Light Scattering
RES	Reticuloendothelial System
rHSA	Recombinant Human Serum Albumin
RI	Refractive Index
ROP	Ring Opening Polymerization
SD	Standard Deviation
SEM	Scanning Electron Microscopy

SPR	Surface Plasmon Resonance
TCR	T Cell Receptor
TH2	T Helper Type 2
TNBC	Triple-Negative Breast Cancer
TSA	Tumor Specific Antigen

ABSTRACT

Cancer is the second most common cause of mortality in the world. Several treatment modalities have been developed for cancer therapy. Recently, immune checkpoint (ICP) therapy has demonstrated promising results. However, low response rates, cancer recurrence and side effects are remaining problems. In this work, we aimed to develop formulations to enhance the effectiveness of ICP therapy which enables the patient's immune system to attack cancer cells and, consequently, requires an environment conductive to a targeted immune response against the cancer cells. To achieve this aim, we developed two types of nanoparticles (NPs) for combinatory chemo-photothermal therapy (PTT) to induce immunogenic cell death (ICD) and target the medication to the tumor site. ICD overall causes the activation of dendritic cells (DC) and T cells to initiate an antitumor immune response and is characterized by the presentation of damage associated molecular patterns (DAMPs). NPs were made from biocompatible polymers, poly(lactic acid)-b-poly(ethylene glycol) and bovine serum albumin. Both NPs were loaded with doxorubicin, a chemotherapeutic agent, and indocyanine green, a PTT agent that can absorb the light in near infrared (NIR) region and convert it to heat. NPs were characterized and confirmed to be suitable for agent delivery. Both types of NPs were shown to significantly reduce the viability of model cancer cells, MDA-MB-231 breast cancer cells and B16F10 melanoma cells, in vitro. Analysis of DAMP presentation after treatment demonstrated that NPs could induce ICD. Next, the potential of NP fabrication on a large scale was studied using a high throughput fiber reactor. Poly(lactic-

co-glycolic acid) was the polymer used in scale-up studies.

1. INTRODUCTION

Cancer is a known disease that is characterized by the uncontrolled growth and spread of abnormal cells. It can result in death if this uncontrollable spread is not stopped. Cancer is the second most common cause of mortality after heart disease. More than 1.8 million new cancer cases are expected to be diagnosed in 2020 worldwide.[4] It is estimated that cancer will cause 606,520 deaths in the U.S. in 2020, which means that about 1,660 patients will lose their battle against cancer per day.[4]

The financial costs of cancer are also high for both the patient and society. The Agency for Healthcare Research and Quality estimates that cancer-related direct medical costs, i.e., all health care expenditures, in the U.S. in 2015 were $80.2 billion.[4] Indirect cost (for example, the inability of the patient to work and earn) added, this disease leaves an enormous negative impact on the economy.[4]

Several cancer treatment methods, including surgery, chemotherapy, radiotherapy, and hyperthermia have been developed and are selected based on the type and stage of cancer. The most recent treatment which gained considerable attention and showed promising outcomes is immunotherapy. Despite the high degree of success that many of these treatments have been able to achieve, most of them are associated with multiple side effects. For instance, many cancer therapies can cause adverse cardiovascular events.[5] Specific cardiac side effects can occur during treatment with some of the immunotherapeutic agents.[6] A recent study showed that a small percentage of patients who were treated with immune checkpoint inhibitors as a class of immunotherapy developed inflammation of the heart muscle, a problem known as myocarditis. This adverse effect killed about 50% of the patients who developed it.[7] Sometimes side effects

may be more manageable if the administered dose of the drug is lowered. Another method to control the side effects is preventing the exposure of healthy cells of the body to the drug by targeting the drug to the tumor site, which can be achieved through nanomedicine.

Cancer recurrence and low response rates are other remaining problems in this field.[8] Several clinical studies on immunotherapy have proved that different patients exhibit different response rates. The percentage of cancer patients estimated to respond to immune checkpoint inhibitor drugs was 12.46% by 2018.[9] The most important leading cause of this problem is believed to be the immunosuppressive tumor microenvironment, which varies in different tumors and different patients.[10] Therefore, there is a great need for the development of a novel approach for the treatment of cancer that can alter the tumor microenvironment to make it more vulnerable against immunotherapeutic drugs while not causing severe side effects.

1.1. Overall Research Project

Rational combination of two or more methods can be considered as a solution that takes advantage of different mechanisms to kill cancer cells and decreases the probability of cancer recurrence. Furthermore, combined methods can work synergistically to improve the efficiency of treatment.[11]

The goal of this project is to develop a formulation for cancer treatment as a pretreatment for immune checkpoint (ICP) therapy. ICP therapy enables the patient's immune system to attack cancer cells and, as a consequence, requires an environment that is conducive to a targeted immune response against the cancer cells. In order to promote a tumor environment suitable for immunotherapy, we utilized a combination of chemotherapy and

photothermal therapy (PTT). Each of these therapeutic modalities has been proved to induce immunogenic cell death (ICD) independently.[12-13] ICD is accompanied by the release of tumor-specific antigens (TSAs) and damage-associated molecular patterns (DAMPs), namely calreticulin, adenosine triphosphate (ATP), and high mobility group box 1 (HMGB1). ICD overall causes the activation of dendritic cells (DC) and T cells.[2] As a consequence, the non-immunogenic microenvironment of the tumor changes into an immunogenic one, which is desirable for ICP therapy.

To accomplish this aim, two biodegradable nano-formulations were developed by utilizing FDA-approved materials to combine chemotherapeutic and PTT agents and deliver them to the tumor site. After studying the cytotoxicity of the formulations, their ability to induce ICD was investigated by identifying DAMP alteration after nanoparticle (NP)-mediated treatment of cancer cells *in vitro*. Figure 1.1 illustrates the overall concept of the project.

Further, the production of NPs on a larger scale was studied using a high throughput fiber reactor. The simplicity of the reactor reduces the need for multiple instrumentation, which makes it easy to meet good manufacturing practice (GMP) regulations and, consequently, decreases associated costs tremendously. A model polymer was used to thoroughly investigate the manufacturing method by identifying the affecting factors on product size and uniformity. The operational parameters were optimized to gain nanoparticles with a desired size and polydispersity index.

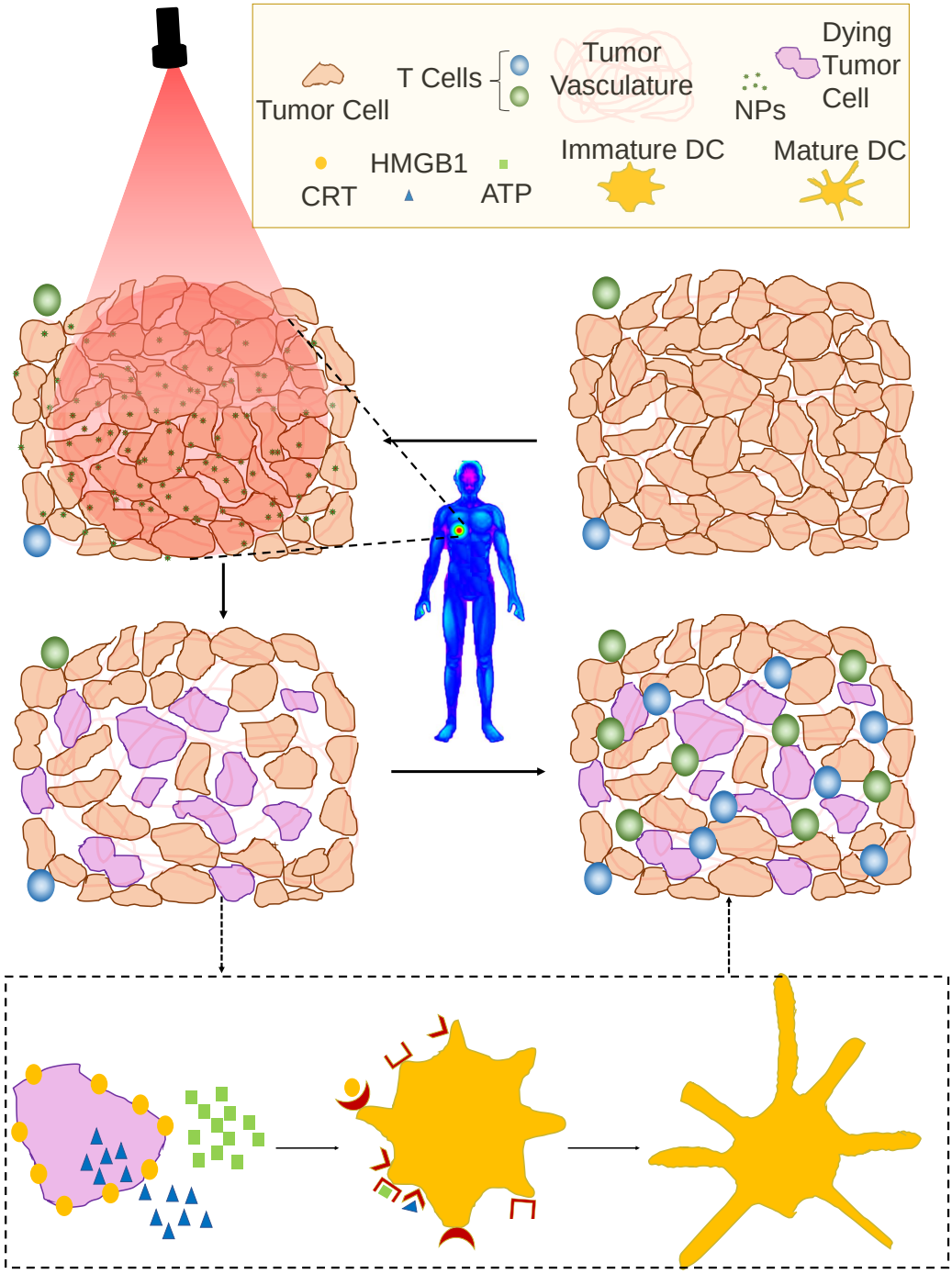

Figure 1.1. The overall concept of the project. NPs are targeted into the tumor site with a low presence of immune cells and irradiated by NIR laser. The PTT agent within the NPs changes the laser light energy to heat and elevate the tumor temperature. Accompanied by the chemotherapeutic agent, this effect undertakes cancer cells to immunogenic cell death (ICD), which is characterized by ATP secretion, HMGB1 release, and CRT surface exposure. As a consequence, not only some of the cancer cells are eradicated but also tumor becomes conductive to the immune cells

1.2. Specific Research Aims

The following specific aims have been addressed in this project

Aim 1: Design and synthesize NPs for synergistic chemo-photothermal therapy

The formulation of two types of NPs was accomplished: one made of poly(lactic acid)-*b*-poly(ethylene glycol) (PLA-PEG) and another made of bovine serum albumin (BSA) with an adjusted size and agent loading. Both formulations contain doxorubicin (Dox) as a chemotherapeutic agent and indocyanine green (ICG) as a PTT agent. PLA-PEG and BSA NPs are made through nanoprecipitation and desolvation/crosslinking, respectively. After confirming the reproducibility of both NP preparation methods, we determined the NP's PTT efficacy and the *in vitro* drug release pattern from the NPs.

Aim 2: Conduct *In-Vitro* studies to demonstrate the synergism of two approaches and ICD induction

We first investigated the viability of MDA-MB-231 metastatic breast cancer cells after treating them with PLA-PEG NPs and near-infrared (NIR) laser exposure. Then, we evaluated the potential for eliciting ICD through this treatment by the determination of levels of DAMPs.

Further studies were carried out with albumin NPs, which were used to treat B16F10 metastatic melanoma cells. The effect of NP concentration and their incubation time with cells on the cells' viability were determined. Quantification of DAMPs after NPs mediated laser irradiation allowed confirmation of the feasibility of ICD induction by this treatment.

Through this aim, we have demonstrated the potential of our NPs as effective formulations for cancer treatment, which can be combined with an ICP therapy for further *in vivo* studies.

Aim 3: Scale up the synthesis process using a high-throughput fiber reactor:

We produced polymeric NPs using a high-throughput fiber reactor and found the optimized conditions which result in higher efficiency and production of monodisperse NPs. By achieving this aim, we gained an understanding of the reactor's behavior. We can predict the products' properties based on the conditions at which the reactor is being operated. This knowledge can be applied to make NPs with a wide range of polymers, including poly(lactic-co-glycolic acid) (PLGA), PLA-PEG and bovine serum albumin (BSA) with controllable size and efficiency of the agent loading through a continuous process.

1.3. Project Outline

Relevant background on ICD, PTT, and nanomedicine is provided in chapter 2. Chapter 3 describes the preparation of PLA-PEG polymer and NPs that are loaded with therapeutic agents and their characterization. PTT ability of the PLA-PEG NPs, *in vitro* drug release from the NPs, NP cytotoxicity against MDA-MB-231 cells, and DAMP presentation in treated cells are explained in chapter 3. In chapter 4, preparation, characterization, and size optimization of BSA NPs are described. PTT efficiency and *in vitro* drug release, *in vitro* viability of the B16F10 cells treated with NPs/laser, and molecular determination of ICD in B16F10 cells are also described in chapter 4. In chapter 5, fiber reactor set up, and optimization is described. Finally, chapter 6 provides a conclusion and summary of our

findings along with the future perspective of this project and related projects which are suggested to be performed in the future.

2. BACKGROUND

2.1. Immune Checkpoint Therapy

James P. Allison and Tasuku Honjo won the Nobel Prize of medicine in 2018 for the discovery of cancer therapy by inhibition of negative immune regulation.[14] Amongst different types of immunotherapy, immune checkpoint (ICP) therapy has gained the most successful outcomes in the treatment of metastatic cancers. The idea behind ICP focuses on interfering with immune checkpoints, which cancer cells use to avoid being recognized by the immune system.[8] For example, the PD-1 checkpoint protein on T cells is activated when it binds to PD-L1, a protein that is overexpressed on cancer cells. Since PD-1 acts as an "off switch" to prevent the immune system from attacking native tissues, its activation by the cancer cells helps them evade the immune system.[8] In ICP therapy, antibodies that target PD-1 or PD-L1 can prevent the binding of these proteins, thereby preventing immune system avoidance by the cancer cells. Figure 2.1 shows the molecular mechanism of ICP therapy.[8]

While ICP therapy has shown significant promise, low response rate, and the potential for high toxicity are the two main drawbacks of this approach.[15] The reason for low response rates is believed to be the non-immunogenic environment of the tumor, which contains numerous factors that help to evade immune system activation and attack.[10] For instance, upregulation of adhesion molecules like ICAM-1/2, VCAM-1, and CD34 prevents T cells from infiltrating the tumor. Moreover, alteration of tumor cells' major histocompatibility complex (MHC) Class I, tumor antigenic peptide complexes and antigen presentation biomolecules lead to T-cell recognition evasion. Production and secretion of numerous

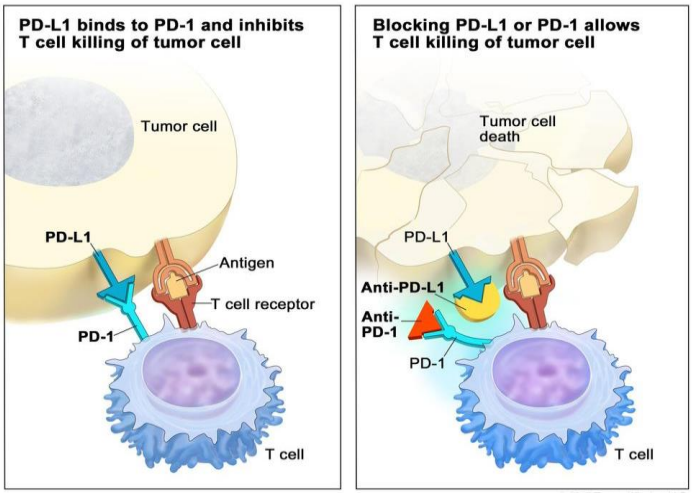

Figure 2.1. Illustration of ICP therapy. Reprinted from National Cancer Institute.[1]

immunosuppressive factors to the microenvironment like gangliosides is one of the most important means that tumors utilize to downplay T-cell function or induce T-cell apoptosis. Overexpression of anti-apoptotic proteins such as Bcl-2 and Bcl-xL is another mechanism for immune response suppression.[10] Because of this, a treatment such as the combinatorial NP-mediated photothermal therapy (PTT) and chemotherapy in this proposal that induces immunogenic cell death to alter the tumor environment and make it ready for ICP therapy is desired.

2.2. Immunogenic Cell Death (ICD)

Immunogenic cell death (ICD) is a form of cell death that can induce an anti-tumor immune response by activation of dendritic cells, thereby initiating a cascade process leading to an antigen-specific T-cell response.[2] ICD is characterized by the secretion or surface presentation of damage-associated molecular patterns (DAMPs), including calreticulin, high mobility group box 1 (HMGB1), adenosine triphosphate (ATP), and heat shock proteins.[16] Each molecule and its role in involving the immune system are briefly described:

2.2.1. Heat Shock Proteins (HSPs)

One of the most critical characteristics of cell death is that the presentation or translocation of specific proteins on the cell membrane.[17] Some of these proteins, such as phosphatidylserine, can initiate the phagocytosis of dying cells by antigen-presenting cells (APCs).[18] Such signals from the plasma membrane of dying cells are received by a specific set of receptors on APCs that, as a consequence, cause a further immunological response.[19]

Heat-shock proteins (HSPs) are molecular chaperones that are responsible for the correct folding or refolding of proteins when cells are under stress. Typically, they exist intracellularly. However, at least two of these molecules, HSP70 and HSP90, can be translocated to the cell surface and activate the immune system. Overexpression of HSPs in cancerous cells has been demonstrated, which can be the result of stress that is applied to the cells.[19] Although overexpression of HSPs within the cells has a cytoprotective effect and inhibits apoptosis, when they overexpress on the plasma membrane, they have different immunological functionality. HSPs that are located on the membrane of cells can bind to the specific receptors on APCs' surface.[20]

It has been shown that HSPs can enhance DCs maturation by binding to CD40 and CD86 receptors on the surface of the DCs.[21-22] HSP90 has also been demonstrated to upregulate CD91 on APCs, another factor that can lead to DC maturation.[23]

Moreover, HSP70 and HSP90 participate in presentation of tumor-derived peptide antigens on major histocompatibility complex (MHC) class I molecules, which leads to the activation of CD8+ T-cells that kill cancer cells, infected cells or other damaged cells. HSPs also stimulate the natural killer (NK) cells, which initiate an immune response to

the tumor formation.[24-25] Therefore, the presence of HSP70 and HSP90 on the cell surface is considered as a determinant of the immunogenicity of stressed or dying cells.

2.2.2. Calreticulin

Calreticulin is a protein that binds to Ca^{2+} ions. Calreticulin is mainly present in the endoplasmic reticulum (ER) lumen, participates in homeostasis of Ca^{2+}, and controls Ca^{2+} dependent cell signals.[26] It is also a chaperone molecule and interacts with several proteins.[27] Similar to HSPs, calreticulin also locates on the plasma membrane dying stressed cells.[28]

Calreticulin presence on the membrane of the cells determines the phagocytosis of dying tumor cells by macrophages and DCs. Although apoptotic cells that lack calreticulin on the surface can still die, phagocytes do not remove them efficiently.[17]

Studies show that translocation of calreticulin on the cell surface accounts for the initiation of an anti-tumor immune response both *in vitro* and *in vivo*. It interacts with various proteins such as thrombospondin, C1q, mannose-binding lectin (MBL), andthe internalization receptor CD91 on phagocytes like DCs, leading to DC activation and engulfment of dying cells.[29-32]

Tumor cells release several molecules into the extracellular matrix when they receive treatment and undergo cell death. These molecules can elicit an anti-tumor immune response. High mobility group box 1 (HMGB1) and adenosine triphosphate (ATP) are the two crucial ones that are discussed here.[19]

2.2.3. High Mobility Group Box 1 (HMGB1)

HMGB1 is a protein that binds to the cell's chromatin and affects nuclear functions like transcription.[33] The release of HMGB1 from the cells can induce an immune response. Both inflammatory cells and cancer cells that undergo necrosis can release HMGB1.[34-35]

Released HMGB1 interacts with the TLR4 receptor on DCs, which is responsible for controlling antigen presentation.[36] Besides, HMGB1 can play a role in stimulating TLR9, which leads to the production of interferon-α (INF-α).[36] Interacting a complex of HMGB1 and DNA with the RAGE receptor can also produce INF-α through the same process.[19, 37]

2.2.4. Adenosine Triphosphate (ATP)

Adenosine triphosphate (ATP) is a nucleotide that can be found in both intracellular and extracellular spaces. Inside the cells, ATP serves as the primary energy source for most cell functions. Extracellular ATP participates in cell signaling, the regulation of renal blood flow, vascular endothelium, and inflammatory responses. When released from damaged cells, ATP acts as a DAMP and informs the immune system of the presence of damaged tissue by binding to P2 purinergic receptors, which are classified as P2Y receptors (P2YR) and P2X receptors (P2XR).[38]

Cells release ATP to the extracellular matrix through plasma membrane channel pannexin 1 when they undergo apoptosis. Released ATP promotes phagocytosis via binding to the macrophages' P2Y2R.[39-40] Interaction of ATP with P2Y2R leads to the release of proallergic biomolecules like the eosinophil cationic protein , interleukin 8 (IL-8) and IL-33 and, as a consequence, induces a T helper type 2 (Th2) immune response against cancer cells.[41-42]

It has been demonstrated that the interaction of ATP with the P2X7 receptor can also cause tumor suppression. Several studies showed that released ATP binds to the P2X7 receptor on DCs and activates it. Then, inflammasomes are activated and result in IL-1β secretion and production of INF-γ by CD8+ T-cells. Ultimately, this chain of processes promotes the clearance of the tumor cells.[38, 43] Figure 2.2 illustrates the effect of ICD on the tumor microenvironment and the role of DAMPs in summary.

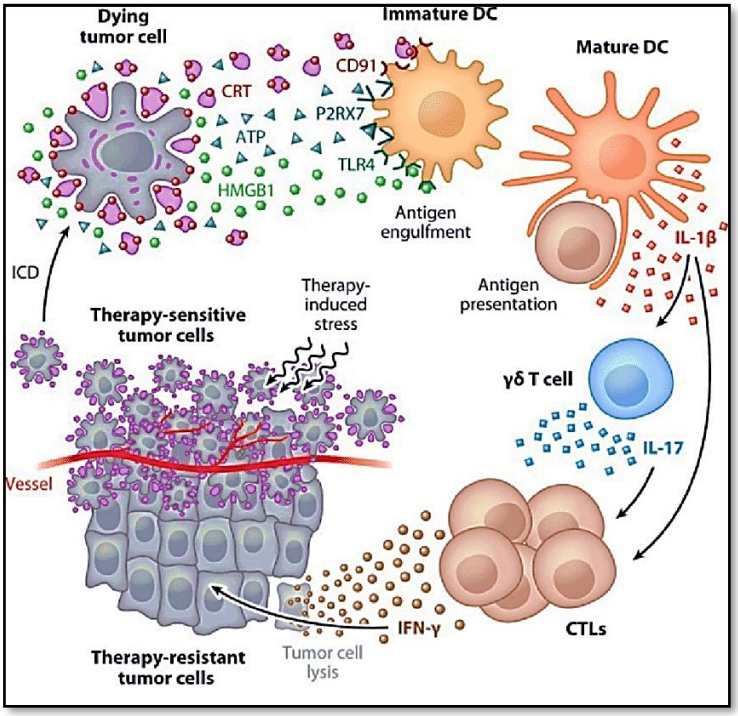

Figure 2.2. Effect of ICD on tumor microenvironment. Reprinted from Annual Reviews in Immunology by permission.[2]

Despite the effect of ICD, which pushes the immune system to destroy the cancer cells, in many cases, the immune response that ICD induces is not enough, and better results might be observed if ICP reinforces the ICD effect. In this work, we utilized NP-mediated combinatorial PTT/chemo to induce the presentation/release of DAMPS as a way to elicit ICD.

2.2.5. Induction of ICD

Temperature rise kills the cells through two different pathways. It might either directly damage the cell because of the applied heat or indirectly stimulate cell death when the heating is ceased. The first pathway is proportional to the amount of provided thermal energy. Tumor biology and microenvironment also affect the efficacy of this method. A promising fact is that because of specific biological features like lower heat-dissipating ability and lower interstitial pH, cancer cells are more susceptible to heat injury in comparison to healthy cells.[44] On the other hand, a chain of factors is involved in enabling the indirect cell death pathway, including apoptosis, microvascular damage, ischemia-reperfusion injury, altered cytokine expression, and alterations in the immune response.[44] Immune response changes through dendritic cell (DC) activation, delivery of tumor-specific antigens (TSA) to the lymph nodes, and activation of T cells with T cell receptors (TCR) specific to the TSA which leads to upregulating inhibitory surface receptors (PD-1 and CTLA-4) resulting in the attack of remaining tumor cells. Therefore, treatments such as PTT, which are based on temperature elevation, are being considered as a method to induce ICD.[45]

Similarly, anticancer therapy with the chemotherapeutic agent doxorubicin has been proved to relieve tumoral immune suppression in the tumor environment or stimulating anti-tumor adaptive immunity.[46] Doxorubicin shows cytotoxic activity by inhibiting DNA replication within cancer cells by intercalation into DNA and inhibition of topoisomerase II. However, its nonspecific action leads to severe side effects, especially in higher dosages.[47] Therefore, a combination of chemotherapy and PTT with moderate dosages can provide an immunogenic microenvironment that is susceptible to immune response.

However, inhibitory ligands on tumor cells would inhibit a full response. Including ICP therapy in the explained combination therapy to block the immune checkpoints allows for an uninhibited immune response. The final ternary treatment is expected to lead to tumor cell killing and immune memory.

2.3. Photothermal Therapy (PTT)

PTT is one treatment approach that has been proposed to induce ICD. PTT consists of the use of electromagnetic radiation of near-infrared (NIR) wavelengths for the treatment of cancer. An agent that absorbs the light in the NIR range is introduced into the body. This agent accumulates in the tumor site through the means which are later explained (Section 2.4). A laser irradiates the tumor site containing the PTT agent at the wavelength that it absorbs the most. By converting the laser energy to heat, the PTT agent increases the tumor temperature over 43 ºC, which is detrimental to cells.[48]

The irradiated light passes through the tissues as deep as a few centimeters in depth (3.4 cm in bovine tissue for 808 nm light at 1 mW/cm^2)[49] to reach the photothermal agent accumulated in the tumor. If other substances in this path, such as hemoglobin, water, etc. absorb the light, these not only decrease the treatment's efficacy by reducing the intensity of light that reaches the target agent but also results in off-target damage caused by heating that substance in noncancerous tissues. NIR wavelength is the most appropriate choice to address this issue since main tissue chromophores are transparent to light in the NIR window of ~ 650-950 nm.[50]

Nanoparticles (NPs) used for PTT purposes are classified into four major types.

1) Metallic NPs: Metallic NPs have a photothermal effect due to surface plasmon resonance (SPR). Plasmon absorption is efficiently converted to heat through electron-electron and electron-phonon relaxations. This rapid photothermal conversion can be harnessed for photothermal therapy through laser irradiation at a wavelength that overlaps the NPs SPR absorption. The ideal NPs for this purpose have an optimal size and a high absorption but low scattering. Optical properties of the parent metal, incident light, surrounding medium, NPs size, and shape affect the heat production of metallic NPs.[51] Gold nanoshells, gold nanorods, and other gold/silver nanostructures have been constructed to have their SPR in the NIR range and have been successfully utilized as PTT agents. AuroShell particle is a core-shell NPs with a silica core and gold shell that is being investigated in clinical trials.

2) Carbon Nanomaterials: Carbon nanomaterials have been extensively used in biomedical applications due to their biocompatibility. Graphite- based nanomaterials, including graphene oxide (GO), carbon nanotubes (CNTs), carbon nanohorns (CNHs), carbon dots (CDs), graphene dots (GDs), and fullerenes have been utilized for photothermal applications.[52] The π-plasmon absorbance background at the NIR range and low luminance make graphite-based nanomaterials a great candidate for photothermal applications. Vibration in carbon lattice due to the optical transitions and relaxations upon laser irradiation elevates the medium temperature. However, the toxicity of these materials limits their biomedical applications.[52]

3) Conductive polymer NPs: various conductive polymer nanoparticles have shown an excellent photothermal conversion effect in the NIR range. Polyaniline is the first conductive polymer that was reported to be utilized as a photothermal agent.[53]

Polypyrrole, and poly(3,4-ethylene dioxythiophene)-poly(styrene sulfonate) (PEDOT:PSS) polymers' maximum absorbance occur in NIR region which makes them potent for PTT.[53] Our group has utilized PEDOT NPs for PTT and reported promising *in-vitro* results.[54]

4) Dye Encapsulated NPs: Several organic dyes, especially the ones that absorb the NIR light wavelengths such as tetrapyrrole structures, cyanine dyes, squaraine derivatives, and boron-dipyrromethane (BODIPY) dyes have been enormously studied for various biomedical applications including imaging and photothermal therapy.[55] Figure 2.3 Shows the chemical structure of a representative dye from each group.

Tetrapyrrole Structures: Tetrapyrrole dyes usually have two distinct absorption bands. The main absorbance peak appears at around 400 nm. In comparison, a minor absorption band exists at longer absorption wavelengths around 600 nm, which is named Q-band and offers photothermal properties to the dye. Tetrapyrrole dyes also have interesting

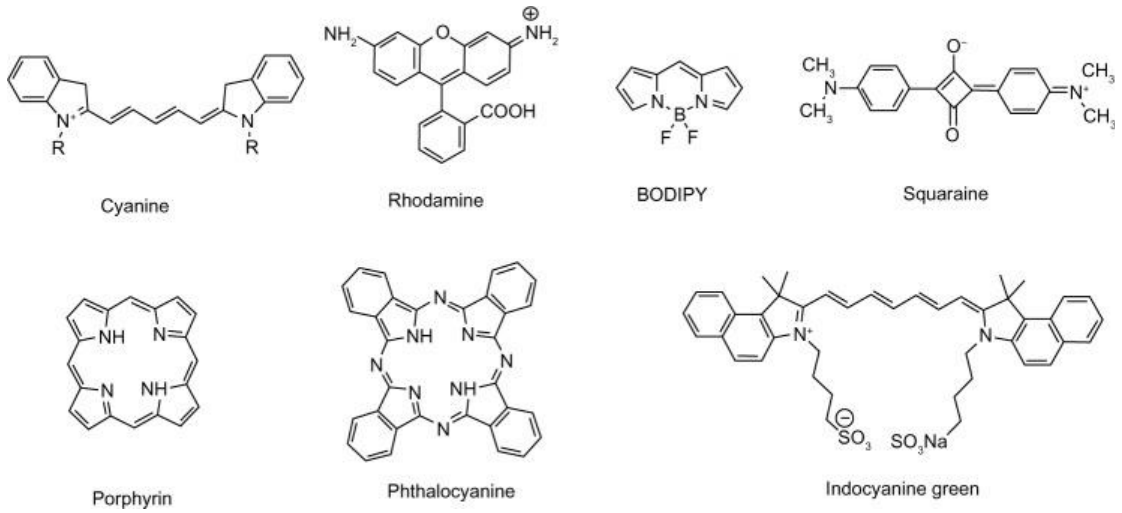

Figure 2.3. Chemical structure of cyanine, rhodamine, BODIPY, Squaraine, Porphyrin, Phthalocyanine and indocyanine green (ICG). Reprinted from Dove Medical Press under CC BY 3.0 License.[3]

chemical properties that allow them to form a complex with transition metals that are

required for magnetic resonance imaging. Natural examples of tetrapyrrole structure include some colored biomolecules such as chlorophyll, heme, and bacteriochlorophyll. Porphyrin and phthalocyanine derivatives are other common examples that have been frequently used for photothermal applications. However, due to the presence of the four phenyl groups or four naphthyl groups in their chemical structure they highly tend to aggregate in aqueous environments which leads to low solubility and decreases their bioavailability.[55]

Cyanine Dyes: Cyanine dyes are small organic molecules that generally exhibit trans geometry. Most of the cyanine dyes absorb light at the NIR region. They have shown a high molar extinction coefficient and high fluorescence quantum yields, which makes them potent candidates for bioimaging, photodynamic therapy, and photothermal therapy.[55] A well-known example of these dyes is indocyanine green (ICG) that has been approved by the U.S. Food and Drug Administration (FDA) for biological imaging.[56] However, their application is limited by their low photostability, uncontrolled aggregation in physiological fluids and high rate of binding to the proteins in the human serum.[56]

Squaraine Derivatives: The main feature of squaraine dyes is their high absorbance at 650 nm-700 nm and sharp fluorescent emission peak in the NIR region. This unique optical property can be utilized for imaging and PTT. However, poor water solubility resulting from their hydrophobic π-conjugated planar structures hinders their functionality in physiological environments.[55]

BODIPY Dyes: BODIPY dyes are good candidates for use in PTT owing to their unique properties, such as high thermal and photostability, high molar extinction coefficient and

high fluorescence quantum yields. However, most BODIPY derivatives' maximum absorbance occurs at the short wavelengths in the visible range. Furthermore, their hydrophobicity reduces their bioavailability. Aza-BODIPY is a modified structure that can be obtained by replacing the carbon atom at the meso position with a nitrogen atom in the chemical structure of BODIPY. This modification leads to the bandgap reduction and shift the spectral bands to the right to the NIR region. Our group has utilized aza-BODIPY entrapped within polymeric NPs for NIR imaging.[55]

According to the previous paragraphs, most of the organic dyes are hydrophobic and can be eliminated readily from the body since they are small molecules. Some of them absorb the light at the visible wavelengths. Two main strategies have been utilized to address these problems. Chemical modification of the dye and introduction of hydrophilic functional groups increases the solubility of the organic dye. However, the delivery of the dye to the tumor site remains unsolved. Encapsulation of the dye within water dispensable NPs is another well-known strategy to increase the organic dye stability. NPs can also deliver the dye to the tumor sites via either passive or active targeting. Moreover, NPs facilitate the combination of two therapeutic agents. For example, two organic dyes, one dye, and either one of the photothermal materials discussed earlier can be loaded within the NPs to reinforce the PTT effect of the NPs. Moreover, PTT can be combined with other treatment modalities such as photodynamic therapy, chemotherapy, or imaging by co-loading the agents within the NPs.

2.4. Nanomedicine

PTT and chemotherapeutic agents can be either injected directly into the tumor site or be targeted through active or passive targeting by encapsulation of the agents in NPs.

Briefly, in passive targeting, NPs that are smaller than 200 nm can penetrate the tumor area, taking advantage of disorganized angiogenic vasculature of the tumor in which, in contrast to normal vessels, epithelial cells are not well aligned and provide wide fenestrations (enhanced permeation).[57] Furthermore, due to the lack of lymphatic drainage, the particle's retention time in the tumor increases compared to healthy tissues (enhanced retention). The combination of these effects is known as enhanced permeability and retention (EPR) effect.[57-58] Figure 2.4 illustrates the EPR effect.

In active targeting, particles are typically functionalized by targeting ligands such as a small molecule like folic acid or a macromolecule like an antibody, which has a great affinity to highly expressed receptors on cancer cells. The affinity that this ligand provides the targeted NP results in more significant accumulation of these particles at tumor sites than other tissues.[58-59] The use of NPs as carriers for therapeutic and imaging agents brings about other advantages such as their favorable potential to increase

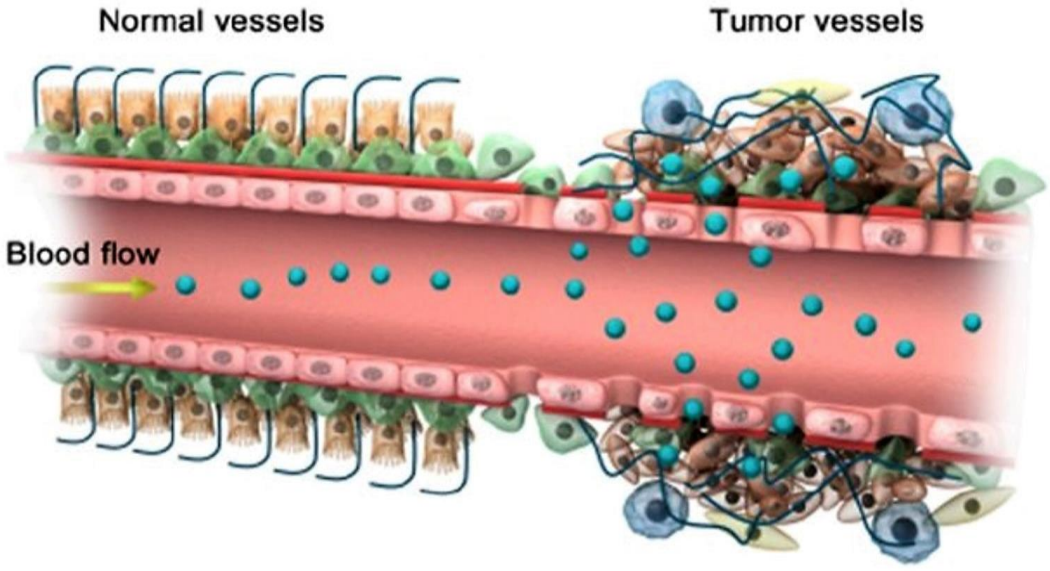

Figure 2.4. Enhanced permeability and retention effect. Reprinted from Ivyspring International Publisher.[2]

solubility and stability of the loading agent, control its release profiles, enhance their accumulation in tumor site and thereby reduce its toxicity, and reduce drug resistancess.

Different types of NPs, such as solid lipid, ceramic, magnetic, and polymeric NPs, have been developed for the delivery of therapeutic agents. Polymeric NPs can be made from either synthetic or natural polymers. In this work, two types of polymeric NP formulations will be made from poly(D,L-lactic acid)-*b*-poly(ethylene glycol) (PLA-PEG) and albumin.

PLA-PEG NPs have been extensively investigated for their potential as controlled and targeted drug carriers over the last decades due to the biocompatibility, biodegradability, and low toxicity of the polymer. This synthetic diblock copolymer contains a hydrophobic (PLA) block and a hydrophilic (PEG) block. The hydrophilic block act as a stabilizer in the physiological environment, and the hydrophobic block is responsible for hydrophobic secondary interactions to form the NP and hold hydrophobic agents. By adjusting the ratio of these two blocks, we can control the size, zeta potential, stability, and degradability of the NPs, which is a fascinating aspect in the field of drug delivery.[60]

Albumin is an attractive natural polymer that can be considered as another ideal candidate to make NPs due to its biodegradability, low toxicity, nontoxic degradation products, non-immunogenic, ease of purification, and water solubility. Albumin is the most abundant plasma protein (35–50 g/L in human serum). Another interesting feature of albumin is the presence of functional groups, which make it possible to bind desired ligands or even drugs to the NPs and cross-link it into an insoluble polymer network.[61]

Both PLA-PEG and albumin biopolymers have been utilized as carriers for the delivery of various therapeutic agents, including photothermal therapeutic and chemotherapeutic agents, and have shown stunning results. In 2007, South Korea approved Genoxol-PM for breast, lung, and ovarian cancer treatment. Genexol-PM is a paclitaxel formulation based on PLA-PEG. Genoxol-PM and several other formulations based on PLA-PEG NPs are under clinical development in the United States. FDA-approved formulations of albumins NPs like Abraxane are evidence for the use of this protein as a suitable material for a drug carrier.[62]

2.5. Large Scale Production of NPs

Several methods have been established for producing polymeric NPs like emulsion-diffusion methods, emulsion-evaporation, desolvation, and precipitation by salting-out.[63] However, the best process to make NPs out of diblock polymers regarding ease and efficacy is nanoprecipitation. Desolvation is another method that is mostly used for charged polymers like proteins. Although the two methods have different molecular mechanisms, their processes are very similar.

1) Nanoprecipitation: The polymer is first dissolved in a water-miscible organic solvent. An aqueous solution containing a stabilizer is introduced to the polymer solution. Reduction of the interfacial tension between the aqueous and organic phase leads to the diffusion of the organic solvent into the aqueous phase, which leads to polymer deposition and NP formation in the interface of the two phases.[64]

2) Desolvation: In this method, the ionic strength of the solution is changed via altering the charge or pH by the homogeneous dispersion of the desolvating agent like ethanol or concentrated organic salt solution in the protein or charged polymer solution. Further, the

formed NPs are hardened by the addition of the cross-linking agent such as glutaraldehyde or 1-Ethyl-3-(3-Dimethylaminopropyl) carbodiimide (EDC).[61, 64]

Some studies have been done to scale these processes up using different types of reactors such as impinging jets, single turbulent jets, rotor-stator mixers, static mixers stirred tank centrifugal pumps, turbulent pipes, and the method that our group has proposed which involves the use of high throughput fiber reactor.[65-69]

A "high throughput fiber reactor" (Figure 2.5) consists of a tube that is packed with a plurality of hydrophilic fibers oriented along its axis.[69-72] A constrained phase is fed to the reactor from the top and wets the fibers and provides a high surface area for this phase. The so-called free phase is then fed through a downstream input port and meets the constrained phase at its very thin layer formed on the fibers. Through this contact, nanoprecipitation occurs and produces NPs that exit the reactor output stream from the bottom.

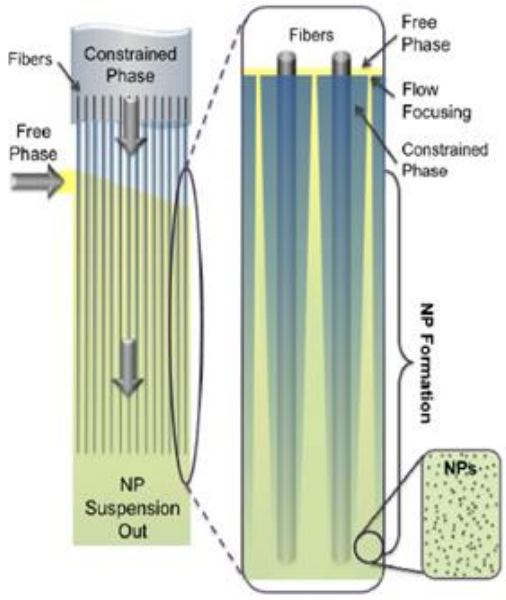

Figure 2.5. Schematic of a high-throughput fiber reactor.

3. *IN VITRO* DETERMINATION OF IMMUNOGENIC CELL DEATH IN METASTATIC BREAST CANCER CELLS INDUCED BY POLY(LACTIC ACID)-*b*-POLY(ETHYLENE GLYCOL) NANOPARTICLES CARRYING INDOCYANINE GREEN AND DOXORUBICIN

3.1. Introduction

The main aim that we followed in this chapter was to develop an anticancer nanomedicine with the least possible side effects on the healthy cells. Furthermore, we desired our nanomedicine to induce the tumor to communicate with the immune system for the purpose of further antitumoral effect. The ideal nanomedicine would be biocompatible and biodegradable to avoid unfavorable immunogenicity.

Poly(lactic acid)-*b*-poly(ethylene glycol) (PLA-PEG) is one of the most prominent amphiphilic copolymers that is utilized in biomedical applications.[73] PLA is a biodegradable polyester that is approved by the FDA for clinical usage.[73] PLA block constructs the hydrophobic portion of the copolymer, which can form the core of the micelles or NPs when the copolymer is put in the presence of the water through strong hydrophobic interactions. The hydrophilic portion, PEG, is exposed to the aqueous environment and stabilizes the micelles or NPs. Hydrophobic interaction of the PLA portion of the NPs with hydrophobic drugs enables drug entrapment within the NPs for controlled drug delivery. PLA has been copolymerized with other hydrophilic agents, including poly(2-methacryloyloxyethyl phosphorylcholine) (PMPC), poly(ethylene oxide) (PEO), and poly(N-isopropyl acrylamide) (PNIPAAm), to form amphiphilic block copolymers and further self-assemble into micelles in several studies.[73] However, among them, PEG is the most popular hydrophilic polymer in biomedicine owing to its unique characteristics such as linearity, lack of charge, low immunogenicity, low polydispersity,

and ease of copolymerization. PLA-PEG NPs have been extensively used in nanomedicine owing to the excellent physicochemical and biological properties, including nontoxicity, delayed protein adsorption, and weak uptake by the reticuloendothelial system (RES).[73]

Accounting for 15% of all cancer deaths in females in the U.S., breast cancer has remained among the top two causes of cancer mortality in women.[74] Breast cancer patients routinely have the expression of estrogen receptor (ER), progesterone receptor (PR), and amplification of HER-2/Neu evaluated. Breast cancer tumors are classified into three groups based on the expression of these markers: 1) hormone receptor-positive tumors, 2) HER-2/Neu amplified tumors, and 3) triple-negative breast cancer (TNBC) cells that do not express ER, PR and do not have HER-2/Neu amplification. The third group is very aggressive and is known as the most devastating form of breast cancer. The patients diagnosed with TNBC typically have poor outcomes. A high risk of early metastasis is expected for the patients that are diagnosed with TNBC. This type of cancer does not respond to the hormone therapeutic agents such as tamoxifen and aromatase inhibitors because it lacks ER and PR. They are also unlikely to respond to HER2-targeted formulations. Therefore, other methods of treatments such as chemotherapy and PTT must be considered to treat this class of tumors.[74-75]

The MDA-MB-231 cell line is a metastatic breast cancer cell line that is negative for ER, PR and E-cadherin, expresses mutated p53, and lacks the HER-2 receptor. Therefore, it is representative of a TNBC cell line. This cell line is commonly used to model the late-stage breast cancer.[74]

In this chapter, we report the preparation of PLA-PEG NPs containing Indocyanine green (ICG)- an NIR organic dye with photothermal capabilities- and Doxorubicin (Dox) –a chemotherapeutic agent which has been reported to induce ICD [46]– through nanoprecipitation of poly(lactic acid)-b-methoxy poly(ethylene glycol) (PLA-b-mPEG), a polymer that is well known to be biodegradable and biocompatible .[60] These NPs were evaluated as agents for dual PTT and chemotherapy to eradicate MDA-MB-231 cells. Also, our studies investigated whether the NP-mediated combination therapy induced ICD *in vitro* through the evaluation of the DAMP presentation by the treated cancer cells.

3.2. Materials and Methods

3.2.1. Materials

Heterofunctional poly(ethylene glycol) methyl ether (OH-PEG-OCH_3, Mn 5 kDa) and bovine serum albumin (BSA) were acquired from Sigma-Aldrich. Tin(II) 2-ethylhexanoate (stannous octoate, $Sn(Oct)_2$), doxorubicin hydrochloride (Dox), and thiazolyl blue tetrazolium bromide (MTT) were obtained from Alfa Aesar (Ward Hill, MA). Indocyanine green (ICG) was obtained from MP Biomedicals (Irvine, CA). ATP Determination Kit was obtained from Invitrogen (Carlsbad, CA). Rabbit anti-calreticulin antibody (ab2907) and rabbit anti-HMGB1 antibody (ab79823) were purchased from Abcam (Cambridge, UK). Goat anti-rabbit IgG (H&L) DyLight 488 conjugate was obtained from ImmunoReagents, Inc. (Raleigh, NC). 4′,6-Diamidine-2′-phenylindole (DAPI) dihydrochloride was purchased from EMD Millipore Corporation (Burlington, MA). 10x phosphate buffer saline (PBS) was received from SeraCare (Milford, MA). Ultrapure deionized water was obtained from a Millipore Direct Q system. All of the other solvents used were ACS grade.

3.2.2. Polymer Synthesis

D,L-Lactide was dissolved in ethyl acetate at 70°C and cooled down to room temperature to recrystallize. These unimers were freeze dried to remove any remaining solvent prior to use. PLA-mPEG was synthesized through ring opening copolymerization (ROP) of D,L-lactide with methoxy-PEG (mPEG) (Mw = 5,000 g/mol) in toluene using stannous octoate ($Sn(Oct)_2$) as a catalyst at 110 ºC for 24 h under an Ar atmosphere, as shown in Figure 3.1.[76] The product was then dissolved in acetone, and the copolymer was precipitated by adding cold (kept at -86°C) ethyl ether and separated through 10 min of 9,798 x g centrifugation at 4°C (Avanti J-26 XPI, Beckman Coulter, US). The purification process was repeated three times and the product was lyophilized and kept at -25°C for further use.

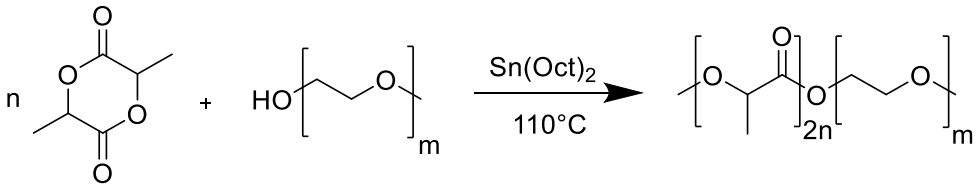

Figure 3.1. Ring opening copolymerization of poly(lactic acid)-b-poly(ethylene glycol) (PLA-mPEG) in the presence of $Sn(Oct)_2$ as a catalyst.

3.2.3. Polymer Characterization

The copolymer was characterized by ^1H NMR spectroscopy using a Bruker Avance III 400 Hz spectrometer to confirm the copolymer synthesis and estimate the molecular weight. Molecular weight was also estimated using a Viskotek gel permeation chromatography (GPC) system with a Viskotek 270 dual detector (Right-Angle Light Scattering (RALS) and Low-Angle Light Scattering (LALS)). The estimated molecular weight was determined relative to polystyrene standards (PS) with molecular weights of

5,200, 13,000 and 30,000 g/mol prepared in HPLC-grade $CHCl_3$ (5 mg/mL). The mobile phase was HPLC-grade chloroform with a flow rate of 1 mL/min. The samples were injected through a solvent delivery system (VE 1122) into a Malvern T3000 GPC/SEC column.

3.2.4. NP Preparation

PLA-mPEG NPs were made through nanoprecipitation. Briefly, 100 µL of an organic phase containing PLA-mPEG (15 mg/mL), ICG (1 mg/mL) and Dox (1.6 mg/mL) in a mixture of acetone and DMSO (ratio 3:2) was added dropwise to 2 mL ultrapure water while stirring at 960 rpm. NPs were separated from unloaded Dox and ICG through one-hour centrifugation at 74,200 x g (Avanti J-26 XPI, Beckman Coulter, US). NPs were then resuspended in water and characterized. Blank NPs were made with the same method except that the organic phase did not contain ICG or Dox. For confirmation of reproducibility of NP preparation, independent NP batches were made and characterized

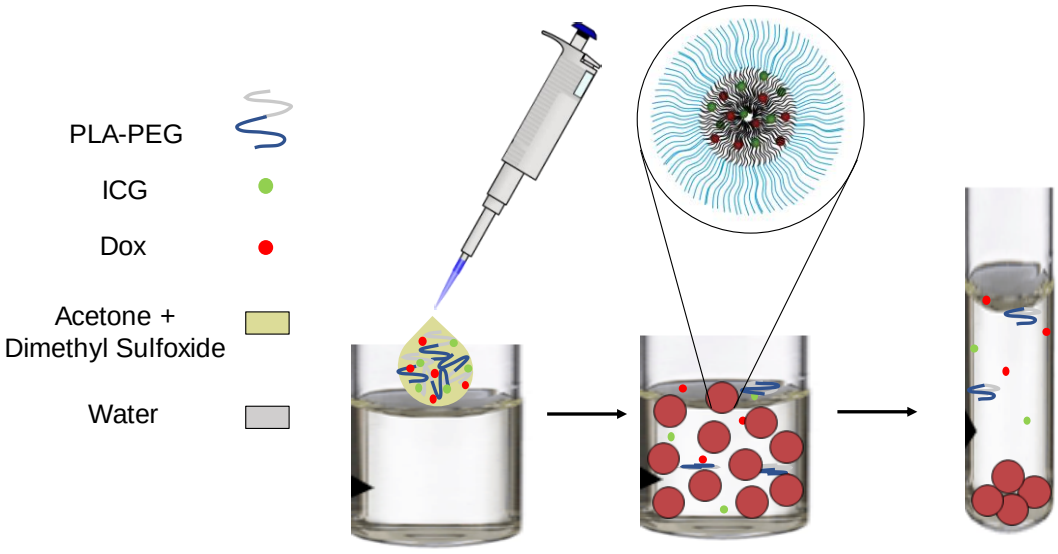

Figure 3.2. NP preparation through nanoprecipitation.

over a period of several months. Figure 3.2 Shows a schematic of the nanoprecipitation method.

3.2.5. NP Characterization

NPs were characterized by dynamic light scattering (DLS) to measure their hydrodynamic size and electrophoretic light scattering to determine their zeta potential using a Malvern ZetaSizer Nano ZS instrument. For measurement of hydrodynamic size, NPs were suspended in water. Zeta potential measurements were carried out in 1 mM KCl. The stability of NPs in complete cell media (described below) at 37 °C was investigated by tracking NP size variation over a period of 72 h.

The morphology of dried NPs was investigated by scanning electron microscopy (SEM) using an FEI Helios NanoLab 400 microscope after coating them with a 2-nm layer of iridium by coating with an Electron Microscopy Sciences EMS150T ES sputter coater.

Drug loading (DL%) was calculated using Equation 1 in which the mass of loaded agents (ICG or Dox) was determined by UV-vis spectroscopy using a Biotek H4 multimode plate reader (λ_{Abs}= 476 nm for Dox and λ_{Abs}=798 nm for ICG). The total mass of NPs was measured by scale after lyophilization.

$$DL\% = 100 \times \frac{Mass\ of\ agent\ in\ NPs}{Total\ mass\ of\ NPs} \qquad \text{Equation 1}$$

3.2.6. NP Degradation

To investigate the degradability of the polymeric NPs, gel permeation chromatography was used to compare the polymer's molecular weight distribution before and after degradation. Blank NPs were made as described earlier, resuspended in phosphate

buffered saline (PBS, pH 7.4) and incubated at 37°C for 30 days. The suspension was then lyophilized and dissolved in HPLC grade chloroform. The resulting mixture was then filtered through Whatman filter paper, 0.2 µm syringe filter and 20 nm syringe filter prior to analysis by GPC.

3.2.7. Agent Release

The *in vitro* drug release behavior of the NPs was studied for 30 days. Release studies were performed by placing 150 µL of 13.3 mg/mL suspension of the NPs in release buffer in a dialysis tube (D-Tube^{TM} Dialyzer Mini, MWCO 6-8 kDa) and immersing these tubes in 4 mL of PBS solution (pH 7.4) containing 5 mg/mL bovine serum albumin (BSA) at 37° C. BSA was included in the release buffer to enhance the stability of ICG in aqueous environment and enable reliable measurement of the concentration of this agent. 100 µL samples were taken from the 4-mL dialysate at predetermined time intervals to determine the concentration of ICG and Dox released by UV-Vis absorption spectroscopy. The volume of the dialysate was maintained through the study by immediately replacing the volume taken with fresh release buffer.

3.2.8. PTT Conversion

NPs were irradiated by an 808-nm laser diode (RLCO-808-1000G, 9 mm; Roithner Lasertechnik GmbH, Wien, Austria) for 10 min at room temperature. An indium antimonide infrared (IR) camera (FLIR Systems, Inc., Wilsonville, OR, USA) was used to measure the temperature change of the samples. The samples were irradiated at an irradiance of 0.3 W/cm^2 (laser power = 84.8 mW, spot diameter = 6 mm). All of the measurements were conducted in 96-well plates with 100 µL of sample. The

concentration of NPs in suspension in complete cell media was 0.3 mg/mL and complete cell media (described below) was used as the control.

3.2.9. Cell Culture

Human mammary adenocarcinoma MDA-MB-231 cells were obtained from the American Type Culture Collection (ATCC) and cultured in complete cell media consisting of Dulbecco's Modified Eagle's Medium (DMEM) without phenol red (Gibco, MD, USA) supplemented with 10% heat inactivated fetal bovine serum (FBS, RMBIO), 1% penicillin/streptomycin (VWR) and 1% 4-(2-hydroxyethyl)-1-piperazineethanesulfonic acid (HEPES, HyClone) in a humidified atmosphere containing 5% CO_2 and 95% air at 37°C.

Laser irradiation of cells was conducted inside a custom-made incubator to simulate physiological temperature, as previously described.[54] In this incubator, temperature was maintained at 37 °C using filament bulbs wired to a STC-1000 probe temperature controller.

3.2.10. NP-Mediated Growth Inhibition Induced by Chemotherapy and PTT

Cells were seeded at a density of 5,000 cells/well in 96 well plates. 24 h later, when cells were attached to the wells, their media was replaced with the following treatments.

a) To study the effect of NP concentration, suspensions of NPs in complete cell media with concentrations ranging from 0.0 to 1.0 mg/mL were added to the cells. After 1.5 h incubation of cells with NPs at 37°C, cells were treated with laser (0.3 W/cm^2, laser power = 118 mW, spot diameter = 7 mm) for 3 min.

b) To investigate the effect of laser irradiation time, the same procedure was followed,

except that the concentration of NPs was set to 0.3 mg/mL and the irradiation time was varied from 0-9 min with a step size of 3 min.

c) To determine the effect of combination therapy, cells were treated with 0.3 mg/mL of NPs or with the equivalent concentration of Dox (12.7 µg/mL = 23 µM), ICG (8.1 µg/mL = 10 µM) or blank NPs (0.3 mg/mL, no ICG or Dox). The first group of the cells was irradiated with laser for 3 min after 1.5 h incubation at 37°C, while the second group was left without laser exposure.

For all three studies, the MTT viability assay was performed after 48 h of incubation post laser irradiation at 37°C. Only viable cells can metabolize MTT reagent using mitochondrial reductase and convert it to formazan crystals which are soluble in DMSO. Formazan concentration, which is proportional to number of viable cells, can be further calculated by UV-Vis spectroscopy. 10 µL solution of 5 mg/mL MTT reagent in media was added to all the cells. Controls included cells that did not receive any treatment (NT) as well as cells that were treated with methanol for 15 min prior to viability assessment. After 2 h of incubation of the cells with the MTT reagent at 37°C, the media was replaced with 200 µL DMSO and plates were shaken for 15 min to allow proper dissolution of formazan crystals. The optical density of the solutions at 555 nm and 900 nm were measured with a Biotek H4 multimode plate reader.

3.2.11. Study of Damage Associated Molecular Patterns (DAMPs)

MDA-MB-231 cells were seeded in 96-well plates at a cell density of 5,000 cells/well. After 24 h, media was replaced with a suspension of NPs (loaded with Dox and ICG) in media with a concentration of 0.3 mg/mL, or with an ICG solution or Dox solution in media with equivalent concentration as in the NP suspension (23 µM Dox or 10 µM

ICG). As a control, one group of cells was not treated (NT). Wells containing PTT agent (ICG or NPs) were irradiated with laser (0.3 W/cm^2) for 3 min after 1.5 h incubation at 37°C. Cells were returned to the incubator after laser treatment. After 30 min, 24 h, 48 h and 72 h, the level of DAMPs were determined as described below.

3.2.11.1 ATP Release to Extracellular Fluid

The ATP Determination Kit (Invitrogen) was used to determine ATP release from the cells. The determination method is based on catalytic reaction of D-luciferin with ATP in presence of firefly luciferase and formation of luminescent oxyluciferin. Thus, the luminescent intensity of the reaction's product is proportional to the ATP concentration. The reagent was prepared per manufacturer recommendations and mixed with the cells' media (reagent: supernatant volume ratio of 1:10). The luminescence of the solutions (peak at 560 nm) was then read with a Biotek H4 multimode plate reader using a 384-well plate.

3.2.11.2. Calreticulin Determination

Immunocytofluorescence was used to determine the level of calreticulin (CRT) exposed on the cells' surface. Briefly, cells were fixed with 100 µL 4% (v/v) formaldehyde for 20 min. Then, 100 µL BSA (1% w/v) was added to block nonspecific absorption. BSA solution was discarded after 30 min, and the cells were incubated with 50 µL rabbit polyclonal anti-CRT antibody (Abcam ab2907, 1:75 dilution in 0.1% w/v BSA) for one hour followed by one-hour incubation with 50 µL of goat anti-rabbit IgG DyLight 488 conjugate (1:1000 dilution in 0.1% w/v BSA) in the dark at room temperature. Cells were then incubated with 1 µg/mL DAPI for 5 min with the purpose of staining cell nuclei for cell count. Multiple images were taken with an EVOS FL microscope and analyzed by

ImageJ to determine the relative fluorescence and number of cells in each image. The relative fluorescence per cell was further calculated for each image.

3.2.11.3. HMGB1 Release Determination

HMGB1 release was determined indirectly by observing the extent of HMGB1 left within the cells via immunocytofluorescence. Briefly, cells were fixed with 4% v/v formaldehyde for 20 min, permeabilized with 0.2% v/v Triton X-100, blocked with 1% BSA for 30 min, incubated for one-hour with rabbit anti-HMGB1 antibody (Abcam ab79823, 1:250 dilution in 0.1% w/v BSA), and finally incubated for one hour with goat anti-rabbit IgG Dylight 488 conjugate (1:1000 dilution in 0.1% w/v BSA). Cells were then stained with 1 µg/mL DAPI and fluorescent images were taken and analyzed with the same method as for CRT.

3.2.12. Statistical Analysis

The experiments were performed in at least triplicate ($n \geq 3$) and the data was reported as the means ± standard deviation (SD). Student t-Test was used for identifying statistical differences between group means.

3.3. Results and Discussion

3.3.1. Polymer Preparation

The PLA-mPEG block copolymer was synthesized through ROP of D,L-lactide, as described in Figure 3.1, and purified to separate unreacted D,L-lactide and PEG. Figure 3.3 shows the ^{1}H NMR spectrum of the copolymer in D-chloroform.

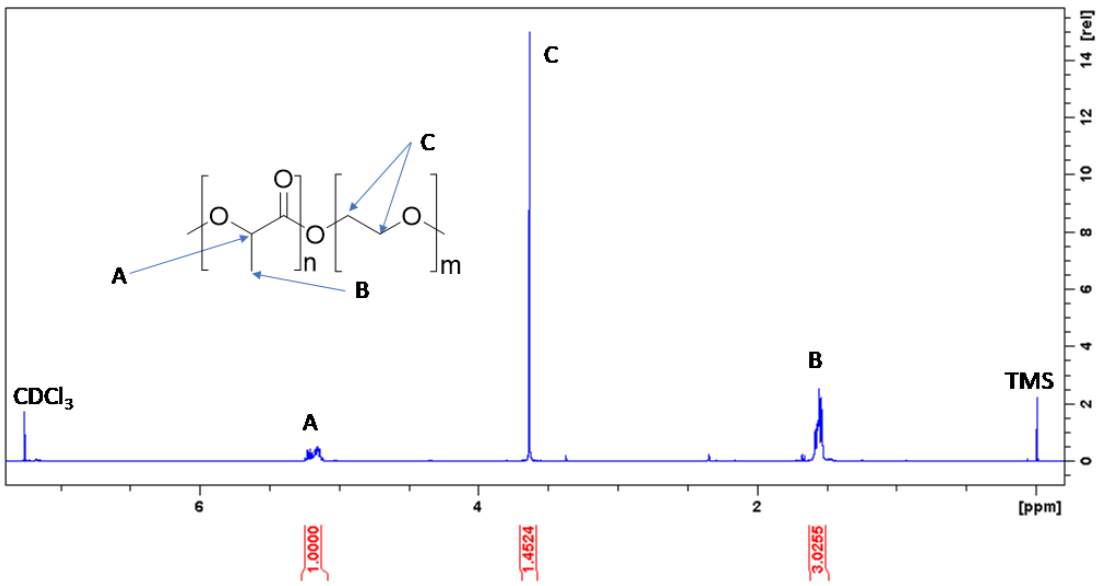

Figure 3.3. NMR Spectrum of poly(lactic acid)-b-poly(ethylene glycol) dissolved in $CDCl_3$.

Peak A at 5.2 ppm belongs to methine proton and peak B at 1.6 ppm to the methyl protons (3 protons) of lactide. Peak C at 3.7 ppm is assigned to the 4 methylene protons in the PEG block.[76-77] The presence of both blocks in the copolymer confirms successful synthesis. Integration of each peak is proportional to the number of protons associated with them in the copolymer. Knowing the Mw of mPEG (5000 g/mol), the M_w of the copolymer was calculated to be 27,533 g/mol.

Molecular weight was also determined based on the data obtained from GPC by linear interpolation of the retention time of the polymer in the plot of log(M_w) versus retention time obtained from PS standard samples. This method estimated the M_w to be 21,197 g/mol. The lower estimate in the M_w of the copolymer by GPC is as expected as a result of differences in its interaction with the mobile phase compared to that of the polystyrene standards.

3.3.2. Nanoparticle Preparation

Nanoparticles were made through nanoprecipitation of PLA-mPEG block copolymer. In this method, a solution of the polymer in a mixture of acetone and DMSO, which dissolves both blocks of the copolymer very well, is added to an excess amount of water. The PLA block of the polymer is highly unstable in aqueous environment, leading to self-assembly of the polymer chains in the form of nanoparticles. Since the PEG block is hydrophilic, it acts as a stabilizer on the surface of the nanoparticles, preventing them from agglomerating and leading to the formation of nanoparticles with a core-shell structure .[78] In this study methoxy-PEG was chosen to make the NPs more stable. However, in future studies we will replace it with PEG-COOH which makes it possible to functionalize the NPs with targeting agents while maintaining other features equal .[76, 79-80] We adjusted the polymer molecular weight and polymer concentration in the organic solvent to make NPs with average size of 108.4 ± 2.1 nm. As Figure 3.4.A shows, NPs had a narrow size distribution with a polydispersity index (PDI) of 0.095 ± 0.022. All the NPs were smaller than 200 nm, which means they can be good candidates for passive targeting based on the enhanced permeability and retention (EPR) effect .[81] The SEM image shown in Figure 3.4.F confirms that the PLA/PEG block molecular weight ratio that we used leads to the formation of spherical NPs.

The distribution of zeta potentials of the NPs is shown in Figure 3.4.B. The average of zeta potential was -7.73 ± 1.17 mV which causes electrostatic repulsion between NPs, thereby contributing to their stability in suspension.[82-83]

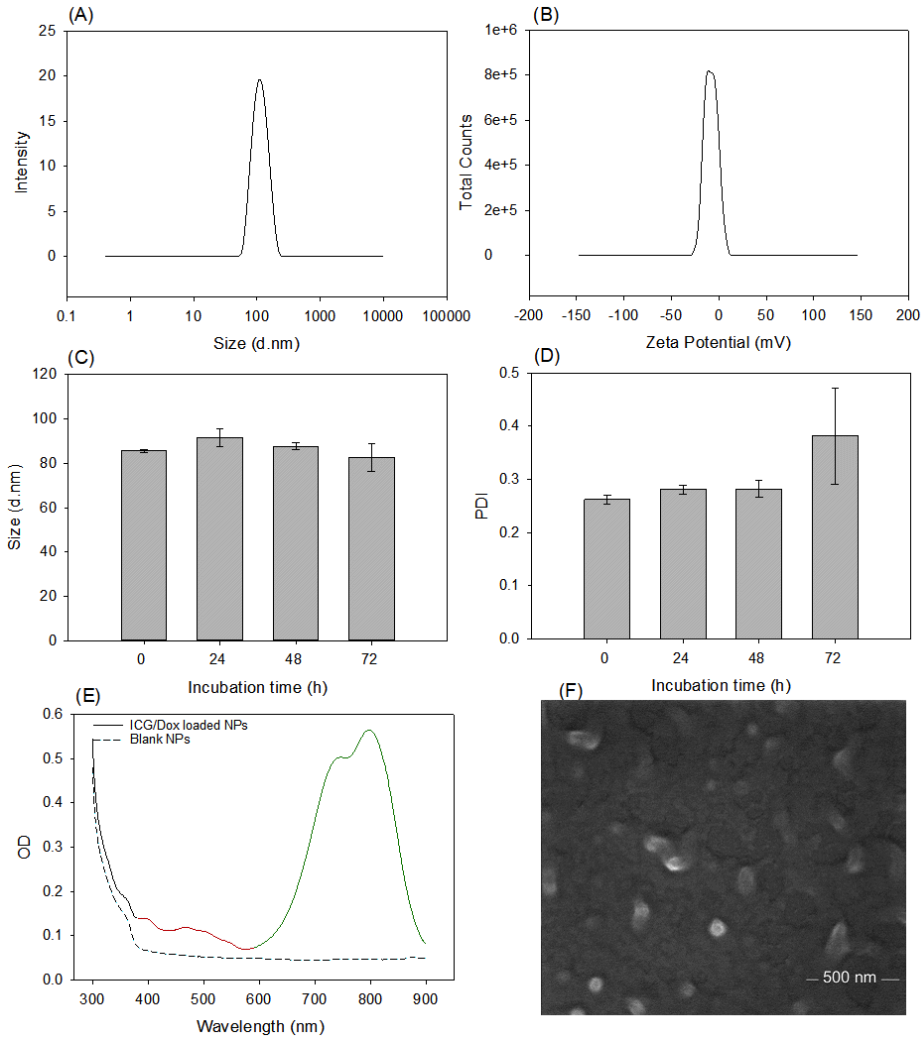

Figure 3.4. NP characterization. A) Size distribution of NPs by dynamic light scattering. B) Zeta potential distribution of NPs. C) Variation of NPs size and D) PDI over 72 h incubation at 37°C. Bars represent the means ± SD (n = 3). E) UV-Vis absorbance spectrum of NPs showing the presence of Dox (red) and ICG (Green). The spectrum of blank NPs (no Dox or ICG) at the same concentration is also shown for comparison. F) SEM image of NPs.

Figure 3.4.C shows the size variation of NPs incubated in cell media at 37°C for up to 72 h. No significant change in the NP size was observed in this time period, demonstrating that the NPs form a stable colloidal suspension even in the presence of proteins and salts. Figure 3.4.D shows that the PDI remains stable up to 72 h, at which point a slight increase in PDI is observed possibly due to the aggregation of some of the NPs; however, the values are not statistically different (P = 0.084).

The hydrophobic core of the NPs makes it possible to load drugs with hydrophobic regions through hydrophobic interactions. Harnessing this property of the NPs, we were able to load two amphiphilic therapeutic agents, ICG and Dox. The absorbance spectrum of the NPs shown in Figure 3.4.E has a peak at 476 nm (red) and another at 798 nm (green) which confirms that Dox and ICG have both been successfully loaded within the NPs, respectively. The mass fraction of the therapeutic agents in the NPs was calculated to be 4.24 ± 0.17 % for Dox and 2.69 ± 0.12 % for ICG, which are both high enough to provide the required therapeutic effect without causing toxicity resulting from the need for a high dose of NPs (as later shown in Figure 3.8.C). These weight percents were used to determine the concentrations of Dox and ICG to use as in cell studies.

3.3.3. NP Degradation

The presence of ester bonds in PLA-mPEG leads to hydrolysis of the polymer in aqueous environments. Figure 3.5 shows GPC chromatograph of the polymer before and after degradation over a period of 30 days. Since the NPs provide a high surface area which can be accessible for water molecules to hydrolyze the polymer, NPs are expected to undergo degradation within the 30 days that they were suspended in PBS. As expected, the elution peak shifted to a later elution time after degradation, confirming that the average molecular weight of the polymer has been decreased about 50% due to chain cleavage. The degradation products are expected to have different mobility in the mobile and stationary phase than PS due to their chemical structure. Their behavior could even be different from that of the original PLA-PEG molecules due to the changes in terminal group chemistry (formation of carboxylic acids and hydroxyl groups with each hydrolysis step) and differences in the ratios of PLA-to-PEG as the PLA block degrades.

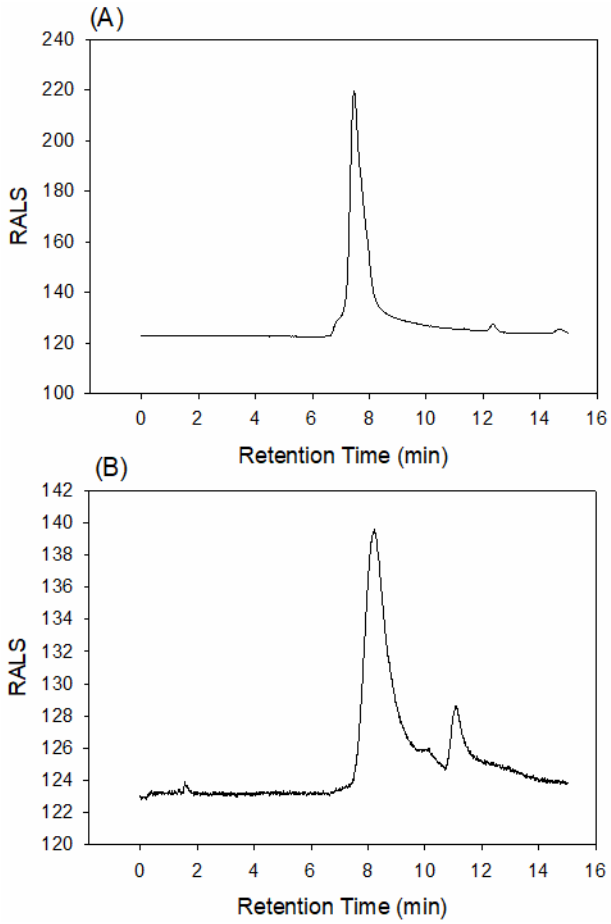

Figure 3.5. GPC chromatograph of A) intact polymer and B) degraded polymer from NPs.

3.3.4. Agent Release

The release kinetics of both loaded agents, Dox and ICG, are shown in Figure 3.6. As Figures 3.5.A and B show, only 13% of ICG releases from the NPs in the first 48 h, leaving sufficient amount of ICG within the NPs to induce a PTT effect through laser irradiation. Similarly, approximately 50% of Dox releases within 48 h, and the rest of the Dox content releases gradually over 31 days.

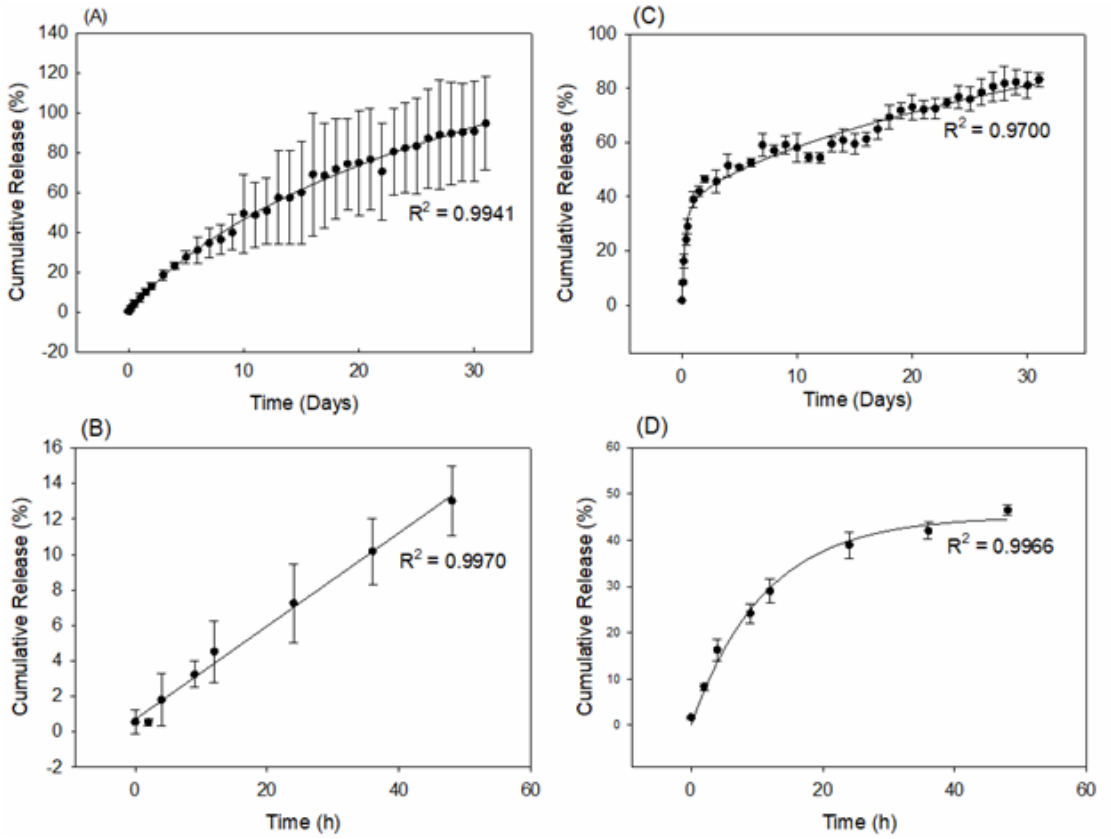

Figure 3.6. A) Release kinetics of ICG over 31 days and B) 48 h. C) Release kinetics of Dox over 31 days and D) 48 h. Data points represent the means ± SD (n = 4).

The best mathematical model which fitted the observed release kinetics was the Peppas-Sahlin equation [84-86] considering the lag time (Equation 2) with R-squared values of 0.9941 and 0.9700 for ICG and Dox, respectively.

$$\text{Released Fraction} = k_1 \cdot (t - T_{lag})^m + k_2 \cdot (t - T_{lag})^{2m} \qquad \text{Equation 2}$$

Here k_1, k_2 and m are constants. As the model describes, drug release from our NPs occurs through Fickian diffusion (first term) accompanied by polymer relaxation (second term) .[85]

3.3.5. PTT Conversion

Figure 3.7.A shows the temperature profile of 100 µL of suspension containing 0.3 mg/mL of NPs which is irradiated by laser at 0.3 W/cm^2 and 3 W/cm^2 irradiance for 10 minutes. As shown, when the irradiance was 0.3 W/cm^2, the solution reaches its maximum temperature (~10°C rise) after ~4 minutes. This temperature rise is high enough to eradicate tumor cells through hyperthermia (would reach > 43°C starting from physiological temperature).[87] Figure 3.7.A also demonstrates the ability of NPs to elevate

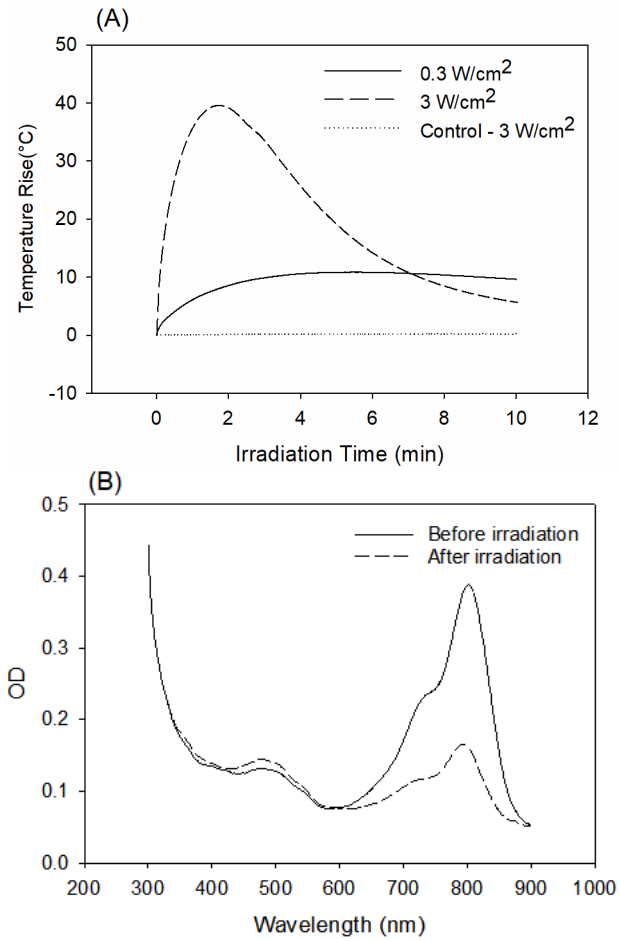

Figure 3.7. A) Temperature profile of NP suspension (0.3 mg/mL) in media irradiated with 808 nm diode laser at irradiance of 0.3 W/cm^2 and 3 W/cm^2 for 10 min. B) Absorbance spectrum of NPs before and after irradiation.

the temperature by up to 40°C by increasing the irradiance to 3 W/cm^2. With both

irradiances, the temperature of the suspensions begins to drop after a few minutes (~ 2 min for 3W/cm^2 and ~ 4 min for 0.3 Wcm^2) due to the thermal instability of our photothermal agent, ICG, which, as the absorption spectrum in Figure 3.7.B shows, decomposes after laser irradiation [88], losing its ability to continue absorbing NIR light.

3.3.6. Cell Growth Inhibition Induced by NP-Mediated Chemotherapy and PTT

The effect of NP concentration and irradiation time on cell growth inhibition was determined. Figure 3.8.A shows the viability of cells treated with NPs at concentrations ranging from 0 – 1 mg/mL for 48 h and irradiated by laser at 0.3 W/cm^2 for 3 min. NPs at or exceeding 0.6 mg/mL in concentration cause a similar level of cell death to that observed in the cells that were killed by methanol exposure. A concentration of 0.3 mg/mL of NPs (between the 0.2 and 0.4 mg/mL tested) was selected for further tests.

Figure 3.8.B shows the viability of cells treated with 0.3 mg/mL of NPs for 48 h and exposed to laser at 0.3 W/cm^2 for different time periods. Although irradiation by laser shows a lethal effect (higher viability is observed when exposure time is zero), increasing the exposure time from 3 min to 9 min does not result in any significant difference ($P > 0.05$) in the viability of the cells. This observation is either due to the decomposition of ICG after laser irradiation as discussed in the previous section, leading to no further absorption of laser light after the maximum temperature is reached and thereby no further photothermal effect, or due to sufficient denaturation of proteins at the thermal dose received in these 3 min such that further heating does not cause added cell death. Further studies were then conducted at with NPs at 0.3 mg/mL and with 3 min of laser irradiation.

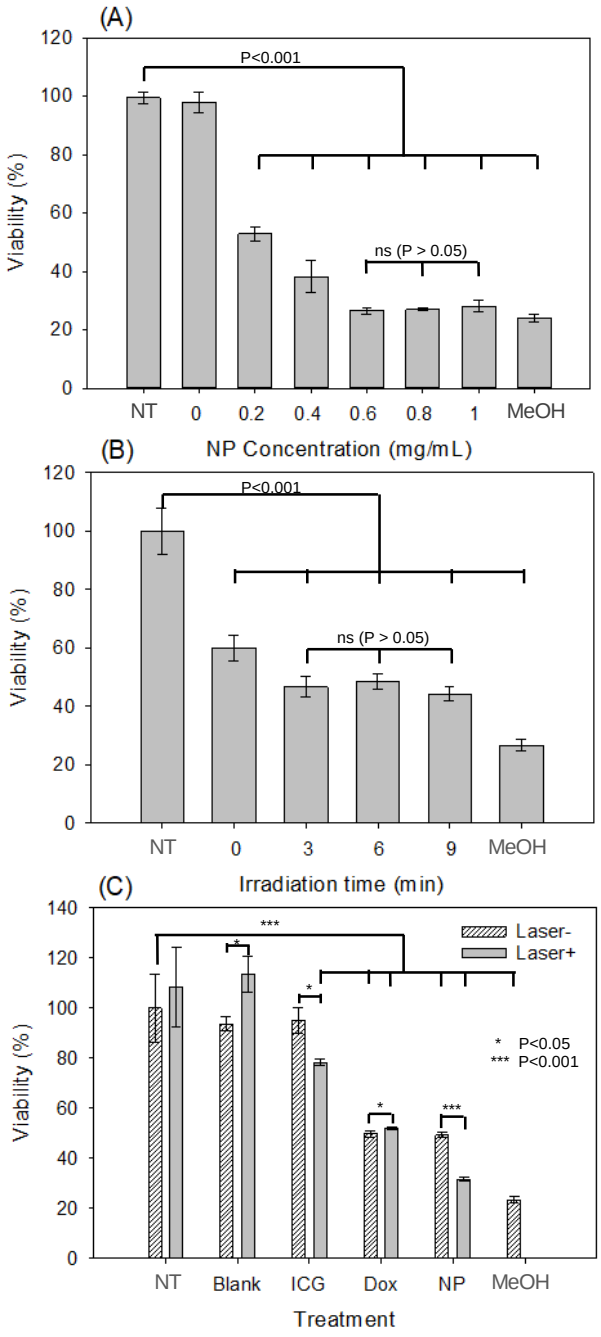

Figure 3.8. Effect of A) NP concentration and B) irradiation time on cell viability. C) Effect of each component of the NPs on cell viability. Cells were exposed to blank NPs, ICG, Dox or NPs for 48 hr before their viability was assessed. Cells exposed to NPs or ICG were also irradiated with laser 1.5 hr after the beginning of the incubation with their respective treatment. NT = No treatment, MeOH = cells treated with methanol for 15 min, ns = no statistically significant difference. Bars represent the means ± SD ($n \geq 3$).

Figure 3.8.C compares the lethal effect of NPs and each of their components. Cells which are treated with NPs are the least viable amongst all. The viability of the cells which are treated with blank NPs both with and without laser exposure are not significantly different from positive control with no treatment ($P > 0.05$) which confirms that the polymeric carrier is not toxic by itself. Cells that are treated with ICG but were not irradiated are as viable as the positive control. However, their viability decreased when they were exposed to the laser beam which means PTT has still a significant effect at this low concentration.

The same reduction in viability is observed when comparing the effect of NPs with and without irradiation. Cell viability reduction caused by Dox did not further decrease upon laser exposure, as expected. NPs in the absence of irradiation also showed the same effect as Dox did. In conclusion, PTT and chemotherapy are responsible for approximately 20% and 50% of the viability decrease, respectively, while the carrier and the 808 nm laser do not decrease the viability of the cells by themselves.

3.3.7. Study of Damage Associated Molecular Patterns (DAMPs)

3.3.7.1. ATP Release

Cancer cells secrete ATP during ICD. Secreted ATP binds to dendritic cells through the P2X7 and P2Y2 receptors leading to their maturation, which further induces an immune response against remaining tumor cells .[89] Figure 3.9 shows the release of ATP from the cells in medium after treatment with NPs (with Dox, ICG and laser irradiation), ICG (with laser irradiation) and Dox after four different incubation times. In all of the four incubation times studied, the cells treated with NPs released the highest amount of ATP to the extracellular medium compared to the other treatments studied. Another notable

observation is that although ICG-mediated PTT accounts for less cell death than treatment with Dox, as discussed in the previous section, it induces a higher ATP release than Dox does even after 48 h, when the maximum effect of chemotherapy is expected.

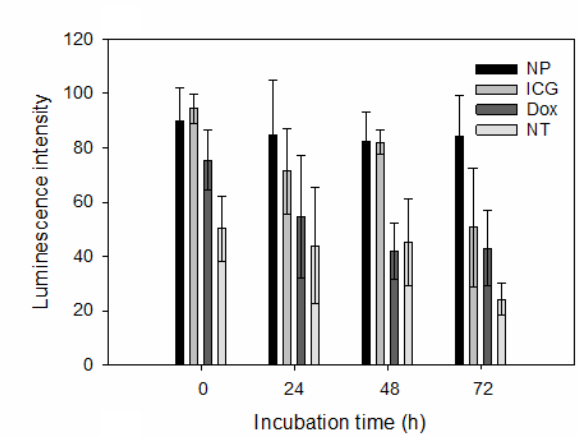

Figure 3.9. Relative level of ATP release from the cells after treatment with NPs, ICG, or Dox, or with no treatment (NT) as a control. All the cells were incubated with their respective treatment 1.5 h prior to the laser irradiation. Incubation time in this figure represents the time that cells were incubated with the treatment after laser irradiation.

3.3.7.2. Calreticulin Presentation

Translocation of calreticulin to the cell surface occurs in ICD. Calreticulin exposure leads to dendritic cell maturation through binding to the CD91 receptor.[90] Since two different treatment approaches with different mechanism of action were used in this study, we traced calreticulin presentation on the cell membrane of the cells for 72 hours to compare the effect of each treatment at each time point. Figure 3.10.B compares the relative fluorescence intensity per cell associated with surface calreticulin obtained from ImageJ for the cells treated with ICG (PTT), Dox (chemotherapy) and NPs (combination therapy), along with a control group which did not receive any treatment. The notable point in this figure is that NPs induced the highest level of calreticulin exposure at all the time points. PTT is the treatment that first imparts its effect.

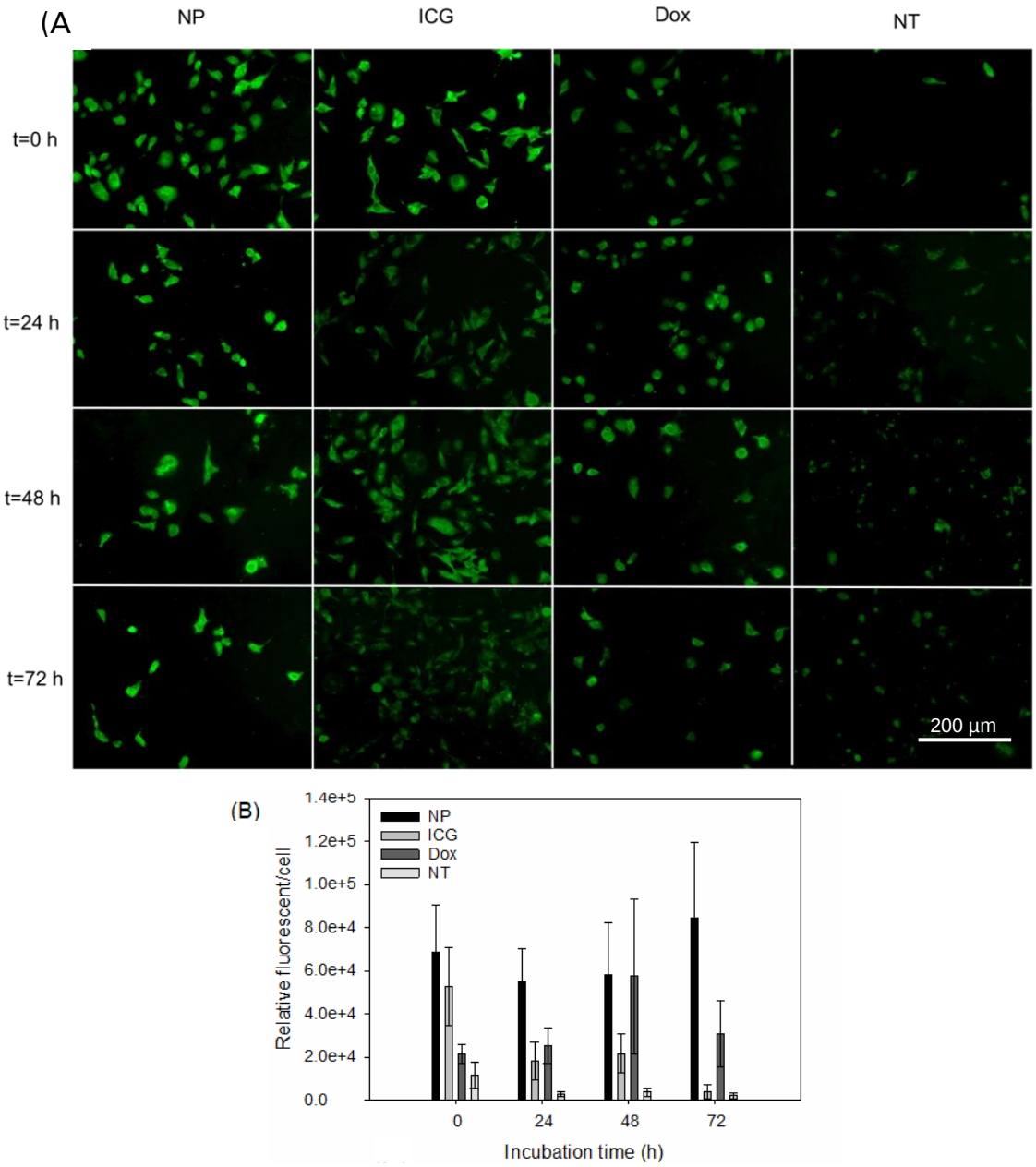

Figure 3.10. A) Representative images of fluorescent labeling of calreticulin exposed on the cell surfaces after treatment over a 72 h incubation time period, and B) their relative fluorescent measured by ImageJ software. Treatments include NP (combination therapy), ICG (PTT), Dox (chemotherapy) and no treatment (NT).

The reduction trend in calreticulin presentation observed over time for cells treated with ICG is due to the proliferation of the remaining cells which are not receiving further treatment. However, the effect of Dox is observed after 48 h, as expected, preventing the

combination therapy (NPs) from ceasing to induce presentation of this DAMP. Figure 3.10 shows one representative image of each treatment.

3.3.7.3. Release of HMGB1

HMGB1 is a nuclear protein that plays an important role in DNA transcription. Cells release HMGB1 from the nucleus to the cytoplasm and eventually to the extracellular medium during the process of ICD.

Therefore, it is expected to observe a reduction in HMGB1 within the cells over time. As the bar graph in Figure 3.11.B shows and as expected, the smallest amount of HMGB1 left in the cells was observed upon combination therapy with NPs. Figure 3.11 shows one representative image of each treatment.

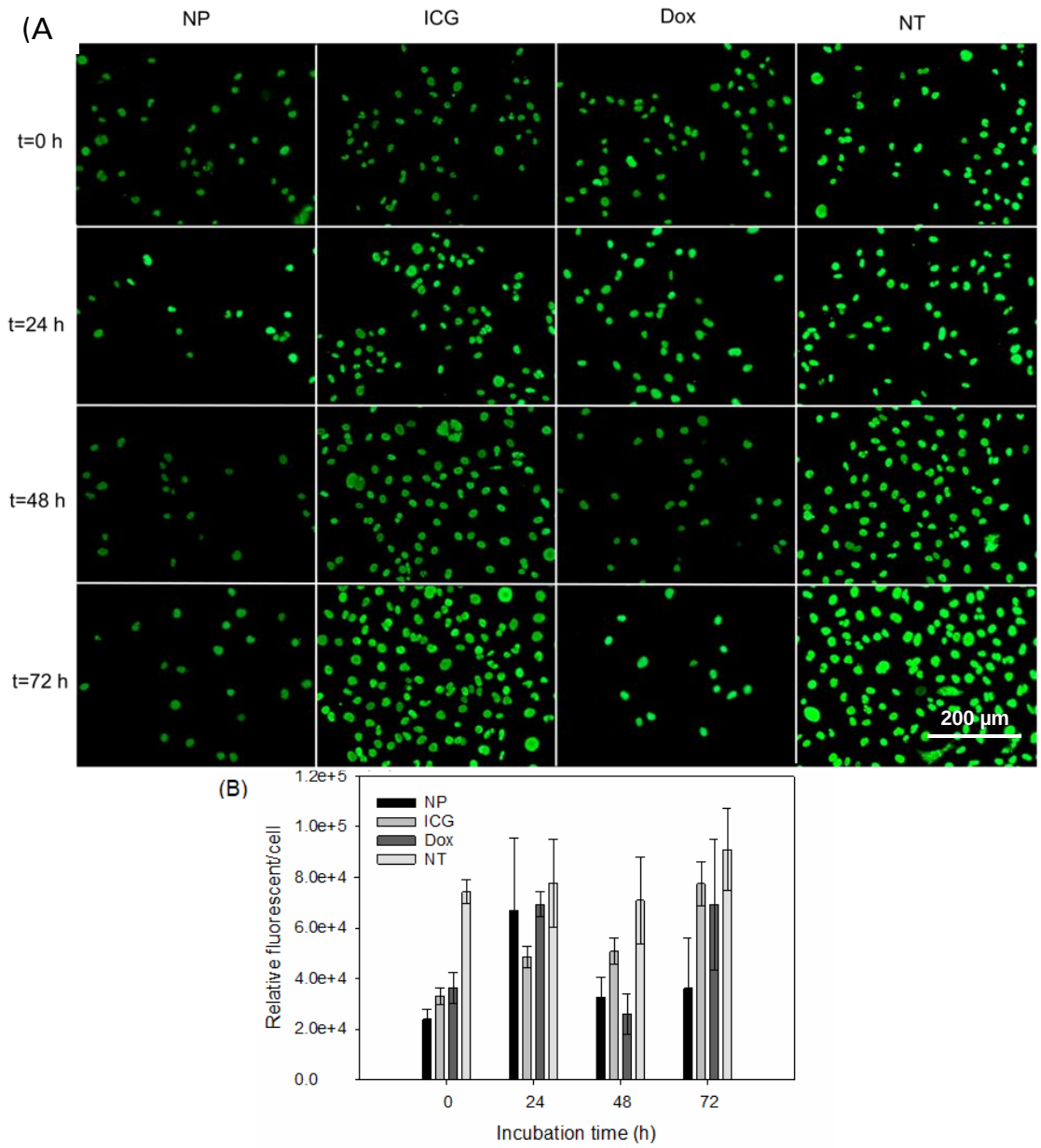

Figure 3.11. Representative images of fluorescent labeling of HMGB1 remaining within the cells after treatment over a 72 h incubation time period, and B) their relative fluorescent measured by ImageJ software. Treatments include NP (combination therapy), ICG (PTT), Dox (chemotherapy) and no treatment (NT).

3.3.8. Discussion

In this work we demonstrate the preparation of biocompatible, biodegradable polymeric nanoparticles for dual chemotherapy and photothermal therapy using a simple nanoprecipitation process. The choice of a known polymer that has been previously

utilized in FDA-approved formulations to enable dual photothermal/chemo-therapy was made specifically in light of the translational potential of the technology. The PLA-mPEG polymer utilized encapsulated Dox and ICG within the core-shell structure of the particles, providing them stability and controlling their release to the physiological environment. ICG was used as the PTT agent since it is a dye that is FDA-approved for bioimaging applications and has a long history of biocompatibility in humans [91], making it an attractive agent for use in therapeutic applications. Dox was selected as the chemotherapeutic agent since it has been proven to relieve tumoral immune suppression and stimulate anti-tumor adaptive immunity.[46] The nanoparticles showed significant colloidal stability as a result of the PEG shell and negative zeta potential, and were able to maintain their size when suspended for up to 72 hr in a physiologically relevant fluid.

In vitro studies demonstrated the ability of the NPs to locally increase the temperature from physiological temperature to over 43 $^{\circ}$C upon irradiation with a NIR laser, which is a sufficient increase to lead to cell death.[48] NIR light (~650-950 nm) can penetrate through tissues as deep as a few cm since tissue chromophores present minimal absorption and scattering in this range,[49-50] thereby making activation of these NPs suitable for the treatment of tumors that are superficial or that can be accessed endoscopically or laparoscopically.

Numerous groups, including our own, have utilized nanomedicines over the past decade for the treatment of primary tumors via chemotherapy or photothermal therapy.[54, 76, 92] In our current work, studies with cultured breast cancer cells demonstrated the ability of the dual treatment to induce a potent anti-cancer effect that resulted from the additive effect of chemotherapy and photothermal treatment. Other groups have also documented the

synergy of nanoparticle-mediated chemotherapy and photothermal therapy on cancer treatment.[93-94] Only recently, however, has the use of these nanomedicines for modulation of systemic immunity against cancer been considered. The effect of localized hyperthermia induced via optical or magnetic stimulation of NPs on immune modulation has been studied by a few groups.[95-100] Similarly, the ability of certain chemotherapies to induce ICD is known [101-103] and the combination of systemic chemotherapy and ICP has been the focus of recent clinical trials. Nonetheless, the work herein reported is, to the best of our knowledge, the first to investigate the interaction of nanoparticle-mediated chemotherapy and photothermal therapy in the induction of ICD.

Our results demonstrate that this combinatorial therapy could potentially act in synergy with cancer immunotherapies that aim to make use of the patient's immune system to target tumor cells for elimination. Effective recognition and attack of cancer cells by killer T cells requires uptake, processing and presentation of tumor-specific antigens (immunogenic aberrant proteins produced by genetic mutations of cancer cells) by dendritic cells to native T cells.[104] Unfortunately, poorly immunogenic tumors fail to initiate the immunogenic cascade. Our work demonstrates that dual chemotherapy and photothermal therapy induced by our NPs leads to ICD which is characterized by the release of tumor specific antigens and the DAMPs calreticulin, ATP and HMGB1. Importantly, our results show that the best response is obtained when the combination treatment utilizing NP-assisted chemotherapy and photothermal therapy is utilized. Future work will investigate if ICD mediated with these NPs could generate an antigen-specific immune response *in vivo*.

3.4. Conclusion

The PLA-mPEG NPs prepared in this study were confirmed to be cytocompatible, yet effective agents for dual photothermal therapy and chemotherapy. The NPs exhibited optimal size in the range of ~ 100 nm and encapsulated sufficient Dox and ICG to mediate a therapeutic effect. This formulation showed promising results since a very low dose of NPs (0.3 mg/mL) and short laser irradiation time of 3 min led to an effective anti-cancer effect in MDA-MB-231 human breast cancer cells due to the additive therapeutic effect of each agent. Our investigation of DAMP presentation after treatment confirmed that the cells undergo ICD in response to our NP-mediated combinatorial treatment approach. Specifically, immunocytochemistry studies demonstrated that cells treated with NP-mediated dual therapy exhibited the highest level of presentation of calreticulin on the cell surface, as well as the highest release of HMGB1 and ATP compared to Dox-mediated chemotherapy or laser assisted ICG-mediated photothermal therapy alone. Thus, this treatment method is expected to be able to modulate the immunogenicity of tumor microenvironment which is believed to be the reason for the low response rate of currently available cancer immunotherapies.

4. *IN VITRO* DETERMINATION OF IMMUNOGENIC CELL DEATH IN METASTATIC MELANOMA CELLS INDUCED BY ALBUMIN NANOPARTICLES CARRYING INDOCYANINE GREEN AND DOXORUBICIN

4.1. Introduction

Similar to Chapter 3, we aimed to produce a nanomedicine that could effectively act as an anticancer agent but that would cause the least possible side effects on other tissues. Besides, we aimed to develop a nanomedicine that was capable of activating an immune response against the remaining cancer cells. The material that we used in this chapter as the carrier for therapeutic agents is a biological macromolecule as opposed to the synthetic polymer that we used in the previous chapter.

Albumin is a protein that has gained attention for drug delivery applications due to its biodegradability, nontoxicity, non-immunogenicity, being metabolized in the body with innocuous degradation products, ease of purification and water solubility.[61] In the work herein described, BSA was utilized for the preparation of the therapeutic NPs as a model for HSA NPs which would be eventually required for human use.

Albumin nanocarriers are considered as an attractive nanomedicine since the unique primary structure of this protein provides multiple binding sites within the NP for incorporation of different types of therapeutic agents. High content of charged amino acids such as lysine in albumin's structure facilitates electrostatic adsorption of therapeutic agents with both positive (for example ganciclovir) and negative (for example oligonucleotide) charges.[61, 105-106] although the protein is water soluble it contains hydrophobic regions that can be targeted for loading of the hydrophobic drugs by hydrophobic interactions. Abraxane® (nanoparticle albumin bound paclitaxel or nab-

paclitaxel), with an approximate diameter of 130 nm, is the first FDA approved nanotechnology based chemotherapeutic formulation that has shown significant benefit in treatment of metastatic breast cancer.[107]

Commercially, albumin is obtained from egg white (ovalbumin), bovine serum (bovine serum albumin, BSA), and human serum (human serum albumin, HSA), as well as from soybeans, milk, and grains. Recombinant human serum albumin (rHSA) is another form of albumin that is genetically engineered and produced with the same structure as plasma-derived HSA. rHSA is highly purified and completely free of virus, fungi, and bacteria.[61] In the work herein described, BSA was utilized for the preparation of the therapeutic NPs as a model for HSA NPs which would be eventually required for human use.

We focused on the evaluation of albumin NPs as agents for the treatment of melanoma. In contrast to the work described in Chapter 3, our shift in focus toward melanoma stems from the fact that optical anti-cancer technologies are expected to have better clinical outcomes when utilized for the treatment of superficial lesions where light would be able to penetrate the tissue. Thus, the potential for clinical translation guided this choice. Malignant melanoma is a malignant tumor that originates from melanocytes. It accounts for only 4% of skin cancers but results in 79% of skin cancer-related deaths. The incidence of melanoma has increased in the past few years.[108] Tumor accessibility for penetration of near infrared (NIR) laser makes photothermal therapy (PTT) a good treatment candidate. In combination with chemotherapy, this treatment can be a promising strategy to reduce the size of the tumor and induce immunogenic cell death (ICD). A syngeneic transplantation model is required for studying the effect of treatment

in combination with immune checkpoint therapy (ICP) *in vivo*. This model allows for the interaction of melanoma cells with immune cells such as dendritic cells (DCs). In this study we used the B16F10 murine metastatic melanoma cell line as a model for melanoma. The results can be translated in *in vivo* models which possess B16F10 syngeneic xenografts.[109]

In this chapter, we describe the development of albumin NPs with appropriate size to encapsulate doxorubicin (Dox), a chemotherapeutic agent, and indocyanine green (ICG), the PTT agent, and deliver them to the tumor site to facilitate NP-mediated combinatorial therapy. Further, we determined whether the NPs were capable of ICD induction through investigation of the presentation of damage associated molecular patterns (DAMPs) in the cancer cells and studied effect of NP concentration on both cell growth inhibition and ICD induction in B16-F10 mouse melanoma cells *in vitro*.

4.2. Materials and Methods

4.2.1. Materials

Bovine serum albumin, glutaraldehyde, sodium chloride, bovine serum albumin and sodium chloride were acquired from Sigma-Aldrich (St. Louis, MO). Glutaraldehyde, doxorubicin hydrochloride (Dox), and thiazolyl blue tetrazolium bromide (MTT) were obtained from Alfa Aesar (Ward Hill, MA). Indocyanine green (ICG) was obtained from MP Biomedicals (Irvine, CA). ATP Determination Kit was obtained from Invitrogen. Rabbit anti-calreticulin antibody (ab2907), rabbit anti-HSP70 antibody (EPR16892, ab181606) and rabbit anti-HSP90 beta antibody (E296, ab32568) were purchased from Abcam (Cambridge, MA). Goat anti-rabbit IgG (H&L) DyLight 488 conjugate was obtained from ImmunoReagents, Inc. (Raleigh, NC). 4′,6-Diamidine-2′-phenylindole

(DAPI) dihydrochloride was purchased from EMD Millipore Corporation (Burlington, MA). 10x phosphate buffer saline (PBS) was received from SeraCare (Milford, MA). Ultrapure deionized water was obtained from a Millipore Direct Q system. All of the other solvents used were ACS grade.

4.2.2. Nanoparticle Preparation and Size Optimization

Bovine serum albumin (BSA) NPs were prepared through desolvation method. Figure 4.1 shows schematics of NP preparation. Briefly, an aqueous solution of BSA was made by adding water containing 2 mM NaCl at a certain pH to BSA. Sufficient amount of a nonsolvent was then added at a constant flow rate to 500 µL BSA solution under stirring at 600 rpm until the solution became turbid. Immediately after nonsolvent addition, 10 µL glutaraldehyde 8% (w/v) was added per each 2.5 mg of BSA to chemically crosslink

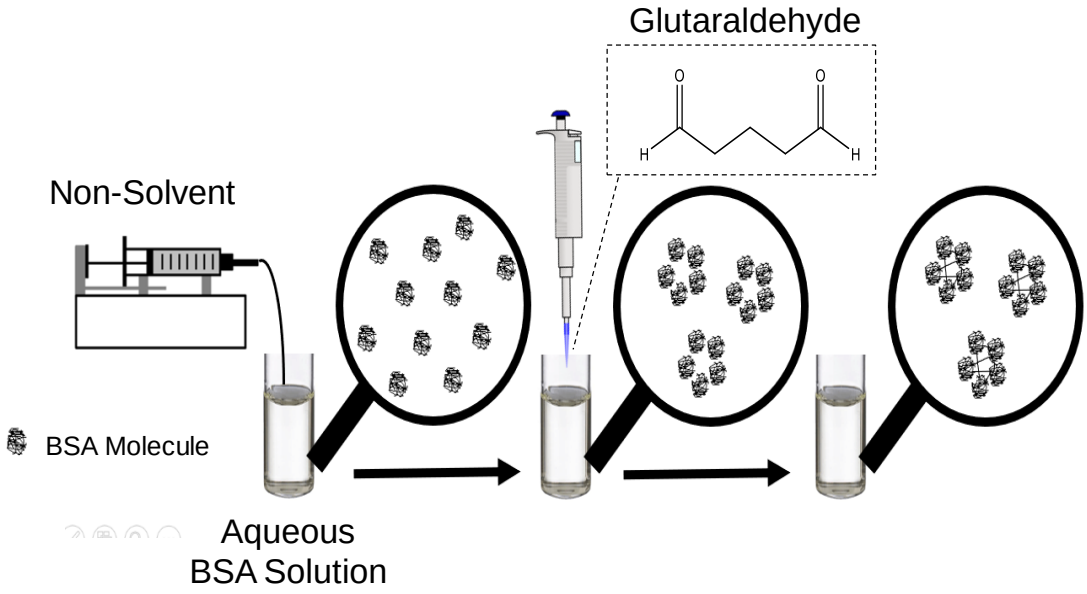

Figure 4.1. NP preparation through desolvation method.

the BSA molecules and thereby form NPs. The crosslinking reaction was allowed to occur for 12 h at room temperature. BSA concentration, pH of the aqueous solvent, the

nonsolvent type and its addition rate were varied to find the optimum condition that resulted in the desired NP size (< 100 nm). According to the results acquired from this size optimization study, optimized conditions were selected for the preparation of NPs for the rest of experiments. Table 1 shows the parameters investigated.

Table 4.1. NP Preparation Parameters.

Test	Study Description	pH	[BSA] (mg/mL)	Nonsolvent	Nonsolvent Addition Rate (mL/min)
1	Nonsolvent identity effect	9.4	30	Ethanol, Methanol, Acetone	1
2	[BSA] effect	9.4	10,30,50	Ethanol	1
3	pH effect	9.4, 10.6, 11.3	10	Ethanol	1
4	Nonsolvent addition rate effect	9.4	10	Ethanol	0.5, 1, 2.5
5	Optimized parameters	11.3	5	Ethanol	2.5

NPs were centrifuged for 30 min at 74,200 x g (Avanti J-26 XPI, Beckman Coulter, US) and resuspended in 200 µL water for further use or characterization.

4.2.3. Agent Loading

To load Dox and ICG within BSA NPs, these agents were loaded via equilibrium partitioning into pre-made NPs. Specifically, 500 µL suspension of 2 mg/mL BSA NPs in water was incubated at room temperature with Dox and ICG while stirring at 600 rpm in the dark for 4 h. Table 2 shows the final concentration of the agents in each experiment. Unloaded ICG and Dox were removed through 30 min of centrifugation at 74,200 x g (Avanti J-26 XPI, Beckman Coulter, US). NPs were then resuspended in water for further characterization.

Table 4.2. Target Dox and ICG Loading in NPs.

Experiment	Target Loading (%) = agent mass/mass of BSAx 100	[ICG] (mg/mL)	[Dox] (mg/ml)
1	5% Dox – 5% ICG	0.1	0.1
2	7.5% Dox – 7.5% ICG	0.15	0.15
3	10% Dox – 10% ICG	0.2	0.2
4	12.5% Dox – 12.5% ICG	0.25	0.25
Selected Parameters	7.5% Dox – 10% ICG	0.2	0.15

4.2.4. Nanoparticle Characterization

NPs were characterized by dynamic light scattering (DLS) to measure their hydrodynamic size, and electrophoretic light scattering to determine their zeta potential using a Malvern ZetaSizer Nano ZS instrument. The morphology of dried NPs was investigated by scanning electron microscopy (SEM) after coating them with a 2-nm layer of iridium by sputter coating.

Drug loading (DL%) was calculated using Equation 1. The mass of agents (ICG or Dox) in the supernatant was determined by UV-vis spectroscopy using a Biotek H4 multimode plate reader (λ= 476 nm for Dox and λ=798 nm for ICG). The total mass of NPs was simply measured by scale after lyophilization.

$$DL\% = 100 \times \frac{Initial\ mass\ of\ agent\ used - Mass\ of\ agent\ in\ supernatant}{Total\ mass\ of\ NPs} \qquad \text{Equation 1}$$

The stability of NPs in complete cell media (described below) at 37 ℃ was investigated by tracking NP size variation over a period of 72 h.

4.2.5. Agent Release

In vitro drug release behavior of NPs was studied for 30 days by determining the concentration of Dox and ICG released at predetermined time intervals into 4 mL of PBS solution (pH 7.4) containing 5 mg/mL bovine serum albumin (BSA) at 37° C. BSA was

included in the release buffer to enhance the stability of ICG in aqueous environment and enable reliable measurement of the concentration of this agent. Release studies were performed by placing 150 µL of 11.6 mg/mL suspension of the NPs in release buffer in a dialysis tube (D-Tube^{TM} Dialyzer Mini, MWCO 6-8 kDa) and analyzing 100 µL samples taken from the 4-mL dialyzate to determine ICG and Dox concentration by UV-Vis absorption spectroscopy.

4.2.6. Photothermal Conversion

NPs were irradiated by an 808-nm laser diode (RLCO-808-1000G, 9 mm; Roithner Lasertechnik GmbH, Wien, Austria) for 10 min. An indium antimonide infrared (IR) camera (FLIR Systems, Inc., Wilsonville, OR, USA) was used to measure the temperature change of the samples. The samples were irradiated at a laser fluence of 0.3 W/cm^2 (laser power = 184.72 mW, spot diameter = 2.8 mm). All of the measurements were conducted in 96-well plates with 100 µL of sample. The concentration of NPs in suspension in complete cell media ranged from 0-0.5 mg/mL, with astep size of 0.1 mg/mL). Complete cell media (described below) was used as the control.

4.2.7. Cell Culture

Cells were obtained from the American Type Culture Collection (ATCC) and cultured in complete cell media consisting of Dulbecco's Modified Eagle's Medium (DMEM) without phenol red (Gibco, MD, USA) supplemented with 10% heat inactivated RMBIO fetal bovine serum, 1% penicillin/streptomycin (VWR) and 1% L-glutamine (VWR) in a humidified atmosphere containing 5% CO_2 and 95% air at 37°C.

4.2.8. Study of Cell Viability After Treatment

Cells were seeded at a density of 5,000 cells/well in 96 well plates. 24 h later, when cells were attached to the wells, their media was replaced with the following treatments.

a) To study the effect of NP concentration, suspensions of NPs in complete cell media with concentrations ranging from 0.0 to 0.5 mg/mL were added to the cells. After 1.5 h incubation of cells with NPs at 37°C, the cell media was replaced with fresh media, and cells were treated with 808 nm diode laser (2 W/cm^2, laser power = 0.74 W, spot diameter = 7 mm) for 2.5 min in a chamber at 37°C and returned to the incubator.

b) To study the effect of incubation time of the cells with NPs prior to the laser treatment, a 0.125 mg/mL NPs suspension in media was added to the cells. After 45 min, 1.5 h, 3 h, 6 h, 12 h, 24 h and 48 h of incubation at 37°C, the cell media was removed, and fresh media was added. Then, the cells were irradiated with laser (same setting as above) for 2.5 min.

c) To investigate the effect of laser irradiation time, the same procedure was followed, except that the concentration of NPs was 0.0625 mg/mL, the incubation time was 1.5 h and the irradiation time varied from 0-10 min with a step size of 2.5 min.

For all the studies, the MTT viability assay was performed 48 h after the NPs were added to the cells. Only viable cells can metabolize MTT reagent using mitochondrial reductase and convert it to formazan crystals which are soluble in DMSO. Formazan concentration, which is proportional to number of viable cells, can be further calculated by UV-Vis spectroscopy. 10 µL solution of 5 mg/mL MTT reagent in media was added to all the cells. Positive control wells did not receive any treatment (100% viable). For the negative control, cells were treated with methanol for 15 min prior to viability assessment. After 2 h of incubation of cells at 37°C, the media was replaced with 200 µL DMSO and plates

were shaken for 15 min to allow proper dissolution of formazan crystals. The optical density of solution at 555 nm and 900 nm were measured with a Biotek H4 multimode plate reader.

4.2.9. Study of DAMPs

B16F10 cells were initially placed in microcentrifuge tubes at a cell density of 100,000 cells/tube. Cells were centrifuged at 200 ×g for 5 min. Then, the supernatant was discarded, and the cells were resuspended in 1 mL of ICG/Dox-loaded BSA NP suspension with a concentration of 0.0625 mg/mL and incubated at 37°C. As a control, one group of cells was not treated. After 1.5 h, NP suspensions were replaced with 100 µL fresh pre-warmed media, and the cell suspension was transferred to a 96-well plate. Cells were irradiated by 808 nm diode laser at power density of 2 W/cm^2 for 2.5 min. Cells were returned to the incubator after laser irradiance. After 30 min, cells were transferred to a 12-well plate and 900 µL pre-warmed media was added to allow the cells to replicate. After 24 h and 48 h, the levels of DAMPs were determined as described below.

Flow cytometry was used to quantitatively determine the level of calreticulin, HSP70 and HSP90 that are exposed on the cells' surface. Flow cytometry is a common method for analyzing characteristics of cells or particles, such as cell size or fluorescence intensity. The instrument focuses the cells into a single-cell stream that is interrogated by a laser beam. The scattered light from each object is detected and measured as forward scatter and side scatter. Fluorescence detectors also measure the amount of emitted fluorescence from fluorescent objects. Briefly, cells were detached from the 12-well plates by 5 min trypsinization at 37°C. After washing with DPBS (without Ca^{2+} and Mg^{2+}), cells were

resuspended in 1000 µL BSA (1% w/v) to block nonspecific absorption. BSA solution was discarded after 30 min, and three independent groups of cells were incubated with 50 µL of either rabbit polyclonal anti-CRT antibody (Abcam ab2907, 1:75 dilution in 0.1% w/v BSA), 50 µL rabbit monoclonal anti-HSP70 antibody (Abcam ab181606, 1:250 dilution in 0.1% w/v BSA), or 50 µL rabbit monoclonal anti-HSP90 antibody (Abcam ab32568, 1:250 dilution in 0.1% w/v BSA) for one hour followed by DPBS washing and one-hour incubation with 50 µL of goat anti-rabbit IgG DyLight 488 conjugate (1:1000 dilution in 0.1% w/v BSA) in the dark at room temperature. Then, cells were washed, resuspended in DPBS and analyzed by flow cytometer (CytoFlex, Beckman, Brea, CA). CytExpert software was used to analyze flow cytometry data. The FITC channel was selected to detect the fluorescence of the AlexaFluor 488. A total of 10,000 events were collected for each sample and histograms illustrating the fluorescent intensity against cell counts were plotted.

4.2.10. Statistical Analysis

Experiments were performed in triplicate and the data was reported as the average ± standard deviation. Student t-Test was used for identification of statistical differences between group means.

4.3. Results and Discussion

4.3.1. Nanoparticle Preparation and Size Optimization

Biodistribution, cellular uptake and clearance of NPs by reticuloendothelial system strongly depends on NP size and surface chemistry. The preferential size for NPs that are used as cancer drug carriers is less than 200 nm.[57] In our work, we aimed to reduce NP size to less than 100 nm while maintaining the size polydispersity index (PDI) below 0.2.

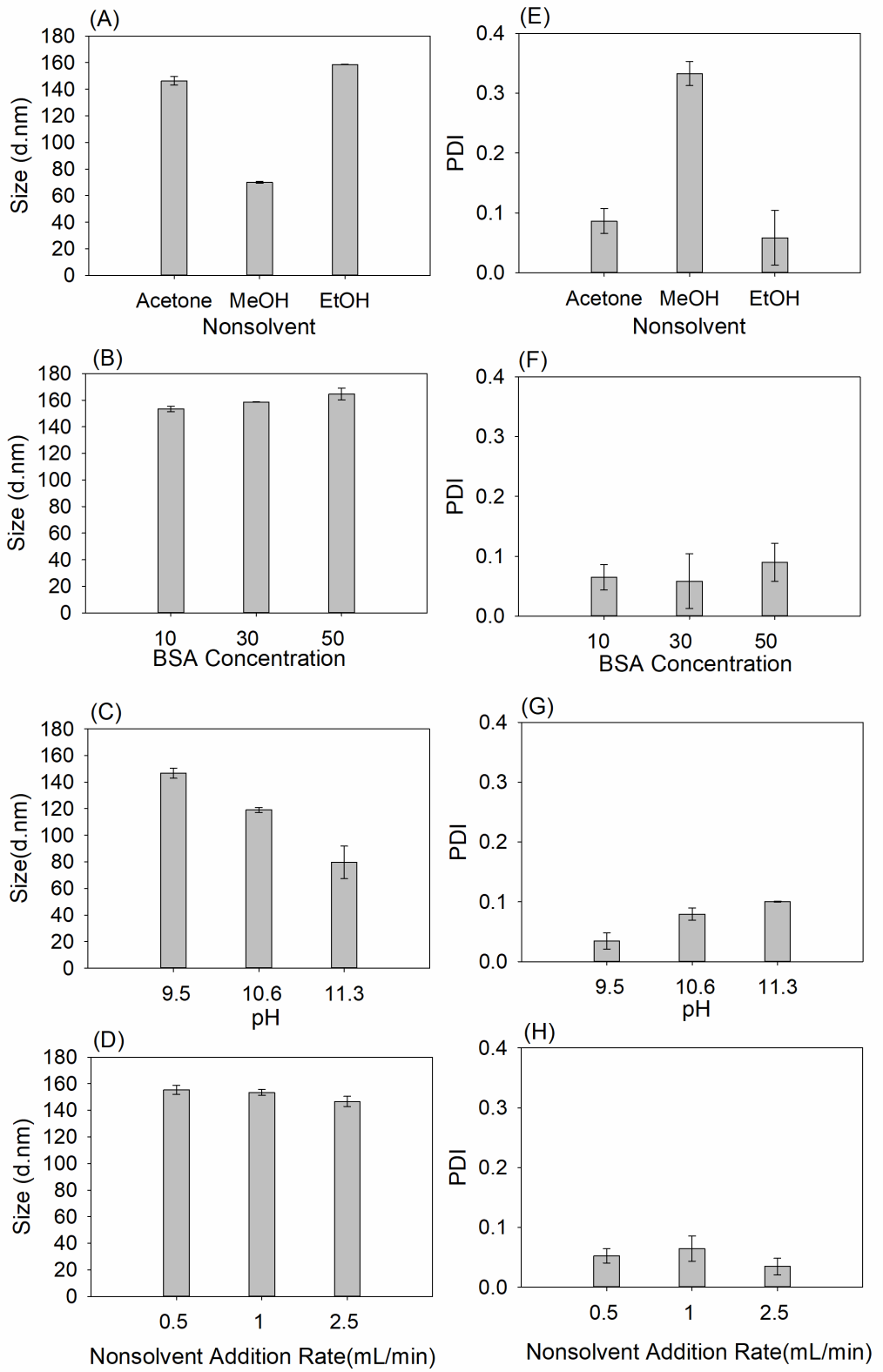

Figure 4.2. Effect of A) nonsolvent type, B) Concentration of BSA solution, C) pH of the BSA solution and D) Nonsolvent addition rate on NPs size. Effect of E) nonsolvent type, F) Concentration of BSA solution, G) pH of the BSA solution and H) Nonsolvent addition rate on NPs PDI.

To this end, we studied the parameters which affect NP size and PDI to find the operating condition applying that can result in the fabrication of the smallest BSA NPs.[110] Figure 4.2 shows the trend and intensity with which each of these parameters alters NP sizes and PDI. Increasing pH of the BSA solution decreased size tremendously. Small NPs have high surface energy which force them to aggregate to bigger and more stable NPs. Since the isoelectric point (pI) of BSA is about 4.9,[111] as the pH value increases, BSA molecules possess higher negative charge which induces stronger electrostatic repulsion that can overcome the high surface energy of small NPs. Thus, the NPs remain stable even with small size. As we targeted to make the smallest possible BSA NPs, pH of the BSA solution was kept at its highest value (i.e. 11.3) for the rest of the study. The second-most effective factor was the type of the nonsolvent. Methanol was the nonsolvent which resulted in the smallest yet the most polydisperse NPs. Therefore, ethanol, the nonsolvent with which the lowest PDI was obtained and which resulted in NP size similar to that obtained with acetone, was chosen as the nonsolvent to make NPs for the remaining studies. Higher BSA concentration increases the degree of saturation, which results in bigger NPs. Figure 4.2.B confirms that increasing BSA concentration increased the NP size slightly. Based on this observed trend and the fact that PDI remained almost constant with BSA concentration, for other studies in this work we decreased the BSA concentration even further to 5 mg/mL. The least effective parameter on NP size that we studied in this paper was the rate of nonsolvent addition. However, the rate which resulted in smallest and the most monodisperse NPs was chosen to make NPs required in the study. Table 4.1, row 5 shows the optimized parameters that are used for the preparation of BSA NPs for all further studies.

4.3.2. Agent Loading

Doxorubicin binds to the carboxyl groups in BSA molecule due to electrostatic attraction.[112] Binding can be increased up to the saturation of albumin NPs by adjusting parameters like concentration of Dox and incubation time of BSA NPs with Dox solution. ICG's ability to bind to albumin is well known and can be the result of either electrostatic absorption or hydrophobic interactions.[113] In this part of the study, we aimed to load the highest possible amount of Dox and ICG within the blank BSA NPs while keeping their

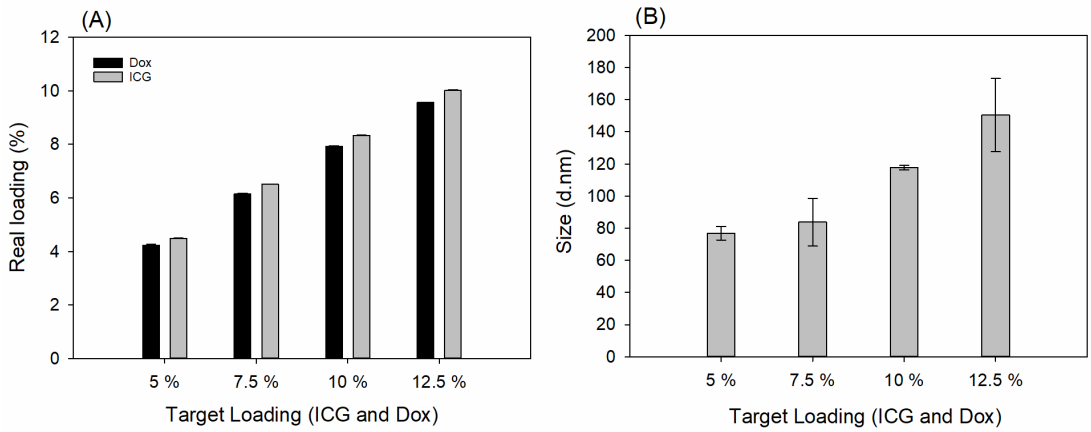

Figure 4.3. Effect of target loading on NPs A) Real Loading % and B) Size

average size at less than 100 nm. Figure 4.3.A shows that by increasing the concentration of both agents (i.e. target loading), more agent was loaded meaning BSA NPs are not saturated by the agents yet. However, as Figure 4.3.B shows, more loading leads to a NP size increase which is not desired. Based on the trend implied from Figure 4.3, target loading of Dox and ICG was chosen to be 7.5% and 10%, respectively which resulted in actual loading of 5.69 ± 0.02% for Dox and 8.55 ± 0.01 % for ICG. It should be mentioned that the selection of unequal target loadings for the two agents was also made in light of further *in vitro* studies that showed unequal anti-cancer potency of ICG and Dox in the NPs.

4.3.3. Nanoparticle Characterization

Size distribution, UV-Vis absorbance spectrum and fluorescence emission spectrum of NPs before and after agent loading are shown in Figure 4.4. The average size of the NPs before loading was 75.47 ± 2.23 nm which increased to 102.6 ± 2.12 nm after loading both agents. As the size distribution in Figure 4.4.A shows, NPs are all smaller than 200 nm and have a narrow distribution both before and after agent loading. Zeta potential of NPs was -7.93 ± 159 mV before loading therapeutic agents and decreased to -27.0 ± 6.10 after loading which provides great colloidal stability. Appearance of the peaks at 476 nm and 798 nm in the absorbance spectrum of NPs confirm loading of Dox and ICG, respectively. Fluorescent emission of NPs excited at 476 nm and 798 nm, as shown in Figure 4.4.C, demonstrates that although Dox is still fluorescent within the NPs, ICG ‘s fluorescent has been quenched due to its aggregation in the NPs, which is favorable in PTT since all the receiving energy is released as heat. Figure 4.4.D shows SEM images of NPs which confirm spherical morphology and monodispersity.

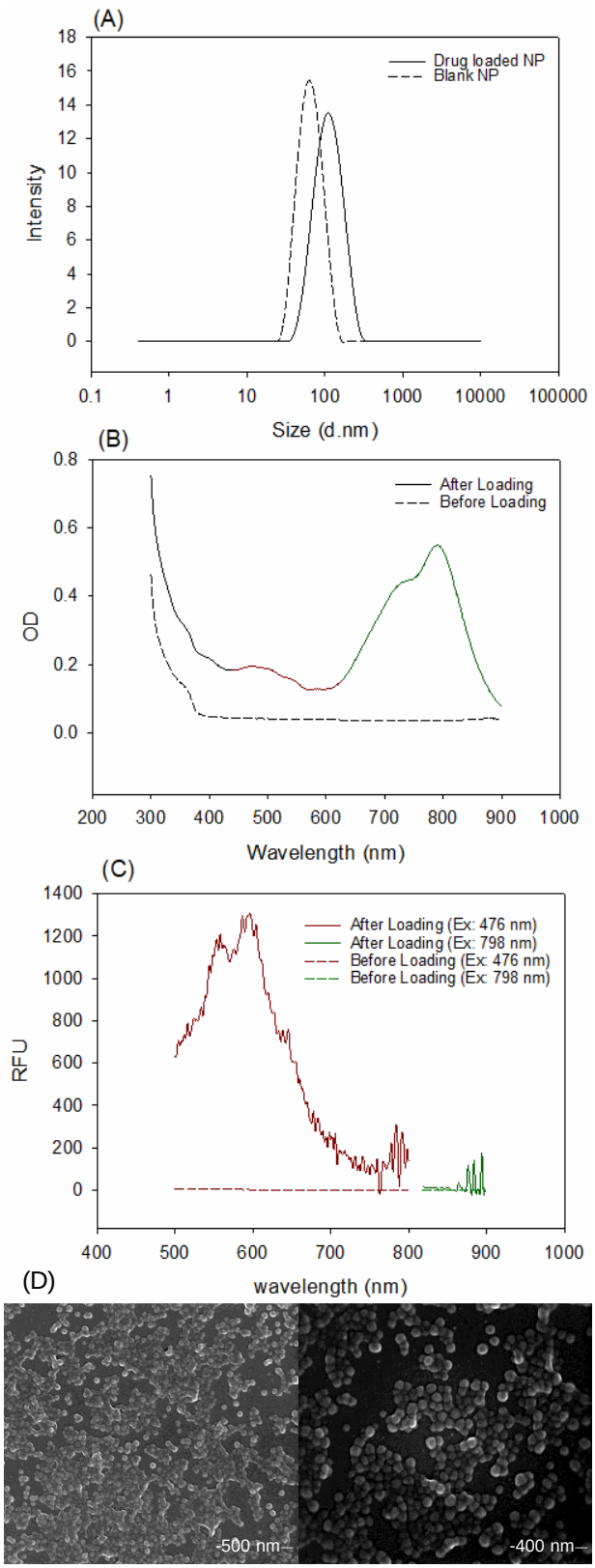

Figure 4.4. A) Size distribution, B) Absorbance spectrum and C) fluorescent spectrum of NPs before and after loading with Dox and ICG. D) SEM image of NPs after loading

4.3.4. NP Stability

High surface energy of nanomaterials leads to the adsorption of blood plasma proteins through different intermolecular forces such as electrostatic interaction, hydrophobic interactions, etc., leading to aggregate formation, which decreases blood circulation time of NPs severely.[114] Figure 4.5 shows that our BSA NPs are stable in size after 72 h incubation in cell media containing 10% serum at 37°C, as the NPs size has not changed

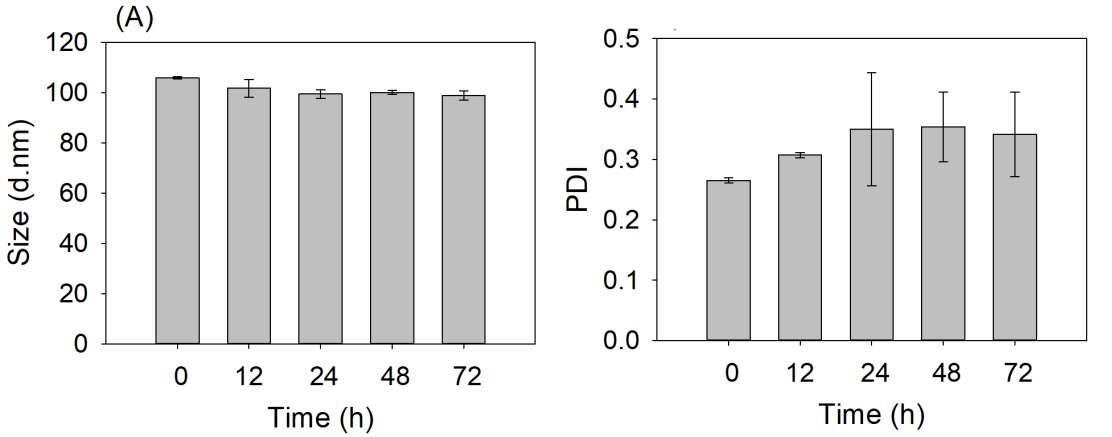

Figure 4.5. Stability of NPs size after 72 h incubation in cell media at 37°C.

significantly in this time frame. The highly negative zeta potential of the NPs may be one reason for this stability as it results in repulsion of biomolecules from the NPs.

4.3.5. Agent Release

In this part we studied releasing kinetics of the therapeutic agents from NPs *in vitro.* Figures 4.5.A and B show the cumulative release of Dox and ICG over 35 days.

The best mathematical kinetics model that fitted the observed release kinetics was the Peppas-Sahlin equation considering the lag time (Equation 1) with R-squared values of 0.9643 and 0.9920 for Dox and ICG, respectively.[85-86]

Released Fraction = $k_1 \cdot (t - T_{lag})^m + k_2 \cdot (t - T_{lag})^{2m}$ Equation 1

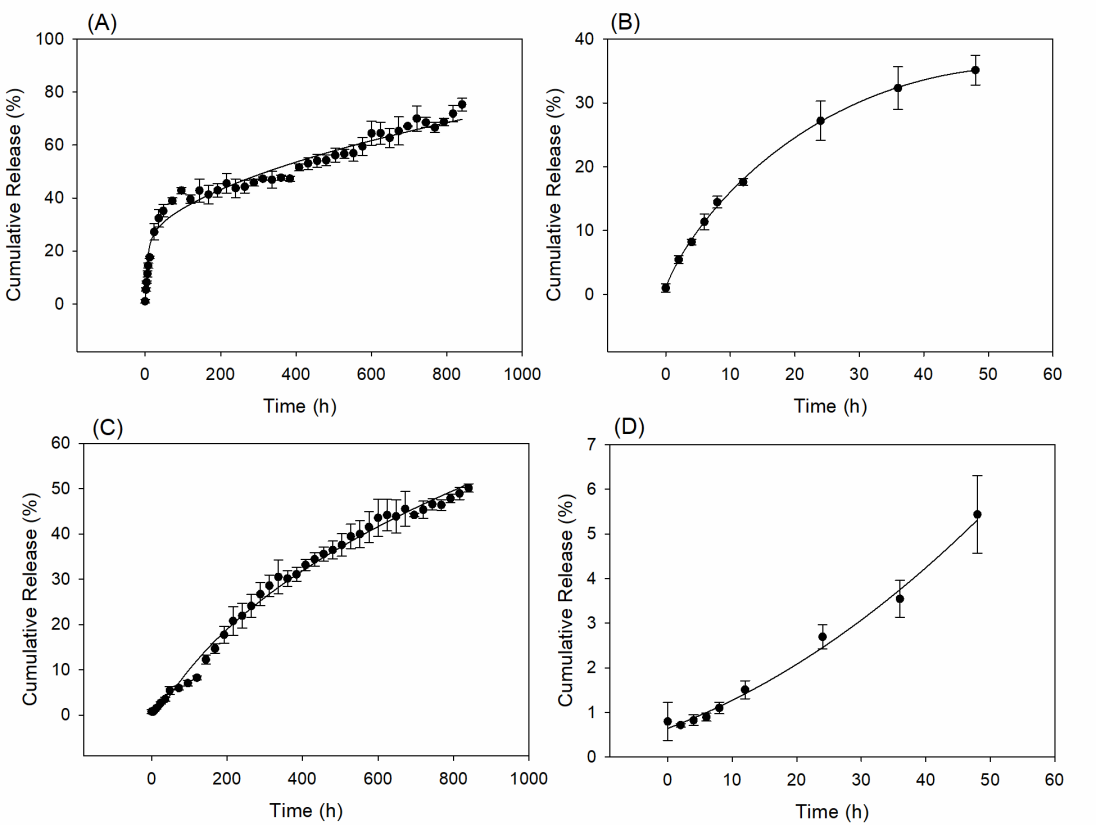

Figure 4.6. Cumulative release of Dox in A) 35 days and B) 48 h, and cumulative release of ICG in C) 35 days and D) 48 h.

Here k_1, k_2 and m are constants. According to the Peppas-Sahlin model, Fickian diffusion and polymer relaxation are the leading causes of drug release from our NPs.

Figure 4.6.A shows that there is an initial burst release of Dox, followed by a slow release from the BSA NPs. This can be explained by initial release of surface adsorbed Dox, followed by controlled release of the drug predominantly via diffusion across the crosslinked BSA network. Dox adsorption to the BSA molecule via intermolecular forces also prevents fast release of the drug.[112]

Release medium contained 5 mg/mL BSA to increase the stability of ICG upon release through absorption to the protein in the dialysis medium and thereby enable collection of more reliable data. Experiments showed that the absorbance of ICG in presence of this amount of BSA only decreases by 7% after 7 days, while this reduction is about 50% when BSA is absent (Appendix A). As discussed earlier in section 4.2.2 on agent loading, the secondary forces that are holding both loaded agents in the NPs are not only hydrophobic interactions but also electrostatic interactions. Having that said, we are expecting a sustained release of the agents from NPs since a relatively strong force is preventing the agent to diffuse out of the NPs to the release medium. Figure 4.6.C shows that only 50% of the dye releases after 35 days. In the first 2 days when the NPs will be irradiated, this value is 5% as Figure 4.6.D demonstrates. Sustained release of ICG not only prevents agent loss before NPs accumulate in the tumor and laser irradiation, but also keeps ICG molecules in the form of aggregates that quench its fluorescence and subsequently enable more photothermal efficiency.

4.3.6. Photothermal Conversion

In this section, the photothermal conversion ability of the NPs was determined. To be effective as a photothermal agent, NPs must provide sufficient heat for increasing the temperature of the tissue by at least 6°C. Figure 4.7 Shows temperature elevation of 100 µL of NP suspension in cell media with concentrations ranging from 0-0.5 mg/mL which

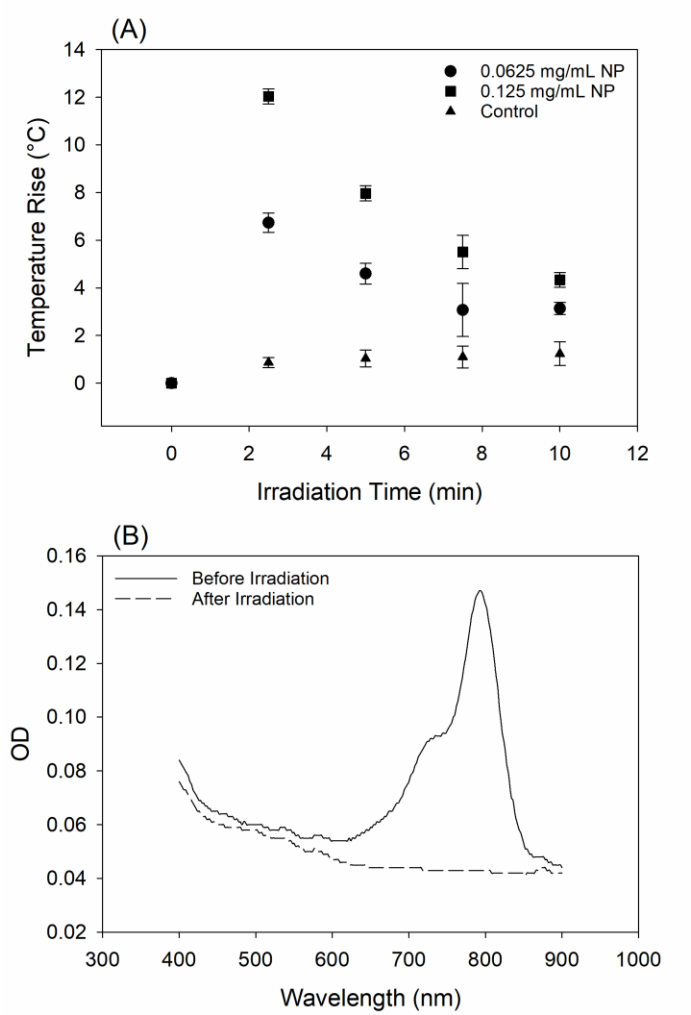

Figure 4.7. A) Temperature elevation of NPs with different concentrations upon 10 min irradiation with a 808-nm laser at 2 W/cm^2. B) UV-Vis absorbance spectrum of NPs before and after irradiation

are irradiated by a 808-nm laser at 2 W/cm^2 for 10 min. The highest temperature elevation was about 12°C when NP concentration was 0.125 mg/mL and about 7°C at 0.0625 mg/mL, whereas the temperature of the irradiated control solution which only consisted of the cell media did not change. The maximum temperature is reached after 2-3 min irradiation, after which the suspension starts to cool down due to the thermal instability of ICG. Figure 4.7.B confirms decomposition of ICG upon extended laser irradiation which, unfortunately, prevents further photothermal conversion. However,

several groups have reported that even this short-term temperature increase can provide an effective anti-cancer effect.[56, 115]

4.3.7. NP-Mediated Growth Inhibition Induced by Chemotherapy and PTT

In this section we studied the effect of NP concentration, incubation time of the NPs with cells prior to laser irradiation, and laser irradiation time on the viability of the cancer cells. Figure 4.8.A which shows the effect of NP concentration on cell viability demonstrates that when the NP concentration exceeds 0.125 mg/mL (which equates to a 12 °C temperature rise based on Figure 4.7), the viability of the cells is the same as the negative control in which cells are killed by treatment with methanol for 15 min. Therefore, a low dose of NPs can cause significant cell eradication. In fact, NPs at 0.03125 and 0.0625 mg/mL lead to sreduction in cell viability to ~ 45% and 27% of that of the NT control, respectively.

Figure 4.8.B compares viability of the cells which were treated with the same NP concentration, but with differing pre- irradiation incubation times. In this study, as in all three of these studies, cell media was changed with fresh pre-warmed media prior to laser irradiation to remove NPs that had not been internalized by the cells. Cell viability decreased significantly when incubation time was 3 h compared to when it was 1.5 or 0.75 h, which can be explained by a higher number of NPs that had been internalized into the cells at this time. Incubation times of 3 hr or longer resulted in complete cell death, with similar results as the negative viability control (MeOH treatment).

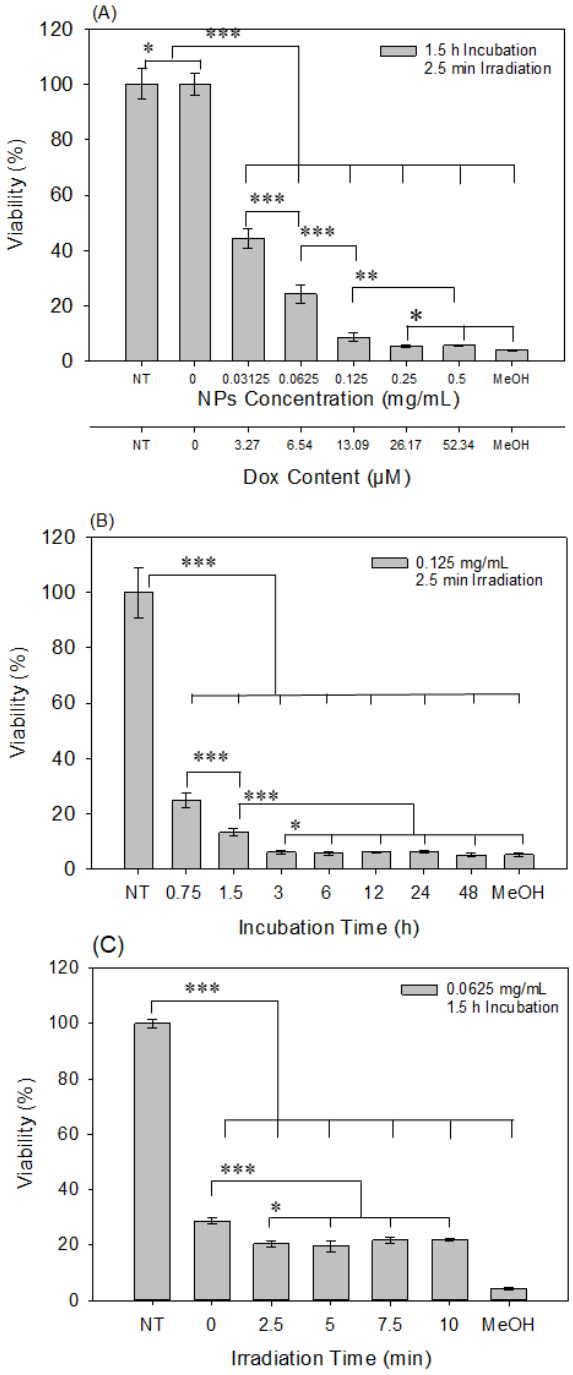

Figure 4.8. Effect of A) NP concentration, B) pre-irradiance incubation time and C) irradiation time on the viability of B16F10 cells. (*** P< 0.01, ** P<0.05, * P>0.05)

Figure 4.8.C shows that laser irradiation decreases cell viability compared to the group which is not exposed to the laser. However, elongating the irradiation time past 2.5 min

does not make a significant change in the viability of the cells. The data from previous section showing photothermal conversion of the NPs can clearly explain this observation, as the temperature starts to drop at t = 2.5 min due to ICG decomposition.

4.3.8. Study of DAMP Presentation

Immunogenic cell death is a crucial factor in enhancing the immunotherapy response.[89] It is important to prescribe a formulation with an optimum dosage that can induce maximal ICD. Three biomarkers that characterize ICD are calreticulin (CRT), 70 kDa heat shock protein (HSP70) and 90 kDa heat shock protein (HSP90), which are exposed on the cell membrane during stress.[19] CRT translocation to the surface of the cells can initiate an antitumor immune response. CRT can bind to CD91 receptors on the surface of DCs and macrophages, encouraging them to engulf the cancer cells and activating an immune response.[28] Translocated HSP70 can also activate the DCs and initiate the antitumor immune response by binding to CD40 and CD86 on the DC surface. HSP90 plays the same role by upregulating the CD91 signal from DCs and macrophages. HSP70 and HSP90 also can participate in the activation of $CD8^+$ T-cells that have the capability of killing the cancer cells if they are activated.[2] Thus, we are looking for a treatment that results in the maximum level of these three biomarkers detected.

In this part of the study we treated B16F10 cells with 0.0625 mg/mL ICG/Dox-loaded BSA NPs for 1.5 hr. Then, cells media was replaced with fresh pre-warmed media, and cells were irradiated with an 808 nm NIR laser diode for 2.5 min at the irradiance of 2 W/cm^2. After 24 h and 48 h of incubation of the cells post irradiation, we quantified the level of CRT, HSP70 and HSP90 on their plasma membrane using flow cytometry and compared the expression of these biomarkers against that of a control group of cells that

had not received any treatment (No Treatment, NT). NP concentration and irradiation time were chosen based on the results that were identified in previous section of cytotoxicity of the NPs against B16F10 cells. To reduce the side effects, we aimed to demonstrate DAMPs presentation on the cells that are treated with lowest possible dosage which is the reason why higher concentrations of NPs were not utilized.

Figure 4.9 shows histograms of fluorescence levels associated with the presentation of each of the three DAMPs. Figure 4.9 shows that this mild treatment could induce exposure of CRT (A), HSP70 (B) and HSP90 (C) since the cell population has shifted to

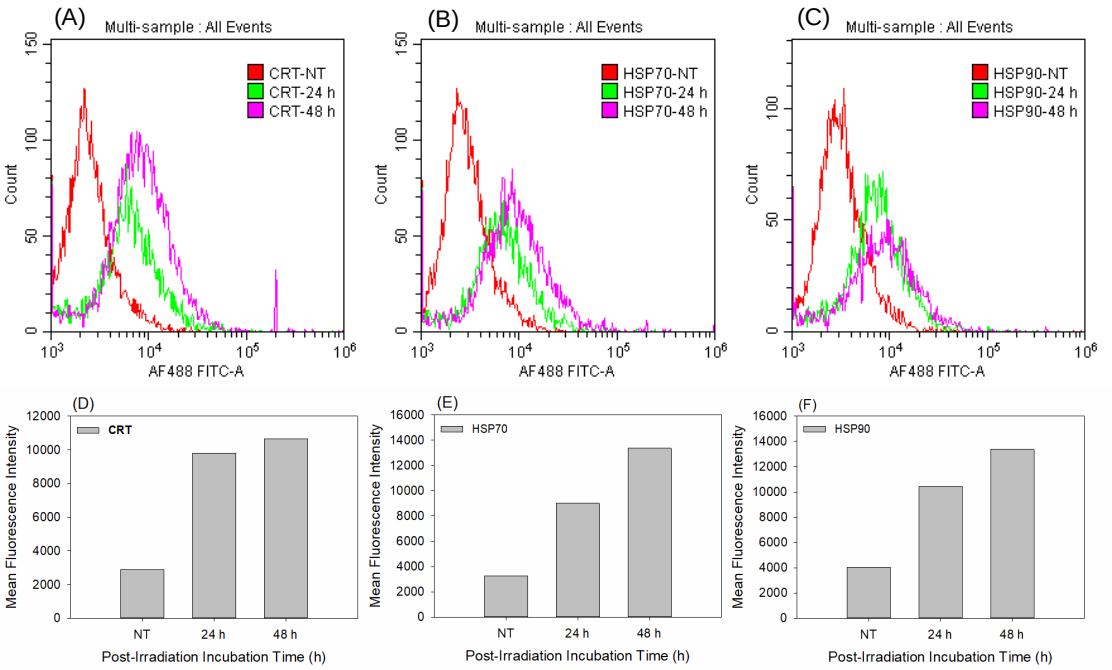

Figure 4.9. Surface expression of A,D) Calreticulin (CRT), B,E) HSP70 and C,F) HSP90 on B16F10 cells 1h, 24 h and 48 h after treatment with 0.0625 mg/mL BSA NPs and 2.5 min of laser irradiation at 2 W/cm^2.

the right and show higher fluorescent intensity compared to the NT group. In addition, the level of DAMP exposure increased over time for all three biomolecules as the peaks

have been shifted to the right and the mean fluorescent intensity increased as the incubation time increased from 24 to 48 hours.

4.4. **Conclusion**

In this work we developed nano-formulation to conduct a combination of chemotherapy and photothermal therapy to treat cancer. Dox and ICG were chosen as the chemotherapeutic and PTT agent since the FDA has approved the formulations that contain these agents individually. BSA was utilized to serve as a biocompatible, biodegradable and nontoxic carrier for these therapeutic agents. Due to the similar properties of BSA and HSA, we expect to obtain similar results when replacing the BSA with HSA which is approved by FDA for clinical use. Albumin allows significant loading of both ICG and Dox due to the presence of amino acids with charged functional groups and hydrophobic moieties within its molecular structure that provide strong intermolecular forces between the agent and the carrier. Several groups have identified the parameters that affect the properties of albumin NPs. By adjusting these parameters, we were able to make NPs with appropriate size and high loading content. Slow release of therapeutic agents and NP colloidal stability *in vitro* certified the capability of the NPs to deliver the therapeutic cargo to the tumor site.

A NIR laser that can penetrate through the tissue for 3-4 cm, is expected to be able to activate fairly low concentration of NPs and increase their medium temperature above about 6°C which is sufficient to kill the cancer cells. NPs with different concentrations demonstrated the ability to inhibit the proliferation of B16F10 metastatic melanoma cells *in vitro* when irradiated with an NIR laser. Treated cells also showed DAMP presentation, which is a characteristic of ICD. According to the fact that ICD is capable

of activating the immune system against any remaining cancer cells, promising *in vivo* results are expected. Furthermore, by encouraging immune cell accumulation in the region, our treatment can provide an enhanced tumor microenvironment for ICP therapy. Future work will focus on synergism of NPs with an ICP agent *in vivo*.

5. LARGE SCALE PRODUCTION OF NANOPARTICLES THROUGH A HIGH-THROUGHPUT FIBER REACTOR

5.1. Introduction

In previous chapters we described preparation of two types of nanoparticles (NPs) for cancer therapy and demonstrated their capability to inhibit the growth of cancer cells as well as induction of immunogenic cell death which enhances their therapeutic effect. However, we made a small amount of NPs each time (i.e. less than 5 mg per batch). In consideration of the need to translate this technology for clinical use, the development of a method that allows massive production of NPs yet maintains NPs' quality and uniformity for clinical tests and for introduction of the product to the market is critical. In this chapter we introduced a method for large scale production of polymeric NPs that are produced through the same methods as we made our NPs (Section 3.2.4 and 4.2.2).

Polymeric NPs have a wide range of applications in various industries and research areas. In the field of nanomedicine, polymeric NPs have been used mostly for drug delivery approaches to facilitate pulmonary, oral, transdermal, and intravenous delivery of therapeutic agents for the treatment of cancer, infection diseases, and inflammation diseases.[116-119] Polymeric NPs are also being used for diagnosis. Conjugates of polymeric NPs with antibodies and genes enable the detection of several biomarkers.[120] Polymeric NPs have also been utilized in the cosmetics industry for the delivery of skincare, antiacne, and antioxidant agents to the skin pores.[121] Highly permeable hair products based on polymer NPs are being fabricated to carry blood flow acceleration, cell activation, and androgen suppression agents.[121] Polymeric NPs have also been studied to be utilized for the separation and purification step in the bioprocesses downstream.[120] The food industry can also benefit from polymer-based NPs for the encapsulation of

phytonutrients and prebiotics.[122] Use of polymeric NPs has been reported in environmental applications, for instance, in bioremediation of soil.[123]

Several methods have been developed to prepare polymeric NPs such as nanoprecipitation, emulsion-diffusion methods, emulsion-evaporation, precipitation by salting-out, and emulsion polymerization.[63] Amongst all, nanoprecipitation, also known as solvent displacement method, has gained the most attention since it is a simple, fast, inexpensive, one-step process. Nanoprecipitation occurs due to the interfacial deposition of the polymer led by introducing a non-solvent which is miscible with the solvent.[124] Several studies have reported the scale-up of this process up using different types of reactors including impinging jets, single turbulent jets, rotor-stator mixers, static mixers stirred tank centrifugal pumps, and turbulent pipes.[65-66, 68, 125] Although favorable results have been reported through these methods, providing homogeneous yet fast mixing which directly affects the product characteristics such as size and polydispersity index (PDI) has remained an important limitation. Similarly, microfluidic processes recently developed enable very reproducible preparation of precursor droplets and consequently nanoparticles.[126] However, the throughput of microfluidic methods prevents their direct adaptation into large-scale manufacture.

In this work, we utilized a high-throughput fiber reactor that we previously utilized for the preparation of nanoparticles through a polymerization method[69] to produce NPs via nanoprecipitation using a model polymer, poly(lactic-co-glycolic acid) (PLGA), which is commercially available and inexpensive, and has been widely used in drug delivery applications. The reactor is made of a stainless-steel tube packed with a plurality of unidirectional stainless-steel fibers, which 1) provides a large surface area that the non-

solvent can be spread over in a thin film and 2) interface the polymer solution when it is introduced to perform nanoprecipitation. The main aim of the paper is to gain a good understanding of the reactor parameters that control NP characteristics to enable on-demand production of NPs with desired properties in a continuous process with the highest efficiency. The possibility of drug loading through this method was further investigated by loading a model dye, rhodamine 6G, within PLGA NPs.

5.2. Materials and Methods

5.2.1. Materials

PLGA (Purasorb PDLG 5002A, 50/50 DL-Lactide/Glycolide copolymer) was a gift from Corbion (Amsterdam, Netherlands). Poly(vinyl alcohol) (87-90% hydrolyzed, avg. mol wt. 30,000-70,000 Da) was obtained from Sigma Aldrich (St. Louis, MO). Rhodamine 6G was purchased from Coherent (Santa Clara, CA). ACS grade acetone was used. A Millipore Direct Q system produced ultrapure deionized water.

5.2.2. Reactor Set Up

A 2 ft long reactor packed with 8 μm diameter stainless steel fibers at a packing density of about 2000 fibers/mm^2 was used in this study. Two syringe pumps (Teledyne ISCO, Model 260D) with capacities of 100 mL and 270 mL were connected to the reactor input ports to feed the reactor. The pumps can either work simultaneously or independently. The reactor was surrounded by a copper cooling coil containing circulating water at set temperatures which is provided by a WKL 230 LAUDA Brinkmann chiller. The cooling coil is insulated with a polymeric foam to improve cooling efficiency. The product was collected from the reactor's output at the bottom. Figure 5.1 shows the described setup.

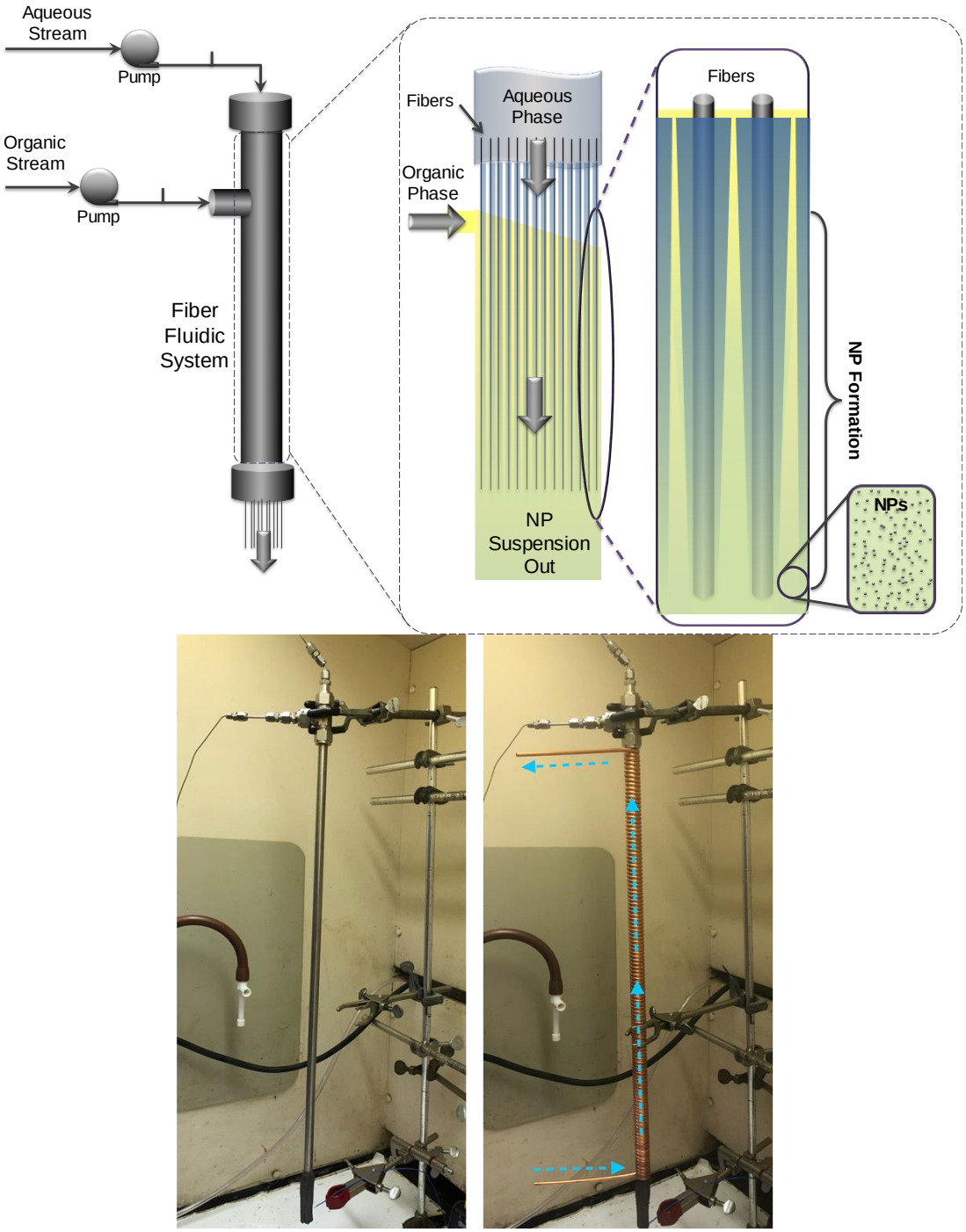

Figure 5.1. Reactor setup.

5.2.3. Fabrication of PLGA NPs Using The Fiber Reactor

PLGA NPs were made through nanoprecipitation. Briefly, syringe pump A and B were filled by 2.5-15 mg/mL solution of PLGA in acetone and 5-25 mg/mL aqueous solution of PVA, which is used as a stabilizer, respectively. Pumps were turned on at the same time to start feeding the reactor simultaneously at set flowrates while the chiller was operating at constant temperature (3°C – 15 °C). The output stream, which contained the formed NPs, was collected and used for further studies. The temperature of the output flow was also recorded by a thermocouple. After each prodcution process, pumps A and B were refilled with pure acetone and pure water to clean the reactor by purging water and acetone, respectively.

5.2.4. Loading Rhodamine 6G within PLGA NPs using the fiber reactor

To confirm the possibility of drug loading using the fiber reactor, we prepared rhodamine 6G-loaded PLGA NPs in the fiber reactor. Pump A fed a 5 mg/mL PLGA solution in acetone containing 0.01 mg/mL rhodamine 6G to the reactor at 3.5 mL/min, while pump B fed a 10 mg/mL PVA aqueous solution at 25 mL/min. The cooling coil was maintained at 10°C.

5.2.5. Size and PDI Measurement

NP size and polydispersity index (PDI) were determined by dynamic light scattering using a Malvern ZetaSizer Nano ZS instrument. Measurements were done at 24°C, and the PVA solution was selected as the dispersant. The viscosity and refractive index (RI) of PVA solutions at specific concentrations matching each sample were measured before sizing, using a glass viscometer and refractometer (data not shown). These values were input to the ZetaSizer software for proper data analysis.

5.2.6. Morphology of NPs

NPs were deposited on silicon wafers, , dried at room temperature, and coated with 2 nm Iridium using a Quorum Technologies EMS150T ES sputter coater. NPs were then visualized using a FEI Helios NanoLab 400 Dual Beam scanning electron microscope (SEM).

5.2.7. Yield Measurement

40 mL aliquots of NPs were centrifuged for 1 h at 75600 ×g (Avanti J-26 XPI, Beckman Coulter, US). Then, the supernatant was discarded, and NPs were resuspended in water and lyophilized (Labconco FreeZone) in pre-weighed vials. The net weight of NPs was measured after lyophilization, and the rate and yield of production were calculated.

5.3. Results and Discussion

Nanoprecipitation occurs due to the nucleation of the polymer and growth of the nuclei, which can either end up with aggregation of the NPs or stabilization of the NPs mediated by a stabilizer such as a surfactant.[127] The nucleation and growth rate, which directly influence NPs size, are controlled by saturation. Saturation is defined as S= C/C* where C is the real-time concentration of the solute, and C* is the solubility of the solute in the mixed solution. When the mixing happens gradually, C and C* gradually change; thus, the level of saturation varies over time until full mixing is achieved. This means that the NPs that are formed in this period are affected by changing conditions, resulting in a variety of sizes and, thus, broad size distribution. On the other hand, if the mixing time is reduced to an amount less than the time which is required for NP formation, all the NPs form under the same saturation conditions, leading to uniform NPs with low PDI.[128] Therefore, mixing time in nanoprecipitation has a crucial role and it is an important issue

to consider when the process is scaled up. In large-scale nanoprecipitation, the focus is on keeping the Damköhler number less than 1 by rapid mixing of the nonsolvent with the polymer solution. Damkohler number for nanoprecipitation is defined as $Da_p = \tau_{mix}/\tau_f$. Where τ_{mix} and τ_f are mixing time and formation time of NPs, respectively.

In our system, when the feed streams are introduced to the fiber reactor, they are divided into a plurality of sub-streams with a diameter of a few μm.[69, 72] Figure 5.2 shows a scheme representing the phase distribution inside the reactor. The flows occupy and share

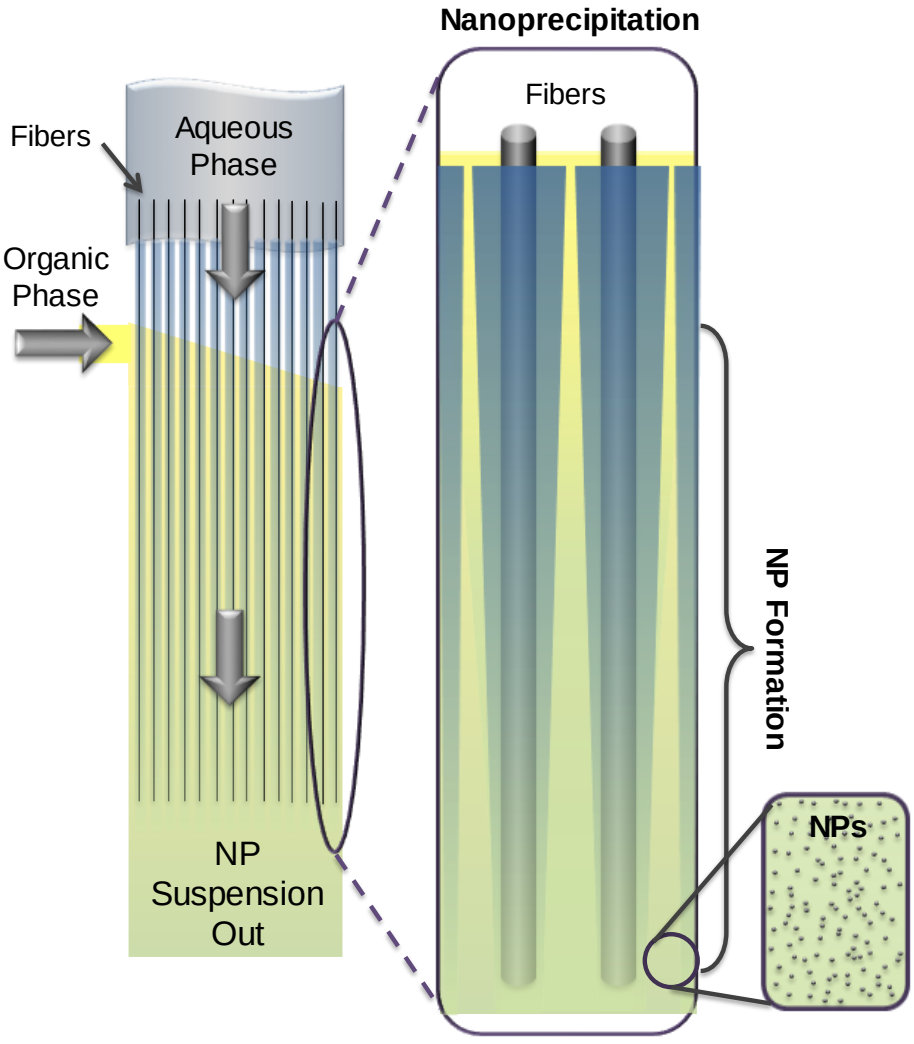

Figure 5.2. Schematics of an inside cross section of the reactor.

the void area between the fibers based on the ratio of their flow rates. The aqueous flow is expected to be in touch with the hydrophilic ss fibers while the organic phase is in the middle, focused in between the aqueous streams. Thus, the maximum diffusion path is half of the distance between two fibers, which is W_d = 6.624 µm. Assuming unidirectional mass transfer (from the organic phase to the aqueous phase) and, according to Fick's second law of diffusion, the required time for the complete mixing is calculated to be 1.78 ms. As long as this value is less than the aggregation time of the polymer, the reactor's products are expected to be uniform.

NP formation, as earlier discussed, includes nucleation and growth of the polymer aggregates under saturation. Therefore, the rate of NP formation can be estimated according to the classical theory of nucleation.[129] The nucleation rate of the polymer per volume unit and time unit is defined as:

$$J = N_0 \upsilon e^{-\frac{16\pi\sigma^3 V_s^2}{3k^3T^3(LnS)^2}} \qquad \text{Equation 1}$$

where S is the degree of saturation, N_0 is the initial number of molecules of solute per unit volume, υ is the frequency of molecular transport to the solid-liquid interface, σ is the interfacial tension at the solid-liquid interface, V_s is the volume of a solute molecule, k is the Boltzmann constant, and T is the temperature. The frequency of molecular transport can be estimated by:

$$\upsilon = \frac{kT}{3\pi a^3 \eta} \qquad \text{Equation 2}$$

where η is the viscosity of the solution and “a” the mean effective diameter of the diffusing species.[130] In general, Equation 1 suggests that as the degree of saturation

decreases, the rate of nucleation and NP formation decreases. For a specific mixing time, τ_{mix}, a decreased rate of nucleation would result in an increased NP formation time, τ_f, and thereby a decreased Da_p. Therefore, the NP properties are controlled by formation process as opposed to the mixing quality.

5.3.1. Effect of PLGA (Copolymer) Concentration

Figure 5.3 shows the effect of the polymer concentration on NP size and PDI. PDI values

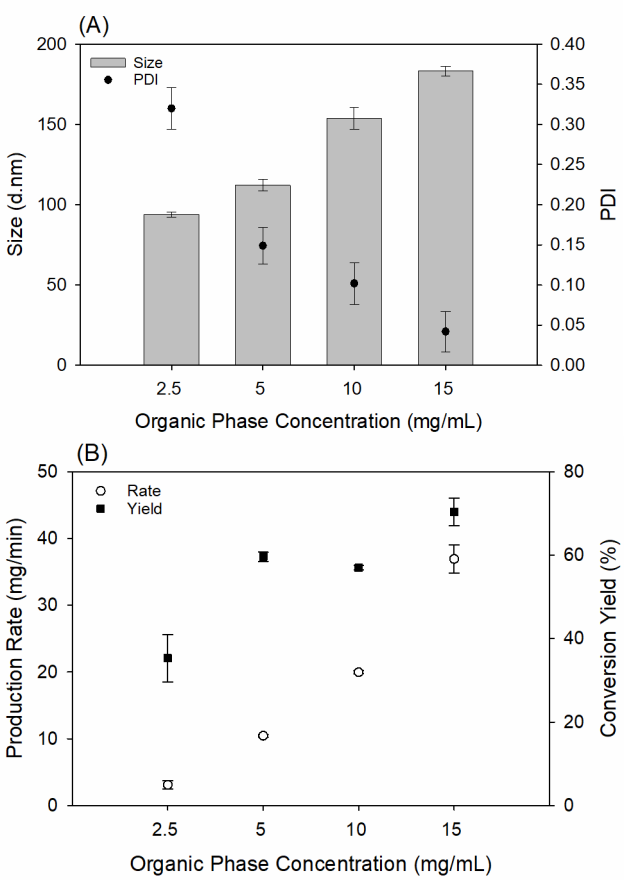

Figure 5.3. Effect of PLGA concentration of A) nanoparticles size and PDI and B) production rate and conversion yield. For this study, the flowrate of the PLGA solution (organic stream) was 3.5 mL/min and the concentration and flowrate of the PVA solution (aqueous stream) was 10 mg/mL and 25 mL/min, respectively.

decreased as the PLGA concentration increased. Due to the lower degree of saturation in lower concentrations, the NP formation time increases. It means that more time is

required for the nuclei to growth and reach a thermodynamic equilibrium state. Therefore, agglomeration of the unequilibrated nuclei which formed in this time occurs. This is the reason why PDI increases when the feed polymer concentration decreases. However, increasing the concentration of the polymer solution led to the formation of larger NPs. This observation can be again explained by the effect of saturation on the nucleation rate and to a greater importance, on the growth rate. Higher concentration leads to higher S, which causes a higher rate of nucleation and growth.[131] At higher saturation level, a greater extent of the polymer tends to precipitate out of the solution phase which provides the required NP building units for the nuclei to growth. Figure 5.3.B shows the variation of production rate and yield percent versus PLGA concentration. Here, production rate refers to the recovery rate of formed and centrifuged NPs, in mg/min. As expected, adding more polymer in the feeding stream results in a higher production rate, which is the result of the higher nucleation rate (higher number of NPs) as well as the higher growth rate (more massive NPs).

5.3.2. Effect of Operation Temperature

As previously explained, the reactor temperature was controlled by circulating water through a copper coil wrapped around the fiber reactor. The organic feed was kept at room temperature before running the reactor, while the aqueous feed was input at 4°C. Figure 5.4 shows the effect of operating temperature on the NPs' size and PDI. Neither the NP diameter nor the PDI changed upon changing the temperature of the cooling coil although, based on equation 1, a significant effect of temperature on size was expected. There are a couple of reasons that could explain the lack of diameter variation with temperature. For instance, temperature not only affects the nucleation rate but also influences the saturation concentrations, diffusion rates, and the solution's viscosity. Thus, these contrasting effects may have been neutralized and led to the experimental observation. This observation is noteworthy from an industrial standpoint since we can eliminate a significant source of energy consumption and instrumentation for temperature adjustment.

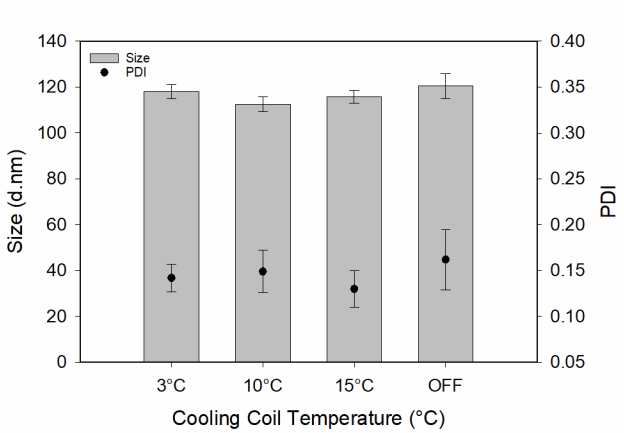

Figure 5.4. Effect of temperature of cooling coil on NP size and PDI. For this study concentration and flowrate of the PLGA solution (organic stream) was 5 mg/mL and 3.5 mL/min and that of the PVA solution (aqueous stream) was 10 mg/mL and 25 mL/min, respectively.

5.3.3. Effect of The Ratio of The Flowrates (Organic Stream / Aqueous Stream)

As Figure 5.5 shows, by increasing the solvent/non-solvent flowrate ratio from 0.06 (1.5 mL/min organic vs. 25 mL/min aqueous flow rates) to 0.1 (2.5 mL/min organic vs. 25 mL/min aqueous flow rates), NPs size decreased, but stayed constant as the organic flow rate and thereby the organic/aqueous ratio further increased. Increasing the flowrate ratio not only increases the amount of the polymer in the final solution but also increases the total volume of the mixture. Thus, although the saturation degree decreases due to increasing the flow rate of the polymer solution while the non-solvent flow rate remains constant, the change is slight. On the other hand, increasing the organic phase volume fraction influences the mixture's viscosity, which can explain our observation.

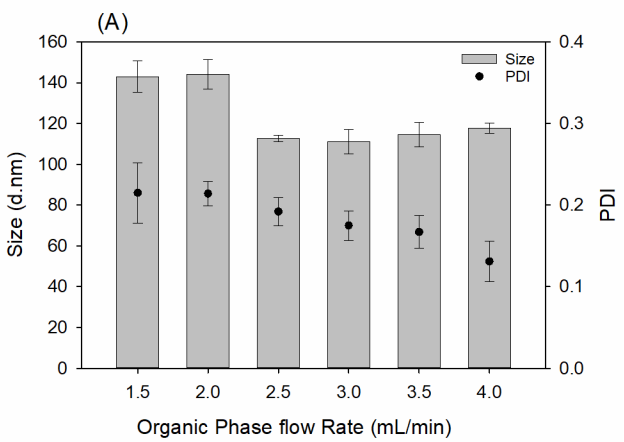

Figure 5.5. Effect of the flowrate ratio on NP size and PDI. For this study, the concentration and flowrate of the PVA solution (aqueous stream) was 10 mg/mL and 25 mL/min, respectively. The concentration of PLGA solution was 5mg/mL and its flowrate varied from 1.5 to 4 mg/mL.

5.3.4. Effect of PVA (Stabilizer) Concentration

The stabilizer comes to part at the end of the nanoprecipitation process and stops further growth of the NPs. So, as the concentration of the stabilizer, which is PVA in this study, increases, NP size decreases. This fact is confirmed by our data presented in Figure

5.6.A. The presence of a stabilizer is required to control NP size and prevent aggregation. However, as the data in Figure 5.6.B shows, the production rate decreases with increasing PVA concentration. While this might be simply a result of decreased recovery rate via centrifugation, for further industrial designs, this factor should be balanced to achieve both optimized production rate and size.

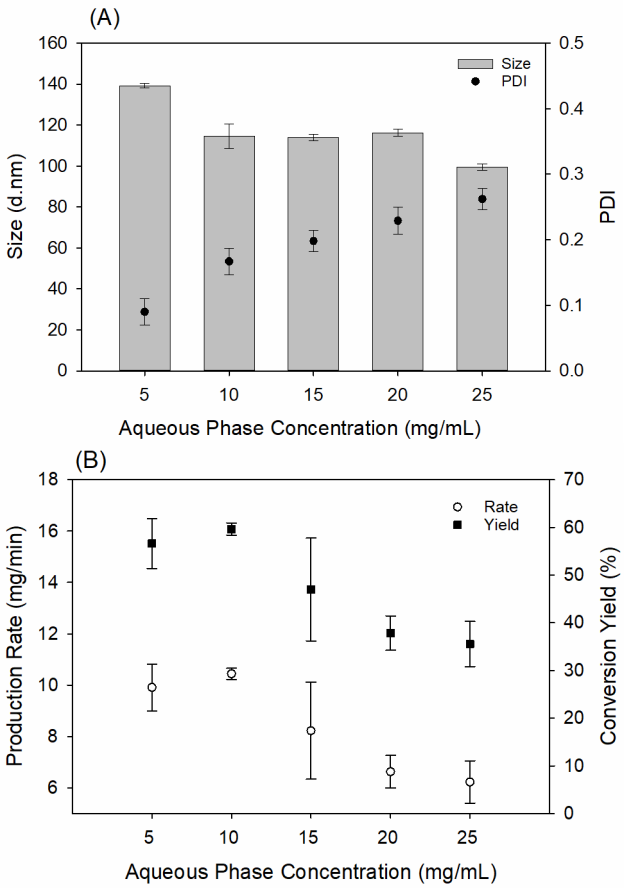

Figure 5.6. Effect of PVA concentration on aqueous phase of A) nanoparticles size and PDI and B) production rate and conversion yield. For this study, the flowrate of the PVA solution (aqueous stream) was 25 mL/min and the concentration and flowrate of the PLGA solution (organic stream) was 5 mg/mL and 3.5 mL/min, respectively.

5.3.5. Loading of Mimic Payload

Rhodamine 6G was the model payload that we used to load within the PLGA NPs on a large scale using the fiber reactor. Figure 5.7.A shows the centrifuged NP pellet, clearly showing entrapment of rhodamine with the polymer NPs from the pink color. The morphology of the resulting NPs is shown in Figures 5.7.B, SEM images of the NPs. These images confirm the uniformity of produced NPs. Figure 5.7.C shows the fluorescence spectrum of the NPs. The presence of the peak at 548 nm in the fluorescence spectrum confirms that the loading was successful. As Figure 5.7.D shows, rhodamine loaded NPs had narrow size distribution similar to that obtained with blank PLGA NPs.

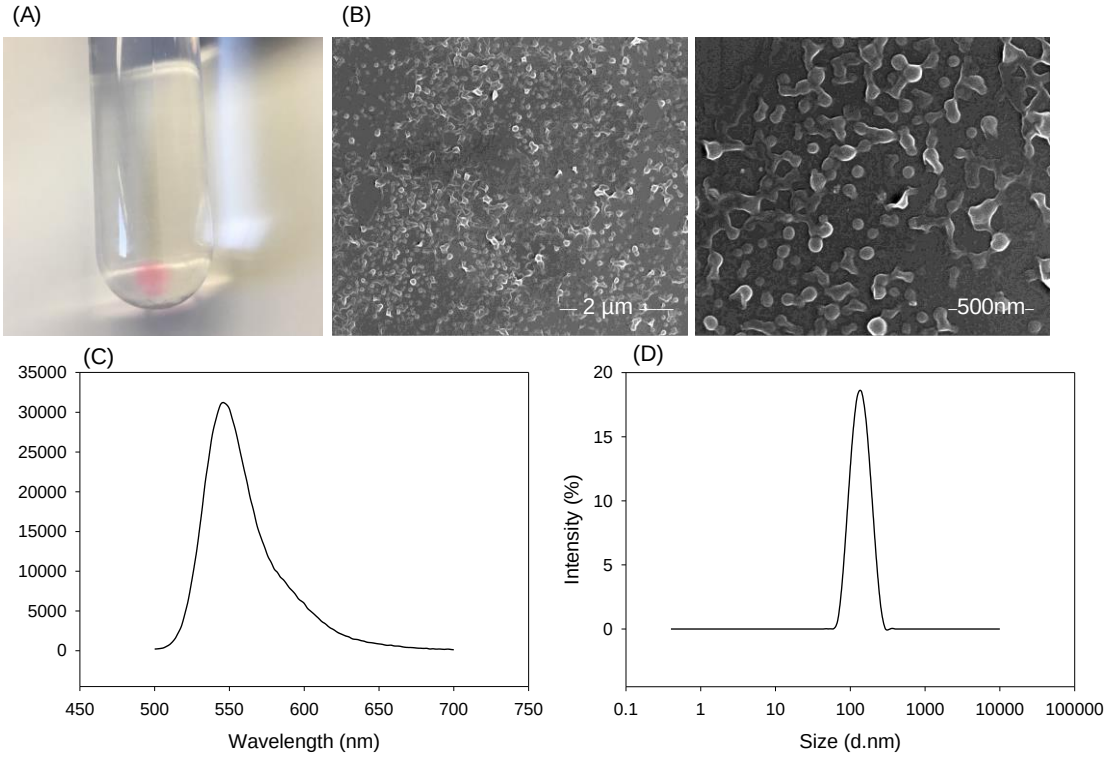

Figure 5.7. A) Rhodamine 6G loaded PLGA nanoparticles and their B) SEM images, C) Fluorescent spectrum (excited at 480 nm) and D) Size distribution.

The average size and PDI of these NPs were 123.94 ±2.02 nm and 0.130 ±0.018, respectively.

5.4. Conclusion

In this work, we introduced a facile and efficient process to make polymeric NPs in a continuous process through nanoprecipitation, which is one of the most common methods, utilizing a fiber reactor system. The fiber reactor is relatively small and straightforward instrument with no moving parts. Results show successful production of monodisperse NPs on a large scale. NP size, which is the most crucial feature of NPs utilized in all of the biomedical applications, was readily adjusted by considering the process factors discussed in the paper, including the concentration and flow rate ratio of the feed streams. The concentration of feed streams had the most influence on the size of the final product. We also fabricated NPs that encapsulated a fluorescent dye, rhodamine 6G, on a large scale. The straightforward design and easy operation of the fiber reactor together with the high level of control over NP size and PDI make this system an excellent candidate for use in the pharmaceutical industry for scale up of nanomedicine formulations, including the formulations that we prepared earlier in this project. Both poly(lactic acid)-*b*-poly(ethylene glycol) NPs and albumin NPs are made through the same procedure through which we made PLGA NPs in this chapter. Therefore, we expect to be able to produce our NPs through this continuous process with adjusted process parameters using the knowledge that we gained in this part of the study.

6. CONCLUSION AND FUTURE WORK

Immunotherapy is a novel approach for cancer treatment which either activates or enhances the patients' immune system against cancer cells. Immune checkpoint (ICP) blockade is a common type of immunotherapy in which an antibody is delivered to the tumor to bind to and block the inhibitory checkpoint molecules presented on the tumor cells which protect them from the immune system.[8] However, checkpoint blockade antibodies can only avoid the suppression of an existing immune response.[132] This is believed to be the reason why ICP therapy has shown low response rates in patients who do not have pre-existing antitumor immunity.[132] Therefore, a pretreatment which leads to activation or restoration of an antitumor immune response by inducing immunogenic cell death (ICD) is required to alter the tumor microenvironment and enhance ICP therapy outcomes.

The ideal pretreatment would not only result in antitumor immunity but would also have the lowest possible side effects. The main reason for why traditional anticancer treatments have severe side effects is that the therapeutic agent affects both normal and cancer cells.[133] As a result, the drug interferes with the normal activity of healthy cells and only a small fraction of the administered drug reaches the cancer cells. Moreover, the half-life of free drugs is relatively low since they get cleared from the blood circulation through renal filtration before or after being metabolized.[134] Therefore, a higher dosage is required to induce the desired therapeutic effect, which in turn reinforce the harmful effect that the drug has on normal cells and results in more severe side effects.

In this work, we aimed to address these two main problems. Several studies have investigated the therapies which can induce ICD through which the tumor’s

microenvironment is altered and conductive to immune cells. Heat mediated therapies such as photothermal therapy (PTT) that can raise the temperature of the cells can be included in this list if the heat dosage is controlled.[13, 135] Some chemotherapeutic agents, such as anthracyclines, can also induce ICD. In this work, we took advantage of both PTT and chemotherapy to induce ICD. We used doxorubicin, a member of the anthracycline family, for chemotherapy, and indocyanine green (ICG), a dye which absorbs light at 808 nm and converts the energy to the heat, for PTT. It is worth mentioning that the FDA has approved both of the agents for clinical use for cancer chemotherapy and biomedical imaging, respectively.[91]

Nanomedicine provides a solution to address the problems associated with side effect and short half-life of the small molecules. Entrapment of the active drug within a biocompatible nanomaterials with optimized size, i.e., smaller than 200 nm, can enhance its delivery to the tumor via enhanced permeability and retention (EPR) effect with minimum effect on normal cells.[57, 136] Appropriate nanoparticle (NP) designs can also protect the active agents from recognition by the immune system, thus increasing the agent's circulation time.[57]

In this work, we designed NPs using biodegradable, biocompatible polymers, poly(lactic acid)-*b*-poly(ethylene glycol) (PLA-PEG) and bovine serum albumin (BSA). NPs were characterized to confirm that they meet the criteria for drug delivery. Both NPs were spherical with an average diameter of less than 110 nm, which enable them to diffuse through the tumor vasculature efficiently. Absorbance and fluorescence spectra of the NPs confirmed the successful and sufficient loading of the therapeutic agents within the NPs.

In vitro releasing profile of the agents from NPs showed that both agents remain within the NPs for a time required for the NPs to reach to the tumor region. Although ICG degrades after its use as a photothermal agent, Dox stays within the NPs for up to about 30 days. Thus, NPs are therapeutically effective for an extended period of time. The ability of the NPs to elevate the temperature of their medium upon laser irradiation was tested to identify the heat dosage.

The NP treatment efficiency was first confirmed *in vitro* in this work using human and murine cells. Human metastatic breast cancer cells, MDA-MB-231, as a model cell line, were treated with ICG/Dox loaded PLA-PEG NPs accompanied with 808 nm laser irradiation. A low dosage of this treatment successfully eradicated most of the cells. We showed a suspension of 0.03. mg/mL of NPs accompanied with less than 3 min laser irradiation is able to reduce cell viability significantly. In this work, release of adenosine triphosphate (ATP) and high mobility group box 1 (HMGB1) from the cells and exposure of calreticulin (CRT) on the surface of the cells confirmed that MDA-MB-231 cells underwent ICD, which was one of the main goals of this project. Similar results (exposure of CRT, heat shock protein 70 –HSP70– and HSP90 on the cell membrane) were obtained when ICG/Dox loaded BSA NPs were used to treat mouse melanoma, B16F10 cells. Therefore, both of the NPs were able to leave the desired impact on the cells when irradiated with a laser.

Despite the promising results that were achieved in this part of the project, further work is required to enhance the treatment and confirm its efficacy in animal models and human patients. Some of the suggested future work follows:

1-Replacing human serum albumin (HSA) with BSA in agent loaded albumin NPs: While BSA was utilized in the studies described in Chapter 4, being a protein of bovine origin, BSA cannot be utilized as a therapeutic agent in humans. HSA would induce lower immunogenicity when administered to humans. It is also the only form of albumin which is approved by the FDA for clinical use.[107] Because of this, future work will require demonstration of combinatorial chemotherapy and PTT utilizing HSA-based NPs. HSA and BSA are very similar in structure and physical properties. Thus, we expect that the protocols developed for the preparation of BSA NPs will translate easily for the preparation of HSA NPs with similar properties. In addition, we expect to see similar results in terms of anti-cancer effect and ICD when cells are treated using HSA NPs as long as the physiochemical properties of the carrier such as NP size, zeta potential and agent loading are maintained.

2- Modification of NPs with a targeting molecule: It is highly suggested to functionalize the NPs with a molecule like folic acid, transferrin, or a monoclonal antibody that is specific to proteins that are overexpressed in cancer cells to increase the targeting ability of the NPs, which in the current design is only based on the EPR effect. Easy functionalization of albumin NPs is feasible due to the presence of several functional groups in albumin, including primary amines and carboxylic acids that lend themselves to easy bioconjugation. However, a slight change is required to be able to attach any ligand to the PLA-PEG NPs. In this work, methoxy-terminated PEG was used to synthesize the block copolymer, which makes the polymer almost chemically inert. In the future, the use of PEG terminated in a carboxylic acid group or primary amine group could offer a

reactive functional group to the NPs through which they could be further functionalized.[137]

3- Signaling with the immune system: Although we showed that NP-mediated therapy induces the patterns through which cancer cells can communicate with immune cells, it is necessary to confirm this communication. At the first level, this study involves an investigation of immature dendritic cell (DC) activation. To achieve this, DCs can be co-cultivated with cancer cells that are treated with NPs and NIR laser irradiation. The interaction of damage associated molecular patterns released from the cancer cells and the DCs is expected to result in DC maturation, which can be detected via immunochemistry.[138-139] In addition, the next step would be to study the alteration of macrophages, which are in contact with the treated cancer cells, to the M1 phenotype, which is capable of invading cancer cells as opposed to the M1 phenotype, which helps the tumor to grow.[140-141]

4- *In vivo* study of synergism of immunotherapy and NP-mediated PTT and chemotherapy combinatory treatment of tumor: the ultimate goal of this project is to enhance the effect of immunotherapy. Therefore, it is essential to conduct an *in vivo* study to prove that the treatment proposed in this dissertation has a positive effect on the immunotherapy results. This study includes administration of an ICP therapeutic agent such as anti-PD-1 or anti-PD-L1 together with our NP/mediated PTT and chemotherapy and study the synergism of the two treatment to prevent the growth of the injected tumor. The animal models that are used in this study must possess active immune system due to the dependence of ICP therapy to the patient's immune system. Thus, we should either

consider using the animal tumor model and animal checkpoint inhibitors or inject human immune cells to immunocompromised animals.[109]

5 – Scale up preparation of ICG and Dox-loaded PLA-PEG and albumin NPs. Finally, the NPs need to be produced in massive quantities when they are going to be introduced to the market. This motivated us to establish an efficient method to fabricate NPs in large scales using a high throughput fiber reactor. We produced PLGA NPs as a model polymer via nanoprecipitation. The effect of several parameters on the production yield and quality was identified. This knowledge can be further used to produce high-yield of the desired NPs. In the future, the production of PLA-PEG NPs and BSA NPs, which were prepared in this project, will be produced using the fiber reactor.

APPENDIX SECTION

Appendix A. Stability of Indocyanine Green in Albumin Solutions

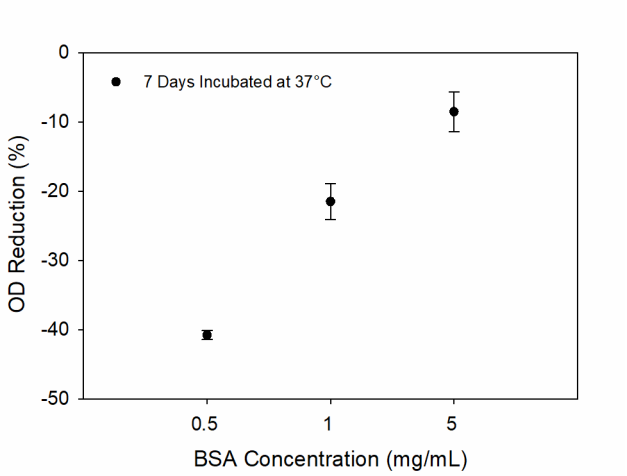

Effect of BSA presence on the stability of ICG in 7 days. Initial concentration of was 0.1 mg/mL

REFERENCES

1. Immune Checkpoint Inhibitors. https://www.cancer.gov/about-cancer/treatment/types/immunotherapy/checkpoint-inhibitors.

2. Kroemer, G.; Galluzzi, L.; Kepp, O.; Zitvogel, L., Immunogenic cell death in cancer therapy. *Annual review of immunology* **2013,** *31*, 51-72.

3. Yi, X.; Wang, F.; Qin, W.; Yang, X.; Yuan, J., Near-infrared fluorescent probes in cancer imaging and therapy: an emerging field. *International Journal of nanomedicine* **2014,** *9*, 1347.

4. Cancer Facts & Figures 2020. https://www.cancer.org/content/dam/cancer-org/research/cancer-facts-and-statistics/annual-cancer-facts-and-figures/2020/cancer-facts-and-figures-2020.pdf.

5. Minami, M.; Matsumoto, S.; Horiuchi, H., Cardiovascular side-effects of modern cancer therapy. *Circulation Journal* **2010**, 1008100855-1008100855.

6. Wang, D. Y.; Okoye, G. D.; Neilan, T. G.; Johnson, D. B.; Moslehi, J. J., Cardiovascular toxicities associated with cancer immunotherapies. *Current cardiology reports* **2017,** *19* (3), 21.

7. Salem, J.-E.; Manouchehri, A.; Moey, M.; Lebrun-Vignes, B.; Bastarache, L.; Pariente, A.; Gobert, A.; Spano, J.-P.; Balko, J. M.; Bonaca, M. P., Cardiovascular toxicities associated with immune checkpoint inhibitors: an observational, retrospective, pharmacovigilance study. *The Lancet Oncology* **2018,** *19* (12), 1579-1589.

8. Sharma, P.; Allison, J. P., The future of immune checkpoint therapy. *Science* **2015,** *348* (6230), 56-61.

9. Haslam, A.; Prasad, V., Estimation of the percentage of US patients with cancer who are eligible for and respond to checkpoint inhibitor immunotherapy drugs. *JAMA network open* **2019,** *2* (5), e192535-e192535.

10. Wu, A. A.; Drake, V.; Huang, H.-S.; Chiu, S.; Zheng, L., Reprogramming the tumor microenvironment: tumor-induced immunosuppressive factors paralyze T cells. *Oncoimmunology* **2015,** *4* (7), e1016700.

11. Moy, A. J.; Tunnell, J. W., Combinatorial immunotherapy and nanoparticle mediated hyperthermia. *Advanced drug delivery reviews* **2017,** *114*, 175-183.

12. Inoue, S.; Setoyama, Y.; Odaka, A., Doxorubicin treatment induces tumor cell death followed by immunomodulation in a murine neuroblastoma model. *Experimental and therapeutic medicine* **2014,** *7* (3), 703-708.

13. Sweeney, E. E.; Cano-Mejia, J.; Fernandes, R., Photothermal therapy generates a thermal window of immunogenic cell death in neuroblastoma. *Small* **2018,** *14* (20), 1800678.

14. The Nobel Prize in Physiology or Medicine 2018. https://www.nobelprize.org/prizes/medicine/2018/summary/.

15. Kourie, H. R.; Klastersky, J. A., Side-effects of checkpoint inhibitor-based combination therapy. *Current opinion in oncology* **2016,** *28* (4), 306-313.

16. Krysko, D. V.; Garg, A. D.; Kaczmarek, A.; Krysko, O.; Agostinis, P.; Vandenabeele, P., Immunogenic cell death and DAMPs in cancer therapy. *Nature Reviews Cancer* **2012,** *12* (12), 860.

17. Gardai, S. J.; Bratton, D. L.; Ogden, C. A.; Henson, P. M., Recognition ligands on apoptotic cells: a perspective. *Journal of leukocyte biology* **2006,** *79* (5), 896-903.

18. Kharitonenkov, A.; Chen, Z.; Sures, I.; Wang, H.; Schilling, J.; Ullrich, A., A family of proteins that inhibit signalling through tyrosine kinase receptors. *Nature* **1997,** *386* (6621), 181-186.

19. Tesniere, A.; Panaretakis, T.; Kepp, O.; Apetoh, L.; Ghiringhelli, F.; Zitvogel, L.; Kroemer, G., Molecular characteristics of immunogenic cancer cell death. *Cell Death & Differentiation* **2008,** *15* (1), 3-12.

20. Arispe, N.; Doh, M.; Simakova, O.; Kurganov, B.; De Maio, A., Hsc70 and Hsp70 interact with phosphatidylserine on the surface of PC12 cells resulting in a decrease of viability. *The FASEB journal* **2004,** *18* (14), 1636-1645.

21. Becker, T.; Hartl, F.-U.; Wieland, F., CD40, an extracellular receptor for binding and uptake of Hsp70–peptide complexes. *The Journal of cell biology* **2002,** *158* (7), 1277-1285.

22. Singh-Jasuja, H.; Toes, R. E.; Spee, P.; Münz, C.; Hilf, N.; Schoenberger, S. P.; Ricciardi-Castagnoli, P.; Neefjes, J.; Rammensee, H.-G.; Arnold-Schild, D., Cross-presentation of glycoprotein 96–associated antigens on major histocompatibility complex class I molecules requires receptor-mediated endocytosis. *The Journal of experimental medicine* **2000,** *191* (11), 1965-1974.

23. Binder, R. J.; Srivastava, P. K., Essential role of CD91 in re-presentation of gp96-chaperoned peptides. *Proceedings of the National Academy of Sciences* **2004,** *101* (16), 6128-6133.

24. Doody, A. D.; Kovalchin, J. T.; Mihalyo, M. A.; Hagymasi, A. T.; Drake, C. G.; Adler, A. J., Glycoprotein 96 can chaperone both MHC class I-and class II-restricted epitopes for in vivo presentation, but selectively primes CD8+ T cell effector function. *The Journal of Immunology* **2004,** *172* (10), 6087-6092.

25. Schild, H.; Arnold-Schild, D.; Lammert, E.; Rammensee, H.-G., Stress proteins and immunity mediated by cytotoxic T lymphocytes. *Current opinion in immunology* **1999,** *11* (1), 109-113.

26. Groenendyk, J.; Lynch, J.; Michalak, M., Calreticulin, Ca 2+, and Calcineurin-Signaling from the Endoplasmic Reticulum. *Molecules & Cells (Springer Science & Business Media BV)* **2004,** *17* (3).

27. Oliver, J. D.; Roderick, H. L.; Llewellyn, D. H.; High, S., ERp57 functions as a subunit of specific complexes formed with the ER lectins calreticulin and calnexin. *Molecular biology of the cell* **1999,** *10* (8), 2573-2582.

28. Obeid, M.; Tesniere, A.; Ghiringhelli, F.; Fimia, G. M.; Apetoh, L.; Perfettini, J.-L.; Castedo, M.; Mignot, G.; Panaretakis, T.; Casares, N., Calreticulin exposure dictates the immunogenicity of cancer cell death. *Nature medicine* **2007,** *13* (1), 54-61.

29. Orr, A. W.; Elzie, C. A.; Kucik, D. F.; Murphy-Ullrich, J. E., Thrombospondin signaling through the calreticulin/LDL receptor-related protein co-complex stimulates random and directed cell migration. *Journal of cell science* **2003,** *116* (14), 2917-2927.

30. Ogden, C. A.; deCathelineau, A.; Hoffmann, P. R.; Bratton, D.; Ghebrehiwet, B.; Fadok, V. A.; Henson, P. M., C1q and mannose binding lectin engagement of cell surface calreticulin and CD91 initiates macropinocytosis and uptake of apoptotic cells. *The Journal of experimental medicine* **2001,** *194* (6), 781-796.

31. Gardai, S. J.; McPhillips, K. A.; Frasch, S. C.; Janssen, W. J.; Starefeldt, A.; Murphy-Ullrich, J. E.; Bratton, D. L.; Oldenborg, P.-A.; Michalak, M.; Henson, P. M., Cell-surface calreticulin initiates clearance of viable or apoptotic cells through trans-activation of LRP on the phagocyte. *Cell* **2005,** *123* (2), 321-334.

32. Garg, A. D.; Nowis, D.; Golab, J.; Vandenabeele, P.; Krysko, D. V.; Agostinis, P., Immunogenic cell death, DAMPs and anticancer therapeutics: an emerging amalgamation. *Biochimica et Biophysica Acta (BBA)-Reviews on Cancer* **2010,** *1805* (1), 53-71.

33. Bianchi, M. E.; Beltrame, M.; Paonessa, G., Specific recognition of cruciform DNA by nuclear protein HMG1. *Science* **1989,** *243* (4894), 1056-1059.

34. Scaffidi, P.; Misteli, T.; Bianchi, M. E., Release of chromatin protein HMGB1 by necrotic cells triggers inflammation. *Nature* **2002,** *418* (6894), 191-195.

35. Wang, H.; Bloom, O.; Zhang, M.; Vishnubhakat, J. M.; Ombrellino, M.; Che, J.; Frazier, A.; Yang, H.; Ivanova, S.; Borovikova, L., HMG-1 as a late mediator of endotoxin lethality in mice. *Science* **1999,** *285* (5425), 248-251.

36. Park, J. S.; Gamboni-Robertson, F.; He, Q.; Svetkauskaite, D.; Kim, J.-Y.; Strassheim, D.; Sohn, J.-W.; Yamada, S.; Maruyama, I.; Banerjee, A., High mobility group box 1 protein interacts with multiple Toll-like receptors. *American Journal of Physiology-Cell Physiology* **2006,** *290* (3), C917-C924.

37. Rovere-Querini, P.; Capobianco, A.; Scaffidi, P.; Valentinis, B.; Catalanotti, F.; Giazzon, M.; Dumitriu, I. E.; Müller, S.; Iannacone, M.; Traversari, C., HMGB1 is an endogenous immune adjuvant released by necrotic cells. *EMBO reports* **2004,** *5* (8), 825-830.

38. Grazioli, S.; Pugin, J., Mitochondrial damage-associated molecular patterns: from inflammatory signaling to human diseases. *Frontiers in immunology* **2018,** *9*, 832.

39. Elliott, M. R.; Chekeni, F. B.; Trampont, P. C.; Lazarowski, E. R.; Kadl, A.; Walk, S. F.; Park, D.; Woodson, R. I.; Ostankovich, M.; Sharma, P., Nucleotides released by apoptotic cells act as a find-me signal to promote phagocytic clearance. *Nature* **2009,** *461* (7261), 282-286.

40. Chekeni, F. B.; Elliott, M. R.; Sandilos, J. K.; Walk, S. F.; Kinchen, J. M.; Lazarowski, E. R.; Armstrong, A. J.; Penuela, S.; Laird, D. W.; Salvesen, G. S., Pannexin 1 channels mediate 'find-me'signal release and membrane permeability during apoptosis. *Nature* **2010,** *467* (7317), 863-867.

41. Kouzaki, H.; Iijima, K.; Kobayashi, T.; O'Grady, S. M.; Kita, H., The danger signal, extracellular ATP, is a sensor for an airborne allergen and triggers IL-33 release and innate Th2-type responses. *The Journal of Immunology* **2011,** *186* (7), 4375-4387.

42. Idzko, M.; Panther, E.; Bremer, H. C.; Sorichter, S.; Luttmann, W.; Virchow Jr, C. J.; Di Virgilio, F.; Herouy, Y.; Norgauer, J.; Ferrari, D., Stimulation of P2 purinergic receptors induces the release of eosinophil cationic protein and interleukin-8 from human eosinophils. *British journal of pharmacology* **2003,** *138* (7), 1244-1250.

43. Ghiringhelli, F.; Apetoh, L.; Tesniere, A.; Aymeric, L.; Ma, Y.; Ortiz, C.; Vermaelen, K.; Panaretakis, T.; Mignot, G.; Ullrich, E., Activation of the NLRP3 inflammasome in dendritic cells induces IL-1β–dependent adaptive immunity against tumors. *Nature medicine* **2009,** *15* (10), 1170.

44. Nikfarjam, M.; Muralidharan, V.; Christophi, C., Mechanisms of focal heat destruction of liver tumors. *Journal of Surgical Research* **2005,** *127* (2), 208-223.

45. Ott, P. A.; Hodi, F. S.; Kaufman, H. L.; Wigginton, J. M.; Wolchok, J. D., Combination immunotherapy: a road map. *Journal for immunotherapy of cancer* **2017,** *5* (1), 16.

46. Mattarollo, S. R.; Loi, S.; Duret, H.; Ma, Y.; Zitvogel, L.; Smyth, M. J., Pivotal role of innate and adaptive immunity in anthracycline chemotherapy of established tumors. *Cancer research* **2011,** *71* (14), 4809-4820.

47. Yoo, H. S.; Lee, K. H.; Oh, J. E.; Park, T. G., In vitro and in vivo anti-tumor activities of nanoparticles based on doxorubicin–PLGA conjugates. *Journal of controlled Release* **2000,** *68* (3), 419-431.

48. Huang, X.; El-Sayed, I. H.; Qian, W.; El-Sayed, M. A., Cancer cell imaging and photothermal therapy in the near-infrared region by using gold nanorods. *Journal of the American Chemical Society* **2006,** *128* (6), 2115-2120.

49. Hudson, D. E.; Hudson, D. O.; Wininger, J. M.; Richardson, B. D., Penetration of laser light at 808 and 980 nm in bovine tissue samples. *Photomedicine and laser surgery* **2013,** *31* (4), 163-168.

50. Smith, A. M.; Mancini, M. C.; Nie, S., Bioimaging: second window for in vivo imaging. *Nature nanotechnology* **2009,** *4* (11), 710.

51. Jain, P. K.; Huang, X.; El-Sayed, I. H.; El-Sayed, M. A., Review of some interesting surface plasmon resonance-enhanced properties of noble metal nanoparticles and their applications to biosystems. *Plasmonics* **2007,** *2* (3), 107-118.

52. Yu, J.; Yang, L.; Yan, J.; Wang, W. C.; Chen, Y. C.; Chen, H. H.; Lin, C. H., Carbon Nanomaterials for Photothermal Therapies. *Carbon Nanomaterials for Bioimaging, Bioanalysis, and Therapy* **2019**, 309-340.

53. Xu, L.; Cheng, L.; Wang, C.; Peng, R.; Liu, Z., Conjugated polymers for photothermal therapy of cancer. *Polymer Chemistry* **2014,** *5* (5), 1573-1580.

54. Cantu, T.; Walsh, K.; Pattani, V. P.; Moy, A. J.; Tunnell, J. W.; Irvin, J. A.; Betancourt, T., Conductive polymer-based nanoparticles for laser-mediated photothermal ablation of cancer: synthesis, characterization, and in vitro evaluation. *International journal of nanomedicine* **2017,** *12*, 615.

55. Cai, Y.; Si, W.; Huang, W.; Chen, P.; Shao, J.; Dong, X., Organic dye based nanoparticles for cancer phototheranostics. *Small* **2018,** *14* (25), 1704247.

56. Sheng, Z.; Hu, D.; Xue, M.; He, M.; Gong, P.; Cai, L., Indocyanine green nanoparticles for theranostic applications. *Nano-Micro Letters* **2013,** *5* (3), 145-150.

57. Rizvi, S. A.; Saleh, A. M., Applications of nanoparticle systems in drug delivery technology. *Saudi Pharmaceutical Journal* **2018,** *26* (1), 64-70.

58. Hirsjarvi, S.; Passirani, C.; Benoit, J.-P., Passive and active tumour targeting with nanocarriers. *Current drug discovery technologies* **2011,** *8* (3), 188-196.

59. Kouchakzadeh, H.; Soudi, T.; Aghda, N. H.; Shojaosadati, S. A., Ligand-modified biopolymeric nanoparticles as efficient tools for targeted cancer therapy. *Current pharmaceutical design* **2017,** *23* (35), 5336-5348.

60. Xiao, R. Z.; Zeng, Z. W.; Zhou, G. L.; Wang, J. J.; Li, F. Z.; Wang, A. M., Recent advances in PEG–PLA block copolymer nanoparticles. *International journal of nanomedicine* **2010,** *5*, 1057.

61. Elzoghby, A. O.; Samy, W. M.; Elgindy, N. A., Albumin-based nanoparticles as potential controlled release drug delivery systems. *Journal of controlled release* **2012,** *157* (2), 168-182.

62. Current Nanotechnology Treatments. https://www.cancer.gov/nano/cancer-nanotechnology/current-treatments.

63. Barreras-Urbina, C. G.; Ramírez-Wong, B.; López-Ahumada, G. A.; Burruel-Ibarra, S. E.; Martínez-Cruz, O.; Tapia-Hernández, J. A.; Rodriguez Felix, F., Nano-and micro-particles by nanoprecipitation: Possible application in the food and agricultural industries. *International journal of food properties* **2016,** *19* (9), 1912-1923.

64. Krishnamoorthy, K.; Mahalingam, M., Selection of a suitable method for the preparation of polymeric nanoparticles: multi-criteria decision making approach. *Advanced pharmaceutical bulletin* **2015,** *5* (1), 57.

65. Baldyga, J.; Bourne, J.; Dubuis, B.; Etchells, A.; Gholap, R.; Zimmermann, B., Jet reactor scale-up for mixing-controlled reactions. *Chemical engineering research & design* **1995,** *73* (5), 497-502.

66. Bourne, J. R.; Studer, M., Fast reactions in rotor-stator mixers of different size. *Chemical Engineering and Processing: Process Intensification* **1992,** *31* (5), 285-296.

67. Robert, J. D.; Bourne, J. R., Rapid micromixing by the impingement of thin liquid sheets (II): Mixing study. *Ind. Eng. Chem. Res* **1989,** *28*, 830-839.

68. D'Addio, S. M.; Prud'homme, R. K., Controlling drug nanoparticle formation by rapid precipitation. *Advanced drug delivery reviews* **2011,** *63* (6), 417-426.

69. Betancourt, T.; Massingill Jr, J. L.; Stretz, H., Fluidic system for high throughput preparation of microparticles and nanoparticles. Google Patents: 2019.

70. Massingill, J. L., Method and system for production of biofuels using a fiber conduit reactor. Google Patents: 2012.

71. Massingill Jr, J. L., Fiber film reactors to effect separation and reaction between two immiscible reaction components. Google Patents: 2009.

72. Jamkhindikar, S. P.; Stretz, H. A.; Massingill Jr, J. L.; Betancourt, T., High throughput fiber reactor process for organic nanoparticle production: Poly (N-isopropylacrylamide), polyacrylamide, and alginate. *Journal of Applied Polymer Science* **2017,** *134* (47), 45524.

73. Oh, J. K., Polylactide (PLA)-based amphiphilic block copolymers: synthesis, self-assembly, and biomedical applications. *Soft Matter* **2011,** *7* (11), 5096-5108.

74. Chavez, K. J.; Garimella, S. V.; Lipkowitz, S., Triple negative breast cancer cell lines: one tool in the search for better treatment of triple negative breast cancer. *Breast disease* **2010,** *32* (1-2), 35.

75. Brenton, J. D.; Carey, L. A.; Ahmed, A. A.; Caldas, C., Molecular classification and molecular forecasting of breast cancer: ready for clinical application? *Journal of clinical oncology* **2005,** *23* (29), 7350-7360.

76. Yildiz, T.; Gu, R.; Zauscher, S.; Betancourt, T., Doxorubicin-loaded protease-activated near-infrared fluorescent polymeric nanoparticles for imaging and therapy of cancer. *International journal of nanomedicine* **2018,** *13*, 6961.

77. Du, Y. J.; Lemstra, P. J.; Nijenhuis, A. J.; Van Aert, H. A.; Bastiaansen, C., ABA type copolymers of lactide with poly (ethylene glycol). Kinetic, mechanistic, and model studies. *Macromolecules* **1995,** *28* (7), 2124-2132.

78. Govender, T.; Riley, T.; Ehtezazi, T.; Garnett, M. C.; Stolnik, S.; Illum, L.; Davis, S. S., Defining the drug incorporation properties of PLA–PEG nanoparticles. *International journal of pharmaceutics* **2000,** *199* (1), 95-110.

79. McCarron, P. A.; Marouf, W. M.; Donnelly, R. F.; Scott, C., Enhanced surface attachment of protein-type targeting ligands to poly (lactide-co-glycolide) nanoparticles using variable expression of polymeric acid functionality. *Journal of Biomedical Materials Research Part A: An Official Journal of The Society for Biomaterials, The Japanese Society for Biomaterials, and The Australian Society for Biomaterials and the Korean Society for Biomaterials* **2008,** *87* (4), 873-884.

80. Özel, T.; White, S.; Nguyen, E.; Moy, A.; Brenes, N.; Choi, B.; Betancourt, T., Enzymatically activated near infrared nanoprobes based on amphiphilic block copolymers for optical detection of cancer. *Lasers in surgery and medicine* **2015,** *47* (7), 579-594.

81. Joshi, M., Opportunities, Challenges and Pathways of Nano-Medicines: A Concise Review. *J Nanomed Res* **2014,** *1* (2), 00013.

82. Honary, S.; Zahir, F., Effect of zeta potential on the properties of nano-drug delivery systems-a review (Part 1). *Tropical Journal of Pharmaceutical Research* **2013,** *12* (2), 255-264.

83. Honary, S.; Zahir, F., Effect of zeta potential on the properties of nano-drug delivery systems-a review (Part 2). *Tropical Journal of Pharmaceutical Research* **2013,** *12* (2), 265-273.

84. Ford, J. L.; Mitchell, K.; Rowe, P.; Armstrong, D. J.; Elliott, P. N.; Rostron, C.; Hogan, J. E., Mathematical modelling of drug release from hydroxypropylmethylcellulose matrices: effect of temperature. *International journal of pharmaceutics* **1991,** *71* (1-2), 95-104.

85. Peppas, N. A.; Sahlin, J. J., A simple equation for the description of solute release. III. Coupling of diffusion and relaxation. *International journal of pharmaceutics* **1989,** *57* (2), 169-172.

86. Zhang, Y.; Huo, M.; Zhou, J.; Zou, A.; Li, W.; Yao, C.; Xie, S., DDSolver: an add-in program for modeling and comparison of drug dissolution profiles. *The AAPS journal* **2010,** *12* (3), 263-271.

87. Herman, T. S.; Sweets, C. C.; White, D. M.; Gerner, E. W., Effect of heating on lethality due to hyperthermia and selected chemotherapeutic drugs. *Journal of the National Cancer Institute* **1982,** *68* (3), 487-491.

88. Gathje, J.; Steuer, R. R.; Nicholes, K., Stability studies on indocyanine green dye. *Journal of applied physiology* **1970,** *29* (2), 181-185.

89. Serrano-del Valle, A.; Anel, A.; Naval, J.; Marzo, I., Immunogenic cell death and immunotherapy of multiple myeloma. *Frontiers in Cell and Developmental Biology* **2019,** *7*.

90. de Bruyn, M.; Wiersma, V. R.; Helfrich, W.; Eggleton, P.; Bremer, E., The ever-expanding immunomodulatory role of calreticulin in cancer immunity. *Frontiers in oncology* **2015,** *5*, 35.

91. Drugs@FDA: FDA Approved Drug Products. https://www.accessdata.fda.gov/scripts/cder/daf/index.cfm?event=overview.process&applno=011525.

92. Wei, W.; Zhang, X.; Zhang, S.; Wei, G.; Su, Z., Biocompatible and bioactive engineered nanomaterials for targeted tumor photothermal therapy: A review. *Materials Science and Engineering: C* **2019**, 109891.

93. Pacardo, D. B.; Neupane, B.; Rikard, S. M.; Lu, Y.; Mo, R.; Mishra, R.; Tracy, J. B.; Wang, G.; Ligler, F. S.; Gu, Z., A dual wavelength-activatable gold nanorod complex for synergistic cancer treatment. *Nanoscale* **2015,** *7*, 12096.

94. Srinivasan, S.; Manchanda, R.; Lei, T.; Nagesetti, A.; Fernandez-Fernandez, A.; McGoron, A. J., Targeted nanoparticles for simultaneous delivery of chemotherapeutic and hyperthermia agents--an in vitro study. *J Photochem Photobiol B* **2014,** *136*, 81-90.

95. Ito, A.; Yamaguchi, M.; Okamoto, N.; Sanematsu, Y.; Kawabe, Y.; Wakamatsu, K.; Ito, S.; Honda, H.; Kobayashi, T.; Nakayama, E., T-cell receptor repertoires of tumor-infiltrating lymphocytes after hyperthermia using functionalized magnetite nanoparticles. *Nanomedicine* **2013,** *8* (6), 891-902.

96. Ito, A.; Tanaka, K.; Kondo, K.; Shinkai, M.; Honda, H.; Matsumoto, K.; Saida, T.; Kobayashi, T., Tumor regression by combined immunotherapy and hyperthermia using magnetic nanoparticles in an experimental subcutaneous murine melanoma. *Cancer science* **2003,** *94* (3), 308-313.

97. Toraya-Brown, S.; Fiering, S., Local tumour hyperthermia as immunotherapy for metastatic cancer. *International Journal of Hyperthermia* **2014,** *30* (8), 531-539.

98. Chen, Q.; Xu, L.; Liang, C.; Wang, C.; Peng, R.; Liu, Z., Photothermal therapy with immune-adjuvant nanoparticles together with checkpoint blockade for effective cancer immunotherapy. *Nature communications* **2016,** *7*, 13193.

99. Bear, A. S.; Kennedy, L. C.; Young, J. K.; Perna, S. K.; Almeida, J. P. M.; Lin, A. Y.; Eckels, P. C.; Drezek, R. A.; Foster, A. E., Elimination of metastatic melanoma using gold nanoshell-enabled photothermal therapy and adoptive T cell transfer. *PLoS One* **2013,** *8* (7), e69073.

100. Toraya-Brown, S.; Sheen, M. R.; Zhang, P.; Chen, L.; Baird, J. R.; Demidenko, E.; Turk, M. J.; Hoopes, P. J.; Conejo-Garcia, J. R.; Fiering, S., Local hyperthermia treatment of tumors induces CD8+ T cell-mediated resistance against distal and secondary tumors. In *HANDBOOK OF IMMUNOLOGICAL PROPERTIES OF ENGINEERED NANOMATERIALS: Volume 3: Engineered Nanomaterials and the Immune Cell Function*, World Scientific: 2016; pp 309-347.

101. Bezu, L.; Gomes-de-Silva, L. C.; Dewitte, H.; Breckpot, K.; Fucikova, J.; Spisek, R.; Galluzzi, L.; Kepp, O.; Kroemer, G., Combinatorial strategies for the induction of immunogenic cell death. *Front Immunol* **2015,** *6*, 187.

102. Kersten, K.; Salvagno, C.; de Visser, K. E., Exploiting the Immunomodulatory Properties of Chemotherapeutic Drugs to Improve the Success of Cancer Immunotherapy. *Front Immunol* **2015,** *6*, 516.

103. Galluzzi, L.; Buque, A.; Kepp, O.; Zitvogel, L.; Kroemer, G., Immunogenic cell death in cancer and infectious disease. *Nat Rev Immunol* **2017,** *17* (2), 97-111.

104. Cassetta, L.; Kitamura, T., Macrophage targeting: opening new possibilities for cancer immunotherapy. *Immunology* **2018,** *155* (3), 285-293.

105. Weber, C.; Coester, C.; Kreuter, J.; Langer, K., Desolvation process and surface characterisation of protein nanoparticles. *International journal of pharmaceutics* **2000,** *194* (1), 91-102.

106. Irache, J.; Merodio, M.; Arnedo, A.; Camapanero, M.; Mirshahi, M.; Espuelas, S., Albumin nanoparticles for the intravitreal delivery of anticytomegaloviral drugs. *Mini reviews in medicinal chemistry* **2005,** *5* (3), 293-305.

107. Pillai, G., Nanomedicines for cancer therapy: an update of fda approved and those under various stages of development. SOJ Pharm Pharm Sci 1 (2): 13. *Nanomedicines for Cancer Therapy: An Update of FDA Approved and Those under Various Stages of Development* **2014**.

108. Tang, J. Q.; Hou, X. Y.; Yang, C. S.; Li, Y. X.; Xin, Y.; Guo, W. W.; Wei, Z. P.; Liu, Y. Q.; Jiang, G., Recent developments in nanomedicine for melanoma treatment. *International journal of cancer* **2017,** *141* (4), 646-653.

109. Olson, B.; Li, Y.; Lin, Y.; Liu, E. T.; Patnaik, A., Mouse models for cancer immunotherapy research. *Cancer discovery* **2018,** *8* (11), 1358-1365.

110. Galisteo-González, F.; Molina-Bolívar, J., Systematic study on the preparation of BSA nanoparticles. *Colloids and Surfaces B: Biointerfaces* **2014,** *123*, 286-292.

111. Peng, Z.; Hidajat, K.; Uddin, M., Selective and sequential adsorption of bovine serum albumin and lysozyme from a binary mixture on nanosized magnetic particles. *Journal of colloid and interface science* **2005,** *281* (1), 11-17.

112. Sawaya, A.; Benoit, J. P.; Benita, S., Binding mechanism of doxorubicin in lon-exchange albumin microcapsules. *Journal of pharmaceutical sciences* **1987,** *76* (6), 475-480.

113. Muckle, T. J., Plasma proteins binding of indocyanine green. *Biochemical medicine* **1976,** *15* (1), 17-21.

114. Kim, D.; El-Shall, H.; Dennis, D.; Morey, T., Interaction of PLGA nanoparticles with human blood constituents. *Colloids and Surfaces B: Biointerfaces* **2005,** *40* (2), 83-91.

115. Zheng, X.; Xing, D.; Zhou, F.; Wu, B.; Chen, W. R., Indocyanine green-containing nanostructure as near infrared dual-functional targeting probes for optical imaging and photothermal therapy. *Molecular pharmaceutics* **2011,** *8* (2), 447-456.

116. Xu, Y.; Kim, C. S.; Saylor, D. M.; Koo, D., Polymer degradation and drug delivery in PLGA-based drug–polymer applications: A review of experiments and theories. *Journal of Biomedical Materials Research Part B: Applied Biomaterials* **2017,** *105* (6), 1692-1716.

117. Yamamoto, H.; Takahashi, C., Application of Polymeric Nanoparticles and Polymeric Micelles for Treatment of Biofilm Infection Disease. In *Nanoparticle Technology Handbook*, Elsevier: 2018; pp 481-486.

118. Amjadi, M.; Sheykhansari, S.; Nelson, B. J.; Sitti, M., Recent advances in wearable transdermal delivery systems. *Advanced Materials* **2018,** *30* (7), 1704530.

119. d'Angelo, I.; Costabile, G.; Durantie, E.; Brocca, P.; Rondelli, V.; Russo, A.; Russo, G.; Miro, A.; Quaglia, F.; Petri-Fink, A., Hybrid lipid/polymer nanoparticles for pulmonary delivery of siRNA: development and fate upon in vitro deposition on the human epithelial airway barrier. *Journal of aerosol medicine and pulmonary drug delivery* **2018,** *31* (3), 170-181.

120. Kondo, A., Development of the Thermoresponsive Magnetic Nanoparticle and Its Deployment in the Biotechnology Field. In *Nanoparticle Technology Handbook*, Elsevier: 2018; pp 427-434.

121. Tsukada, Y.; Sasai, A.; Tsujimoto, H.; Yamamoto, H.; Kawashima, Y., PLGA Nanosphere Technology for Novel Nanomedicine and Functional Cosmetics. In *Nanoparticle Technology Handbook*, Elsevier: 2018; pp 461-467.

122. Shewan, H. M.; Stokes, J. R., Review of techniques to manufacture micro-hydrogel particles for the food industry and their applications. *Journal of Food Engineering* **2013,** *119* (4), 781-792.

123. Tungittiplakorn, W.; Lion, L. W.; Cohen, C.; Kim, J.-Y., Engineered polymeric nanoparticles for soil remediation. *Environmental science & technology* **2004,** *38* (5), 1605-1610.

124. Hornig, S.; Heinze, T.; Becer, C. R.; Schubert, U. S., Synthetic polymeric nanoparticles by nanoprecipitation. *Journal of Materials Chemistry* **2009,** *19* (23), 3838-3840.

125. Demyanovich, R. J.; Bourne, J. R., Rapid micromixing by the impingement of thin liquid sheets. 2. Mixing study. *Industrial & engineering chemistry research* **1989,** *28* (6), 830-839.

126. Bramosanti, M.; Chronopoulou, L.; Grillo, F.; Valletta, A.; Palocci, C., Microfluidic-assisted nanoprecipitation of antiviral-loaded polymeric nanoparticles. *Colloids and Surfaces A: Physicochemical and Engineering Aspects* **2017,** *532*, 369-376.

127. Tao, J.; Chow, S. F.; Zheng, Y., Application of flash nanoprecipitation to fabricate poorly water-soluble drug nanoparticles. *Acta pharmaceutica sinica B* **2019,** *9* (1), 4-18.

128. Johnson, B. K.; Prud'homme, R. K., Mechanism for rapid self-assembly of block copolymer nanoparticles. *Physical review letters* **2003,** *91* (11), 118302.

129. Saad, W. S.; Prud'homme, R. K., Principles of nanoparticle formation by flash nanoprecipitation. *Nano Today* **2016,** *11* (2), 212-227.

130. Guozhong, C., *Nanostructures and nanomaterials: synthesis, properties and applications*. World scientific: 2004.

131. Shiau, L.-D., Determination of the Nucleation and Growth Kinetics for Aqueous L-glycine Solutions from the Turbidity Induction Time Data. *Crystals* **2018,** *8* (11), 403.

132. Rivera Vargas, T.; Apetoh, L., Can immunogenic chemotherapies relieve cancer cell resistance to immune checkpoint inhibitors? *Frontiers in immunology* **2019,** *10*, 1181.

133. Zulfiqar, B.; Mahroo, A.; Nasir, K.; Farooq, R. K.; Jalal, N.; Rashid, M. U.; Asghar, K., Nanomedicine and cancer immunotherapy: focus on indoleamine 2, 3-dioxygenase inhibitors. *OncoTargets and therapy* **2017,** *10*, 463.

134. Guo, H.; MacKay, J. A., A pharmacokinetics primer for preclinical nanomedicine research. In *Nanoparticles for Biomedical Applications*, Elsevier: 2020; pp 109-128.

135. Li, X., The inducers of immunogenic cell death for tumor immunotherapy. *Tumori Journal* **2018,** *104* (1), 1-8.

136. Maeda, H., Polymer therapeutics and the EPR effect. *Journal of drug targeting* **2017,** *25* (9-10), 781-785.

137. Tian, H.; Tang, Z.; Zhuang, X.; Chen, X.; Jing, X., Biodegradable synthetic polymers: Preparation, functionalization and biomedical application. *Progress in Polymer Science* **2012,** *37* (2), 237-280.

138. Musella, M.; Manic, G.; Galassi, C.; Vitale, I.; Sistigu, A., Cytofluorometric assessment of dendritic cell-mediated uptake of cancer cell apoptotic bodies. *Tumor Immunology and Immunotherapy-Cellular Methods* **2020**, 39.

139. Alev, M.; Egenberger, L.; Mühleisen, L.; Weigel, B.; Frey, B.; Friedrich, R. P.; Pöttler, M.; Alexiou, C.; Janko, C., Targeting of drug-loaded nanoparticles to tumor sites increases cell death and release of danger signals. *Journal of controlled release* **2018,** *285*, 67-80.

140. Dehne, N.; Mora, J.; Namgaladze, D.; Weigert, A.; Brüne, B., Cancer cell and macrophage cross-talk in the tumor microenvironment. *Current opinion in pharmacology* **2017,** *35*, 12-19.

141. Kimura, T.; Nakamra, N.; Hashimoto, Y.; Kishida, A., Induction of immunogenic cell death of cancer cell by using chemical detergent treatment and its activation of immune system. *The FASEB Journal* **2018,** *32* (1_supplement), 664.2-664.2.